

POLITECNICO DI TORINO

Master of science in Mechanical Engineering

Master's Degree Thesis

Variation of Flow Factors during the Run-in Process



RWTHAACHEN
UNIVERSITY

ifas Institute for
Fluid Power
Drives and Systems

Academic Supervisor:

Prof. Terenziano Raparelli

Prof. Luigi Mazza

Dott. Achill Holzer

Ing. Giacomo Maculotti

Candidate:

Luca Pirini Casadei

Academic Year 2020-2021

Abstract

The study of Flow Factors variation during run-in is carried out. A method to overcome the limitation of the input matrix dimension in the simulation program is developed. In particular, the software, which is used for the simulation of Flow Factors (Tribo-x), takes a matrix of 300 times 300 points as input, while the microscope measurement points are many more. So, the PSD of the surface is studied in order to find a relevant distance between two measurement points for the construction of the input matrix. Furthermore, the use of a Gaussian filter to reduce the measurement noise is discussed. At the end, all the results are presented and the behavior changes under different loads, temperatures and times are compared.

Contents

Introduction	1
1 State of the art	1
1.1 Introduction to Tribology.....	1
1.2 Solid Surface Topography.....	2
1.2.1 Geometric Characteristics of Solid Surfaces and Measurement Methods.....	3
1.2.2 Analysis of Surface Roughness	5
1.2.3 Contact between solid	7
1.2.4 Adhesion	8
1.3 Friction and Wear	9
1.3.1 Friction	9
1.3.2 Wear.....	16
1.4 Fluid Film Lubrication.....	21
1.4.1 Viscosity	22
1.4.2 Stribeck Curve	24
1.5 Run-in	28
1.6 Flow Factors.....	30
1.6.1 Pressure Flow Factors (ϕ_x, ϕ_y)	33
1.6.2 Shear Flow Factors (ϕ_s)	35
1.6.3 Tribo-x	37
1.7 Test Bench	37
2 MATLAB Code	41
2.1 Data Structure	41
2.1.1 Z-Matrix Construction	42
2.1.2 Missing points	46
2.2 Gaussian Filter	47
2.3 Power Spectral Density.....	48
2.3.1 Welch's Method	52
2.3.2 PSD computed directly from FFT.....	54
2.4 Cut-Off Frequency.....	55
2.4.1 Area method to determine cut-off frequency	56
2.4.2 Minimum method to determine cut-off frequency	60
2.4.3 Error method to determine cut-off frequency.....	61

2.4.4	Comparison between filter and no filter surfaces.....	61
2.4.5	Grid size influence	63
3	Experimental Tests and Results	65
3.1	<i>Samples</i>	65
3.2	<i>Experimental tests</i>	66
3.3	<i>Surface Variation during run-in period</i>	68
3.4	<i>Flow Factors</i>	74
3.4.1	Influence of Time	75
3.4.2	Influence of Load.....	78
3.4.3	Influence of Temperature	81
4	Conclusion and Future Work	85
4.1	<i>Future Work</i>	87
5	Appendix.....	89
5.1	<i>Appendix A</i>	89
	Bibliografy	93

List of Figures

Figure 1.1: Geometric characteristics of solid surfaces [2].	3
Figure 1.2: Error due to finite dimensions of stylus tip [2].	4
Figure 1.3: Comparison of three types of reference line: (a) mean; (b) ten-point average; (c) least squares [2].	6
Figure 1.4: The height distribution (left) and the Abbot curve (right) [4].	7
Figure 1.5: Real contact area of rough surfaces in contact [1].	8
Figure 1.6: Contact stresses between the asperities [1].	8
Figure 1.7: Schematic illustration of adhesive force to detach two surfaces put in contact. W is the load applied to bring them into contact and W^l is the tensile force needed to separate them (adhesive force).	9
Figure 1.8: Schematic illustration of friction force. On the top there is a body sliding on a surface, on the bottom its relative free body diagram [3].	11
Figure 1.9: Static friction force, F_{static} and kinetic friction force, F_k as a function of time [3].	11
Figure 1.10: Force equilibrium for a body on an inclined plane [3].	12
Figure 1.11: Two apparently contradictory aspects for the mechanism of static friction. On the top, the adhesive force act at the tip of the asperities in contact and keep the two surfaces together, resisting relative motion. At the bottom, horizontal components of repulsive force originated by the interaction between interpenetrating asperities resist relative motion [5].	13
Figure 1.12: Effect of time exposure to air on static friction coefficient of cleaved salt surfaces [5].	14
Figure 1.13: Effect of time on the static friction force between metals [5].	14
Figure 1.14: Schematic illustration of the transition from static contact to sliding contact for a hard asperity on a soft surface [1].	15
Figure 1.15: Schematic illustration of mechanisms of sliding frictional energy dissipation [1].	16
Figure 1.16: Schematic illustration of two break possibilities: at the interface (1) or at the weakest region of one body (2) [3].	17
Figure 1.17: Schematics of (a) a rough, hard surface or a surface mounted with abrasive grits sliding on a softer surface, and (b) free abrasive grits caught between the surface with at least one of the surfaces softer than the abrasive grits [3].	19
Figure 1.18: Optical microscope picture of a surface after the test. The sliding direction was along the vertical axis and it can be noticed that the scratches caused by abrasive wear are all parallel to the sliding direction.	20
Figure 1.19: Schematics of abrasive wear processes as a result of plastic deformation by three deformation models [3].	20

Figure 1.20: Schematic representation of the fluid separating the two surfaces [1].....	22
Figure 1.21: Viscosity-temperature characteristics of selected oils [1].	23
Figure 1.22: Stribeck curve and different lubrication regimes [3].	25
Figure 1.23: Principle of hydrodynamic pressure generation between non-parallel surfaces [1].	26
Figure 1.24: Eight common form of friction-time curves [5].	30
Figure 1.25: Film thickness [9].....	32
Figure 1.26: Model for flow factor simulation [9].	33
Figure 1.27: Typical contact areas for longitudinally oriented ($\gamma > 1$), isotropic ($\gamma = 0$) and transversely oriented ($\gamma < 1$) surfaces [9].	34
Figure 1.28: The pressure flow factors ϕ_x and ϕ_y for isotropic surfaces [9].	34
Figure 1.29: Effect of directional properties of roughness on pressure flow factor [9].	35
Figure 1.30: Shear Flow Factor ϕ_s [10].	36
Figure 1.31: Test bench: disc on disc tribometer [14].	38
Figure 1.32: Tribometer scheme [14].	39
Figure 2.1: Data structure after the microscope scan (a) and z-Matrix including all the z(x,y) surface values (b).	42
Figure 2.2: Construction of 'diff_y' and 'Index_diffY'	43
Figure 2.3: x sorted values used to find the vector with all x-values	44
Figure 2.4: Structure of matrix 'Supp' used to build z-matrix.	46
Figure 2.5: Real structure of z-matrix.	46
Figure 2.6: 2D Gaussian distribution with mean(0,0) and $\sigma = 0,5$	48
Figure 2.7: Gaussian filter's effect. Panel (a) shows the original surface, without filter, panels (b)-(d) shows the filter's effect increasing standard deviation (σ). Respectively $\sigma=2$ (b), $\sigma=5$ (c) and $\sigma=7$ (d).	49
Figure 2.8: Power Spectral Density where shows an example of what the cut-off frequency means.	50
Figure 2.9: Example of Flow Matrix creation.....	51
Figure 2.10: Construction of the Flow Matrix. On the left there is the z-matrix and an explanation of how the Flow Matrix is built, whereas on the right there is the Flow Matrix.....	51
Figure 2.11: Welch's method segmentation [18]	53
Figure 2.12: Hamming window	53
Figure 2.13: Comparison between PSD with Welch's method and PSD computed directly from FFT. Two surfaces are analysed: in the first one (a) the two results look very similar, in the second one (b) the two PSD are a little bit different, especially with large wavevector.	54
Figure 2.14: Normalization of PSD computed directly from FFT.....	55
Figure 2.15: Cut-off frequency determined with area method.....	57

Figure 2.16: Variation of $nArea$ in cut-off area method. With $nArea = 50\%$ (a) the cut-off frequency is smaller, so the relevant distance is greater, with $nArea = 70\%$ (b) the cut-off value is bigger (relevant distance smaller).	58
Figure 2.17: x-section of the sample $F0,5_{40grad_5min}$ compared with its Flow Matrix graph with different values of $nArea$: 60% (a), 50% (b), 40% (c) and 30% (d). The relevant distance ωx and $errperc$ as $SurfaceErr\%$ is also indicated.	59
Figure 2.18: Magnification of Figure 2.17(c).	59
Figure 2.19: Cut-off frequency determined with area method.....	60
Figure 2.20: Power Spectral density in x-direction (a) and y-direction(b) for different value of filter intensity.	62
Figure 2.21: Relevant distance for the same surface and same percentage of the cut-off method but with different intensity of the filter: no filter (a), $\sigma = 1$ (b) and $\sigma = 3$ (c).....	62
Figure 2.22: Influence of grid size in the calculation of Power Spectral Density.....	63
Figure 2.23: Grid size influence on the determination of the relevant distance ωy . The surface, the cut-off method and the percentage of the cut-off method are the same for all the graphs. The only difference is the grid size of the measurement scanning: $0,18\mu m \times 0,18\mu m$ (a), $0,36\mu m \times 0,36\mu m$ (b), $0,72\mu m \times 0,72\mu m$ (c) and $1,44\mu m \times 1,44\mu m$ (d).	64
Figure 3.1: Photos of the two sample. The stationary steel disc is on the left and the rotating brass disc is on the right.	66
Figure 3.2: Coefficient of friction as a function of time for different load pressures. The blue dotted lines specify the duration for which tests are carried out.	69
Figure 3.3: Relative contact area computed as the ratio between the real contact area and the nominal contact area after 5 minutes runtime for different loads.	70
Figure 3.4: Coefficient of friction as a function of time for different oil temperature. The load is set to 2 MPa.	71
Figure 3.5: Coefficient of friction as a function of time for different oil temperature. The load is set to 1 MPa.	72
Figure 3.6: Relative contact area computed as the ratio between the real contact area and the nominal contact area. (a) is for a pressure of 0,5 MPa, (b) for 1 MPa, (c) for 2 MPa and (d) for 3 MPa.....	73
Figure 3.7: Abbot curve direction of 5 min runtime tests for different loads. On the left the Abbot curve of the stationary discs in the radial direction and on the right the one of the rotating discs, always for the radial direction.	74
Figure 3.8: Surface of brass disc after 10 minutes of work under 2 MPa of normal load and 40° of oil temperature. The grooves are verticals because the sliding was in y-direction.	75
Figure 3.9: Pressure flow factor in x- and y-direction with 1 MPa of pressure load.	76

<i>Figure 3.10: Pressure flow factor in x- and y-direction with 2 MPa of pressure load.</i>	<i>76</i>
<i>Figure 3.11: Steel surface after 5 minutes of testing with 1 MPa. Note that the scratches are not perfectly vertical so the flow factor along y is not negative.</i>	<i>77</i>
<i>Figure 3.12: Shear flow factor in x- and y-direction with 1 MPa of pressure load.</i>	<i>78</i>
<i>Figure 3.13: Shear flow factor in x- and y-direction with 2 MPa of pressure load.</i>	<i>78</i>
<i>Figure 3.14: Pressure flow factor in x- and y-direction for 5 minutes runtime.</i>	<i>79</i>
<i>Figure 3.15: Pressure flow factor in x- and y-direction for 15 minutes runtime.</i>	<i>79</i>
<i>Figure 3.16: Pressure flow factor in x- and y-direction for 60 minutes runtime.</i>	<i>80</i>
<i>Figure 3.17: Shear flow factor in x- and y-direction for 5 minutes runtime.</i>	<i>80</i>
<i>Figure 3.18: Shear flow factor in x- and y-direction for 15 minutes runtime.</i>	<i>81</i>
<i>Figure 3.19: Pressure flow factor in x- and y-direction for different oil temperature and 15 minutes runtime with 1 MPa of contact pressure.</i>	<i>82</i>
<i>Figure 3.20: Pressure flow factor in x- and y-direction for different oil temperature and 15 minutes runtime with 2 MPa of contact pressure.</i>	<i>82</i>
<i>Figure 3.21: Shear flow factor in x- and y-direction for different oil temperature and 15 minutes runtime with 1 MPa of contact pressure.</i>	<i>83</i>
<i>Figure 3.22: Shear flow factor in x- and y-direction for different oil temperature and 15 minutes runtime with 2 MPa of contact pressure.</i>	<i>83</i>
<i>Figure 4.1: Example that shows the tiny portion of the total microscope data considered by taking a 300x300 submatrix. On the left there is the total surface scanned by the microscope, on the right there is the submatrix taken by conspiring a submatrix of 300x300 points. This is tiny and it is not representative of the total surface topography.</i>	<i>85</i>
<i>Figure 4.2: Portion of surface taken by studying the PSD. It is clearly bigger and it is representative of the surface roughness.</i>	<i>86</i>
<i>Figure 4.3: Surface rotation around z-axis in order to have vertical oriented lay.</i>	<i>87</i>

List of Tables

<i>Table 1.1: ‘Alicon Infinite Focus G4’ Technical Specifications.</i>	5
<i>Table 1.2: Technical specification of the Test Bench.</i>	38
<i>Table 2.1: Optimal nArea value for different samples. The two relevant distances (ω_x and ω_y), errperc, the roughness Ra and the length of the Flow Matrix in x-direction (Range x) and in y-direction (Range y are also indicated).</i>	58
<i>Table 2.2: Optimal nMin value for different sample. The two relevant distance (ω_x and ω_y), errperc, the roughness Ra and the length of the Flow Matrix in x-direction (Range x) and in y-direction (Range y) are also indicated.</i>	61
<i>Table 3.1: Material proprieties.</i>	65
<i>Table 3.2: Time, load and oil temperature values for the performed tests.</i>	66
<i>Table 3.3: Plan of the tests for load and time influence, oil temperature set to 40°.</i>	67
<i>Table 3.4: Plan of tests for oil temperature influence.</i>	67
<i>Table 3.5: Roughness variation of the test with 3 MPa for different durations.</i>	70
<i>Table 3.6: Roughness variation of the 15 min runtime and 1 MPa tests for different oil temperature.</i>	72
<i>Table 3.7: Roughness variation of the 15 min runtime and 2 MPa tests for different oil temperature.</i>	72
<i>Table 5.1: Roughness variation of the test with 0,5 MPa for different durations.</i>	89
<i>Table 5.2: Roughness variation of the test with 1 MPa for different durations.</i>	89
<i>Table 5.3: Roughness variation of the test with 2 MPa for different durations.</i>	90
<i>Table 5.4: Roughness variation of the test with 3 MPa for different durations.</i>	90
<i>Table 5.5: Roughness variation of the 5 min runtime tests for different loads.</i>	90
<i>Table 5.6: Roughness variation of the 10 min runtime tests for different loads.</i>	91
<i>Table 5.7: Roughness variation of the 15 min runtime tests for different loads.</i>	91
<i>Table 5.8: Roughness variation of the 60 min runtime tests for different loads.</i>	91
<i>Table 5.9: Roughness variation of the 15 min runtime and 1 MPa tests for different oil temperature.</i>	92
<i>Table 5.10: Roughness variation of the 15 min runtime and 2 MPa tests for different oil temperature.</i>	92

Nomenclature

Acronyms

AFM	“atomic force microscope”.
EHD	“Elastohydrodynamic lubrication”.
FFT	“Fast Fourier transform”, it is an algorithm that computes the discrete Fourier transform of a sequence, or its inverse.
HD	“Hydrodynamic lubrication”.
IFAS	“Institute for Fluid Power and Systems”.
PSD	“Power Spectral Density”.
RMS	“Root mean square”, it is the square root of the mean square.

Notation

dx	Microscope resolution in x-direction. It is the distance between two measurement points along x.
dy	Microscope resolution in y-direction. It is the distance between two measurement points along y.
<i>Flow Matrix</i>	It is the 300x300 matrix used as input for the simulation software.
R_a	Arithmetical mean deviation of the surface profile.
R_q	Root mean squared of the surface profile.
$z(x,y)$	It is the height value of the surface for the point (x, y) .
$z_i(x,y)$	It is the height value of the surface for the point (x, y) referred to the reference plane.

Introduction

The aim of this thesis is the study of the flow factor variation during the run-in process. Flow factors are particular coefficients used inside an average type of the Reynolds equation in order to take into account the surface roughness influence in the lubrication regimes. In fact, when the lubricant film is thin, the asperities of the surface influence the lubricant flow and its pressure, thus considering roughness effect is crucially important to better understand the complex behavior of tribosystems. Flow factors are computed by numerical flow simulation with the software *Tribo-x*. This software takes in input a matrix whose dimension is 300x300; after the microscope scanning, many more points are obtained. For instance, the optical microscope used can scan up to 10000x10000 data points for 1 mm^2 of surface at highest resolution. Therefore, a very small surface would be considered by taking a submatrix of 300x300 data points from the microscope scanned data and it would not characterize the roughness of the total surface. The idea to avoid this was to study the power spectral density of the surfaces in order to find a relevant distance between two measured data points. Once this distance is found, the input matrix of the software is built by taking each point at a distance equal to the relevant distance from the previous one. In this way, the surface area considered by the input matrix is bigger and it characterizes best the surface topography. The relevant distant is computed by choosing a correct cut-off value of the PSD: in fact, over a certain value the information is not important anymore. Anyway, finding the correct value is fundamental, otherwise some errors may occur: if the cut-off value is too big, the relevant distance will be small and will not characterize the surface topography; if it is too small, the relevant distance is large, and a lot of information gets lost. Three different methods to calculate the cut-off frequency are analyzed.

The thesis is organized in four chapters:

Chapter 1 shows the state of the art of tribology. It gives the most important information of this fascinating and complex phenomena. In the first part of this chapter surface topography, friction, wear and lubrication regimes are explained. After that, the run-in process is analyzed and at the end a detailed explanation of flow factor is carried out.

Chapter 2 presents how the cut-off problem has been managed and how the MATLAB code is built to provide the input matrix of the software from the 3D vector obtained by the microscope scan. Several issues are presented: the management of the missed points, the construction of a square matrix from the 3D vector scanned by the microscope and so on. Furthermore, the use of Gaussian filter is

implemented in order to reduce the noise from the data. This is very important because the noise could influence the PSD.

Chapter 3 presents the experimental test carried out and the parameter that had been changed and the reason why they were chosen. Then, it shows the results of the experimental test and their explanation. The variation of flow factor with different load, test duration and lubricant temperature is analyzed. Furthermore, the variation of surface topography and friction under the same parameter variation is performed.

At the end, the last chapter contains the conclusion and possible further works.

Chapter 1

State of the art

1.1 Introduction to Tribology

Tribology is a science defined in 1967 by a committee of the Organization for Economic Cooperation and Development, chaired by Dr. H. Peter Jost. Its purpose is the study of interacting surfaces in relative motion and includes the application of the principles of friction, lubrication, and wear. The word “tribology” derives from the Greek word “τριβος” (tribos), meaning “rubbing” and the suffix “logy” for “the knowledge of”, so the literal translation would be “the science of rubbing”.

However, the scientific study of tribology has been related to human invention since ancient history. A drawing, found in a grotto at El Bersheh (Egypt), was dated to about 1880 BD. It shows the inclusion of liquid while building pyramids to avoid friction. Furthermore, Leonardo da Vinci studied for almost 20 years the friction behavior and it is clear that he was fully familiar with the basic tribological concepts of friction. Although the two fundamental laws of friction were enunciated by Guillaume Amontons in 1699, the concepts attributed to him are paralleled in the detailed explanations in Leonardo da Vinci’s studies (1452–1519). The two previously mentioned laws are:

1. The force of friction is directly proportional to the applied load.
2. The force of friction is independent of the apparent area of contact.

In spite of these “laws of friction” are not always obeyed, they are commonly used because of their simplicity. Still, the well-informed engineer will learn to use these concepts with due caution because there are a number of cases in which these simple laws do not hold.

Surface interactions in a tribological interface are highly complex, and their understanding requires knowledge of various disciplines, including physics, lubrication, chemistry, solid mechanics, thermodynamics, fluid mechanics, machine design, applied mathematics, thermodynamics, heat transfer, materials science, rheology, performance, and reliability.

By definition, tribology is focused on friction, wear and lubricant. Friction is the phenomenon of motion opposition. According to classical mechanical approach, the friction coefficient usually takes on either one of two characteristic values: kinetic value or static value. The kinetic friction is defined as the force generated between two surfaces in the direction of motion. On the other hand, the static friction is defined as the necessary force to cause motion and the system force is lower than the friction one. In general, the friction force is described in terms of a coefficient of friction (μ):

$$\mu = \frac{F}{W} \quad (1.1)$$

where F is the friction force and W is the normal load acting between both surfaces. The coefficient is called either static (μ_s) or dynamic (μ_k) coefficient of friction, depending on the friction case.

Wear is the degradation of material surfaces. It is the major cause of material wastage and loss of mechanical performance. Friction is a principal cause of wear and energy dissipation and savings can be made by improved friction control. It is estimated that one-third of the world's energy resources in present use is needed to overcome friction in one form or another [1]. There are different kinds of wear: abrasive wear, adhesive wear, fatigue wear, impact wear, etc.

Lubrication is fundamental to control friction and wear. A thin layer of gas, liquid and solid is interposed between two surfaces in order to separate contact surfaces and to reduce damage. These layers are usually very thin, in the range from 1 to 100 μm , so it is usually difficult to observe. Liquid lubrication is the most used and sometimes additives may be added to improve some properties, for instance the viscosity, which is the most important one. There may be three different lubrication regimes: fluid film lubrication, boundary lubrication, and mixed lubrication. Each of them will be discussed in the following sections. The main aim of lubrication is reduced friction, wear and surface adhesion but, in some cases, lubrication could be useful to control the interface temperature in tribo-systems. Without lubrication, components can rub against each other causing heat and local welding: if it is not controlled, their failure will occur.

The purpose of this chapter is to realize an analysis of the state of the art of Tribology, in order to explain how this fascinating phenomenon works. The running-in phenomenon and the Flow Factor. will also be discussed [1][2][3][4][5].

1.2 Solid Surface Topography

The importance of a surface description, even in a fine-scale, is well demonstrated in tribology. The improper microlevel surface shape can cause the breakdown of lubrication layers, with the consequence of an increasing in friction and wear that causes energy lost and, in the worst cases, it

could cause the failure of the system. For this reason, surface accuracy and surface refinement requirements have significantly increased over time [2].

Solid surfaces contain deviation or irregularities compared to the prescribed geometrical form, whatever the method of formation is. Also the most precise machining method is not able to produce a molecularly flat surface. The surface consists of low and high spots, which are called “asperities”. These irregularities could be of various order, from shape deviations to irregularities of interatomic distance orders, even the smoothest one. In addition to surface irregularities, most solid surfaces are chemically reactive, with the exception of noble metals, and all of them are made up of several layers having different physic-chemical properties [3].

1.2.1 Geometric Characteristics of Solid Surfaces and Measurement Methods

According to Hamrock *et al.* [2], the geometric characteristics of surfaces, also known as texture, could be divided into three main categories, as shown in Figure 1.1:

- *Error of form*: errors in the manufacturing process leads to obtain a surface that deviates from a well-defined pattern.
- *Waviness*: unwanted vibration in machine tool systems always occurs during the processing so, relatively long waves in the surface profile can be created.
- *Roughness*: besides error form and waviness, some irregularities are typical in the cutting and polishing process during production.

However, it is difficult to outline a real distinction between these categories. Roughness is the parameter that is usually taken into account and it simply concerns the wavelength of the surface texture (horizontal spacing). But both the horizontal direction (or wavelength) and the vertical direction (or amplitude parameter) should be evaluated to characterize surfaces for tribological analysis. Furthermore, lay and flaws can occur. Lay is the predominant direction of the surface pattern [2][3].

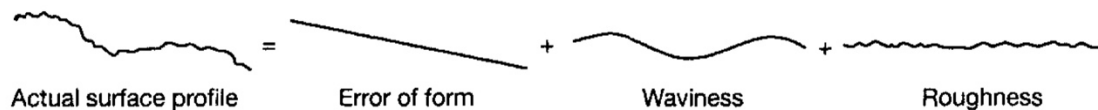


Figure 1.1: Geometric characteristics of solid surfaces [2].

In order to measuring surface finish, two general methods are commonly used:

- contacting method using stylus techniques;
- non-contacting method.

Chapter 3 of [2] includes all the microscope models which are usually used in surface characterization. Regarding contacting microscopes, stylus profilometry is the most common method of measuring surface roughness because it is very flexibility and low-cost. It uses a stylus with a tiny tip, which touches the surface and it transforms the vertical motion of the tip into an electrical analogue voltage. The stylus is normally made of diamond and its tip radius is usually 2 μm . This dimension is relatively large in comparison with the typical roughness and it can distort the surface profile, as shown in Figure 1.2. It can be seen that the peaks are broadened, and the valleys are narrowed due to stylus radius.

Thus, if the surface is very smooth, standard stylus profilometry will not characterize the surface features. In order to characterize very smooth surfaces, the atomic force microscope (AFM) can be used. There are different types of AFM microscopes but each one moves the cantilever or specimen in raster manner, recording the height distribution of the surface [2].

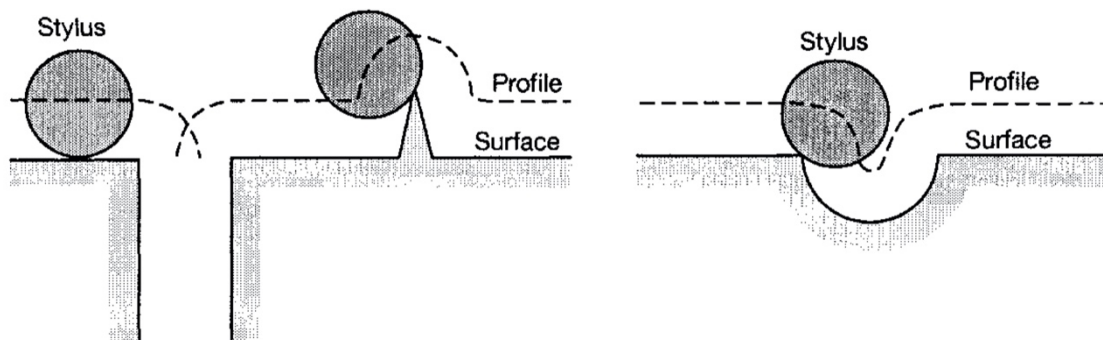


Figure 1.2: Error due to finite dimensions of stylus tip [2]

On the other hand, the noncontracting microscopes uses different principles (light, electron, air, etc.) to determine the characteristic of surface. There are different types of noncontracting microscopes (laser, optical, electron, etc.). In this thesis the optical microscope is used to characterize the sample surface after the tests. The model is ‘*Alicona Infinite Focus G4*’ and its technical specifications can be seen in Table 1.1.

Objective Magnification	-	2,5x	5x	10x	20x	50x	100x
Working distance	mm	8.8	23.5	17.5	19	11	4.5
Lateral measurement range (X,Y)	mm	5.63	2.82	1.62	0.81	0.32	0.16
(X x Y)	mm ²	31.7	7.85	2.62	0.66	0.01	0.03
Vertical resolution	nm	2300	410	100	50	20	10
Height step accuracy (1 mm)	%	n.a.	0.05	0.05	0.05	0.05	0.05
Max. measurable area	mm ²	10000	10000	10000	10000	3965	990
Optional	mm ²	40000	40000	40000	24780	3965	990
Min. measurable roughness (Ra)	μm	7	1.2	0.3	0.15	0.06	0.03
Min. measurable roughness (Sa)	μm	3.5	0.6	0.15	0.075	0.03	0.015
Min. measurable radius	μm	20	10	5	3	2	1

Table 1.1: 'Alicona Infinite Focus G4' Technical Specifications.

1.2.2 Analysis of Surface Roughness

In order to compute the surface analysis after the microscope scan and find the parameter that define the surface texture, some defined reference lines need to be found. There could be several methods to calculate the reference line, Figure 1.3 shows the three most used methods. With the mean method, the mean line is selected as the centroid of the profile; with the ten-point average methods the five highest peaks and the five lowest valleys are found and the average of these 10 points gives the reference line. At the end, the last squares method identifies the line which minimizes the square errors between the surface points and the reference line. This reference line is usually sloped so it can be used to compensate for the linear error of form [2]. The reference line can be measured either along the single profile section (2D) or along all the surface area (3D). In the second case, a reference plane is found instead of a line. In this thesis, a reference plane using the mean method is found. In this way, the average of height values $z_i(x, y)$ is zero.

Let $z_i, i = 1, 2, \dots, N$ be the height values of the surface referred to the reference plane and N the total number of the scanned points, several surface parameters can be found. The most common average roughness parameters are [2]:

- Arithmetic average, called R_a :

$$R_a = \frac{1}{N} \sum_{i=1}^N |z_i| \quad (1.2)$$

- Root mean square (rms), denoted by R_q :

$$R_q = \sqrt{\frac{1}{N} \sum_{i=1}^N z_i^2} \quad (1.3)$$

- Maximum peak-to-valley height distribution, denoted by R_t :

$$R_t = \max(z) - \min(z) \quad (1.4)$$

Other height parameters, less commonly used, are skewness (Sk), kurtosis (K), maximum peak height (R_p), maximum valley depth (R_v), etc. All of them are clearly presented in chapter 2 of [4].

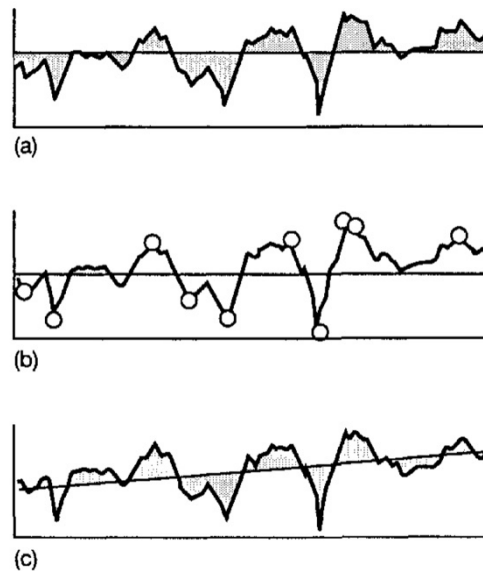


Figure 1.3: Comparison of three types of reference line: (a) mean; (b) ten-point average; (c) least squares [2].

The Abbot curve, also known as ‘bearing length curve’, is an important function and it is often used to characterize the height of the surface. This curve is the cumulative curve of the height distribution, which is a histogram of the surface height. It evaluates the percentage of points on the surface that lie at a given height. The Abbot curve includes the height value from the highest point on the surface, where the curve is equal to 0% (since there is no material above), to the lowest point, where the value is 100% [4], Figure 1.4 shows an example of Abbot curve.

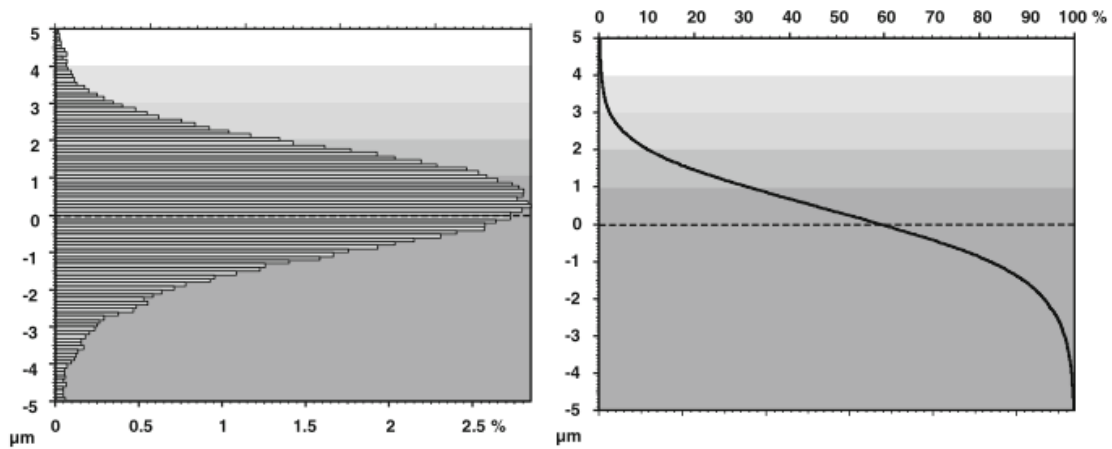


Figure 1.4: The height distribution (left) and the Abbott curve (right) [4].

All the parameters previously described depend only on the profile heights. They do not take into account the spacing between heights. There are some functions that can incorporate the spacing between height, for instance the autocorrelation function and the power spectral density. These functions are more complicated than the previous parameter, but they contain much more information. In this thesis the power spectral density function is used. The reason why it has chosen, and its meaning are presented in §2.3.

1.2.3 Contact between solid

When two surfaces are placed in contact, the real contact area is smaller than the apparent one because of the roughness of the surfaces. In fact, the contact occurs only in the highest asperities of either surface. Figure 1.5 gives a graphic view of this behavior. Let A_i be the area of the i -th contact between asperities, according to Figure 1.5, so the true area of the contact, A_r , will be:

$$A_r = \sum_{i=1}^n A_i \quad (1.5)$$

where n is the number of asperities [1]. Thus, local high pressure can occur in correspondence of the asperities as shown in Figure 1.6. These peaks of pressure cause a local deformation of the surface, which can be either elastic or plastic, depending on the load applied and on the material hardness. The relationship between the true area of contact and the load has been extensively studied and several models were created because it is critically important since it affects the laws of friction and wear. The most common is the Hertz theory, which considers the single asperity contact as a problem of

deformation of two elastic solids with geometries defined by quadratic surfaces. This theory and some other approaches are analyzed in §3.2 of [3]. Furthermore, other models are presented in §10.3 of [1].

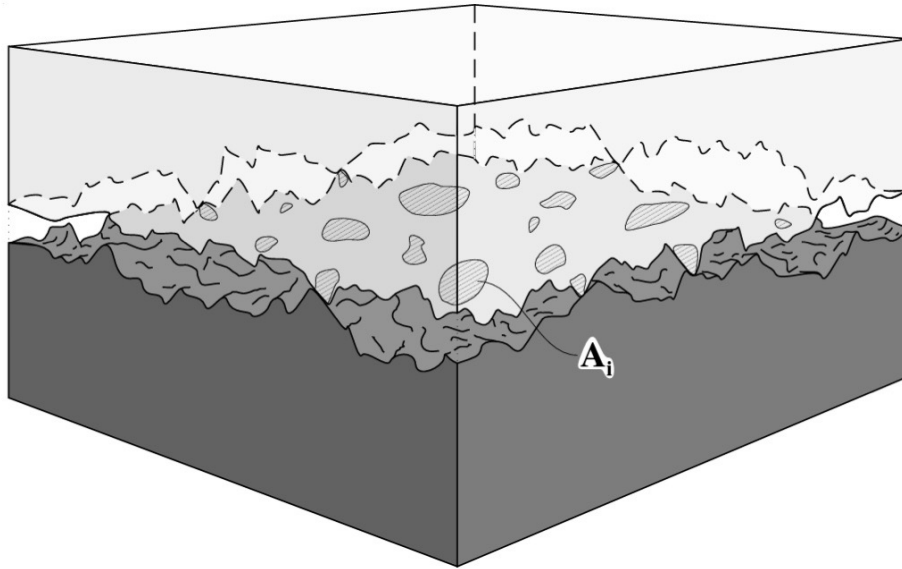


Figure 1.5: Real contact area of rough surfaces in contact [1].

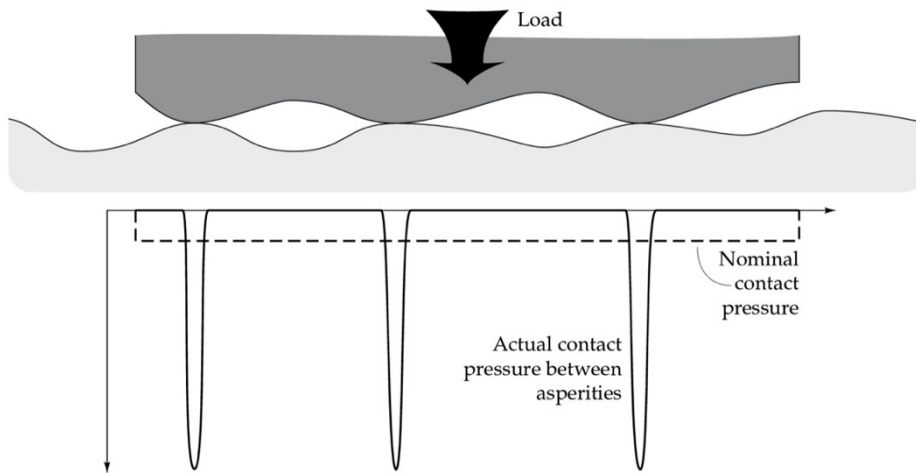


Figure 1.6: Contact stresses between the asperities [1].

1.2.4 Adhesion

When two solid surfaces are put in contact under a normal force, adhesion between the asperities can occur. In order to separate the two solids, a tensile normal force, called adhesive force, is required, Figure 1.7. A coefficient, known as coefficient of adhesion μ' , is often defined as the ratio of the

normal tensile force W' required for separation to the normal compressive force W initially applied [3],

$$\mu' = \frac{W'}{W}. \quad (1.6)$$

Adhesion can occur both in solid-solid contact and lubricated contact. Of course, if the surfaces are without any films of lubricant, the adhesion and bounding is usually stronger. It is a complex phenomenon that involves different variables, like chemical interaction between surfaces and environment, normal load, duration of contact, temperature, roughness, etc. For instance, the presence of oxide on a surface generally decreases the adhesion. Again, the temperature reduces the ductility of the material, expanding the real contact area and thus the adhesion becomes stronger. Furthermore, the diffusions across the interface increases significantly with high temperature, which results in stronger adhesion [3]. In §4.2 of [3] various surface interactions which may cause adhesion are clearly discussed.

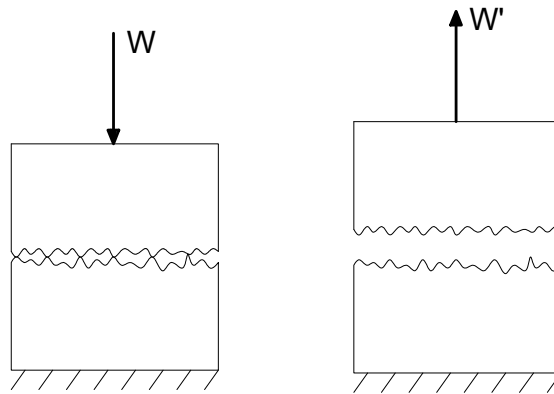


Figure 1.7: Schematic illustration of adhesive force to detach two surfaces put in contact. W is the load applied to bring them into contact and W' is the tensile force needed to separate them (adhesive force).

1.3 Friction and Wear

1.3.1 Friction

Friction is the resistance to relative motion between two surfaces in contact. Friction force is the resistive tangential force which is generated between two solid bodies in contact and whose direction is opposite to the direction of motion, Figure 1.8. There are two conventional rules which are generally

respected in most of the engineering applications. The first rule affirms that the friction force, F , is directly proportional to the nominal load, W :

$$F = \mu W \quad (1.7)$$

where μ is defined as the coefficient of friction and it can assume two values: static, μ_s , or kinetic, μ_k , according to the type of system. In fact, if two solid bodies have no relative motion, the static friction force, F_s , is defined as the tangential force required to initiate motion and the coefficient of static friction, μ_s is used. On the other hand, when two solid bodies are sliding against each other, the kinetic (or dynamic) friction force, F_k , is defined as the tangential force required to maintain the relative motion and the coefficient of kinetic friction, μ_k , is used, Figure 1.9. The static friction force, and thus the coefficient of static friction, is either higher than, or equal to, the kinetic friction force and to the coefficient of kinetic friction.

There is an alternative way to express the coefficient of static friction in terms of friction angle θ , which is sometimes more convenient. It is defined by:

$$\mu_s = \frac{F_s}{W \cos(\theta)} = \tan(\theta) \quad (1.8)$$

where F_s is the static friction force, W is the load and θ is the limit angle of an inclined plane from the horizontal, such that any body of any weight placed on that plane with an inclination either inferior or equal to θ will remain stationary. But, if the value of the angle is greater than θ , the body will start to slide down, Figure 1.10.

The second rule affirms that the friction force is independent of the apparent area of contact between the surfaces in contact. So, if two bodies are brought into contact, they will have the same coefficient of friction regardless of their size. It is important to notice that friction is referred to a system and it is not a material propriety

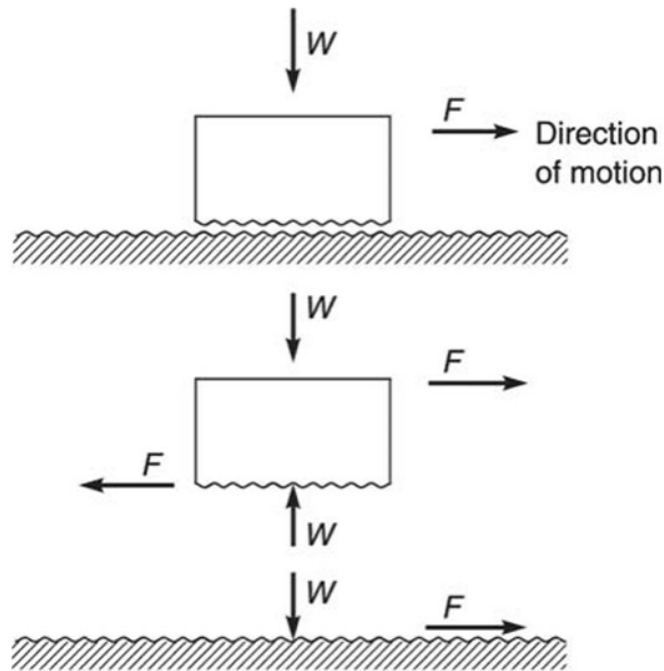


Figure 1.8: Schematic illustration of friction force. On the top there is a body sliding on a surface, on the bottom its relative free body diagram [3].

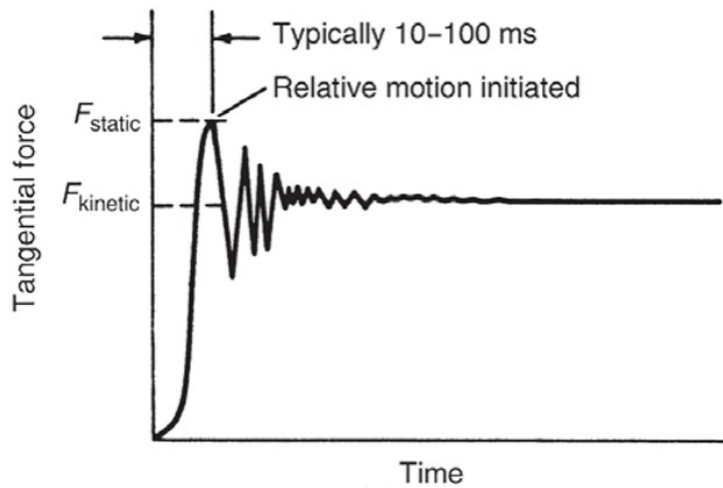


Figure 1.9: Static friction force, F_{static} and kinetic friction force, F_k as a function of time [3].

Friction is the cause of energy loss and wear of all mechanical elements which have relative motion against other elements. Anyway, it is not always an undesired phenomenon: without friction it would be impossible to grab objects, walk or drive a car (tires transfer motion thanks to friction). Moreover, many mechanical devices use friction to carry out their function, for instance car brakes or belt drive [3].

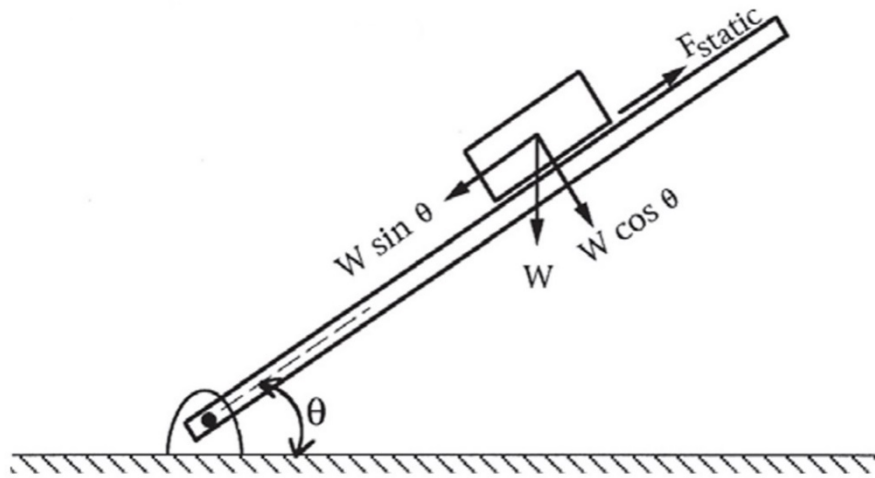


Figure 1.10: Force equilibrium for a body on an inclined plane [3].

In engineering application there are two main types of friction, dry friction and fluid friction. In the first one, two dry surfaces are brought in contact without interposing anything between them. The fluid friction occurs when fluids are inserted between the two surfaces, in this case the friction will be lower.

Friction depends on several parameters, as temperature, nominal pressure, humidity, sliding condition, materials, etc. So, the only coefficient of friction μ is not able to fully characterize this complex phenomenon. It is strictly constant only for a given pair of materials under a given set of operating conditions, in the other cases it could change. Thus, it should be useful to know that the result may not be correct [3].

1.3.1.1 Static Friction

Historically, static friction has been related to adhesion and the breaking of bonds between atoms on the opposing surfaces, but these are not the only causes of static friction. In fact, when two surfaces are brought in contact, some of the asperities may fill the pits due to the presence of valleys on the surface. Thus, a strong mechanical joint is built, and this is not caused by adhesions, Figure 1.11. So, sometimes surfaces may adhere, but adherence has not the same meaning as adhesion because it does not involve molecular bonding. The repulsive force, seen at the bottom of Figure 1.11, must be also overcome in order to exceed static friction and move the bodies. This can happen either by asperities climbing over one another or by deforming one another.

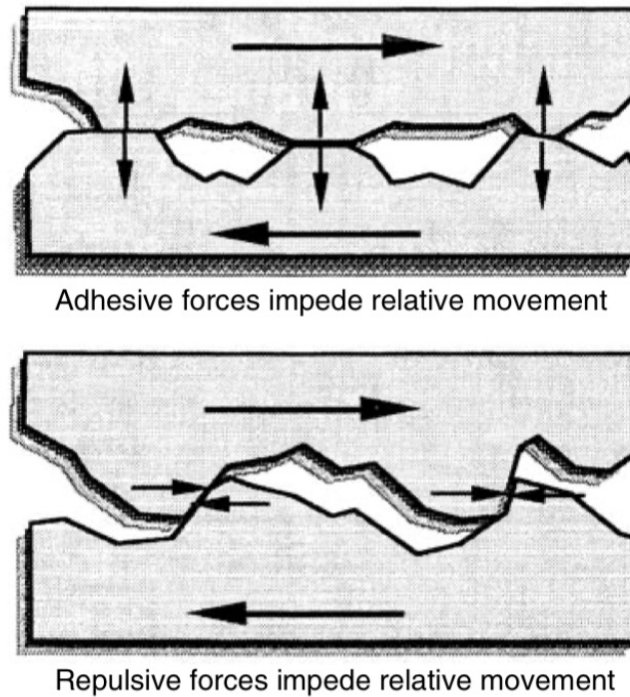


Figure 1.11: Two apparently contradictory aspects for the mechanism of static friction. On the top, the adhesive force act at the tip of the asperities in contact and keep the two surfaces together, resisting relative motion. At the bottom, horizontal components of repulsive force originated by the interaction between interpenetrating asperities resist relative motion [5].

Static friction force is directly proportional to the normal load W . The coefficient of proportionality is the coefficient of static friction, μ_s :

$$F_s = \mu_s W \quad (1.9)$$

The coefficient of static friction is measured under certain conditions of temperature, load, time, environment conditions, etc. Anyway, this coefficient will be different if these conditions change. For instance, if there is a contaminated environment, and so there is the presence of adsorbed gases, the value μ_s will be lower than the one occurring with well-cleaned surfaces and no reactive gases. Furthermore, it is studied that the coefficient of static friction is affected by the length of time contact between the two bodies. There can be two different possibilities:

- the contact becomes contaminated with species which have lower shear strength and so the friction declines;
- the contact is clean and the interfacial bond becomes stronger. In this case, the friction will tend to grow.

The first case is observed in freshly cleaved rock salt, Figure 1.12, for metals the opposite behavior is typically observed instead, Figure 1.13.

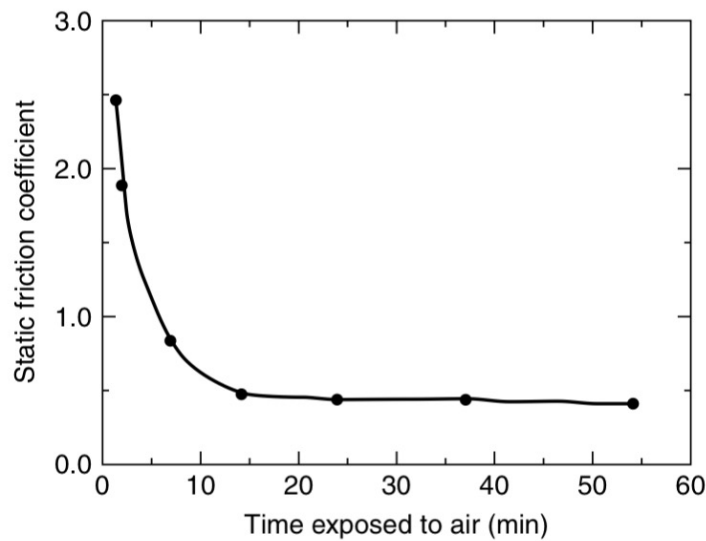


Figure 1.12: Effect of time exposure to air on static friction coefficient of cleaved salt surfaces [5].

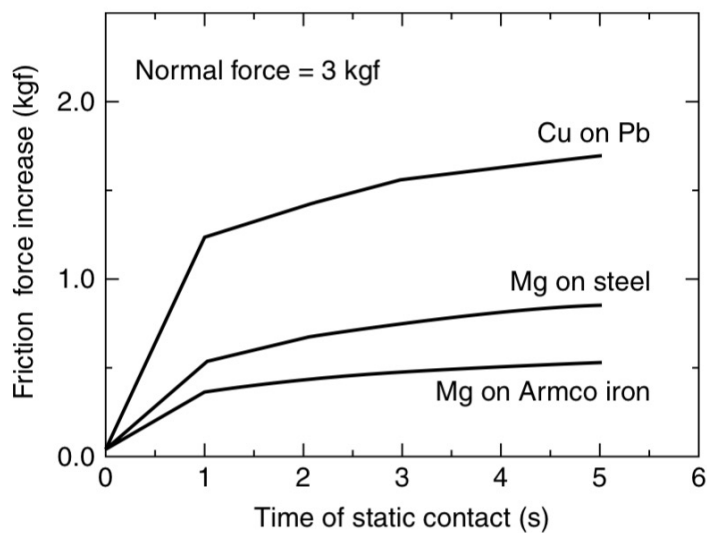


Figure 1.13: Effect of time on the static friction force between metals [5].

When two metal surfaces are brought in contact and pressed together, some interaction between the atoms on their surfaces occurs. The quantity of interactions and their strength will depend on several parameters: temperature, contact pressure and the degree of chemical reactivity that the species have for each other: for this reason, the value of static friction changes with the duration of contact. This phenomenon is very important in all those mechanisms which are supposed to have long periods of inactivity: when restarted, they will be able to overcome starting friction.

The most effective strategy to reduce the static friction is to interpose lubricant between the contact bodies or coating the surface with treatment to avoid the formation of adhesive bonds [5].

1.3.1.2 *Sliding friction*

When the tangential force is greater than static friction force, the sliding between the two body will start. After that moment the tangential force resisting the movement of one surface over another one is the kinetic friction force, F_k , which can be either lower than or equal to the static one. Its formula is:

$$F_k = \mu_k W \quad (1.10)$$

where μ_k is the kinetic friction coefficient and W is the normal load. The transition from static contact to sliding contact can be qualitative describe by studying the asperity interactions of a hard material indenting with a softer one, Figure 1.14. Initially, the tangential force is low, so the hard asperity is supported on both sides. When increasing the force until the critical value, the flank where the force is acting becomes unloaded and the asperity sinks into the softer material. In this way the increasing of contact area, due to the extra depth, causes the maximum in tangential force that opposes to motion. Once the asperity begins to move, the soft material gets deformed and provides sufficient support for the asperity to rise above the level of static contact, the tangential force declines [1].

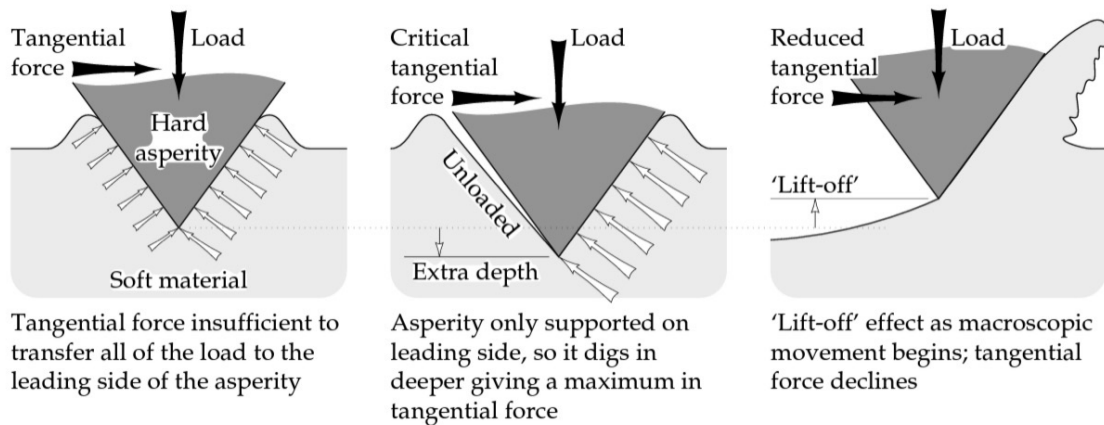


Figure 1.14: Schematic illustration of the transition from static contact to sliding contact for a hard asperity on a soft surface [1].

Sliding friction is a complex phenomenon that involves several physical mechanisms. In literature a lot of different models are presented which try to describe it but none of them is capable of accounting for all possible variables. Anyway, for each contact condition at least one of them predict quite correctly the friction process¹. A schematic illustration of the main mechanisms involved in

¹ A set of interfacial mechanisms that, when acting together in an interface, produces a characteristics resistance to sliding [5].

different contact condition is shown in Figure 1.15. In lubricated contact, a thick film of lubricant separates the two bodies, so the wear is negligible. In this case, the friction force is a result of viscosity shearing within the lubricant and the regime of the lubricant affects both the value of the kinetic friction coefficient and the friction force. In §1.4 all the lubricant regimes are clearly explained. On the other hand, in unlubricated or boundary lubricated contacts, the surfaces are not separated anymore and the asperities of one body come into contact between the asperities of the opposing body or between the surfaces wear debris or hard contaminants. Surface adhesion, elastic and plastic deformation can occur between asperities. In presence of plastic deformation two different behaviors may take place: ploughing (pushing material up and aside) and wedge formation (driving a wave of plasticity deformed material across the surface). In boundary lubricated contact a very thin film of lubricant prevents surface adhesion, so only elastic and plastic deformation occur. When the surfaces are unlubricated and no superficial contaminant layers are present (e.g., oxides), adhesions between the opposing asperities may occur, in addition to plastic and elastic deformations [1].

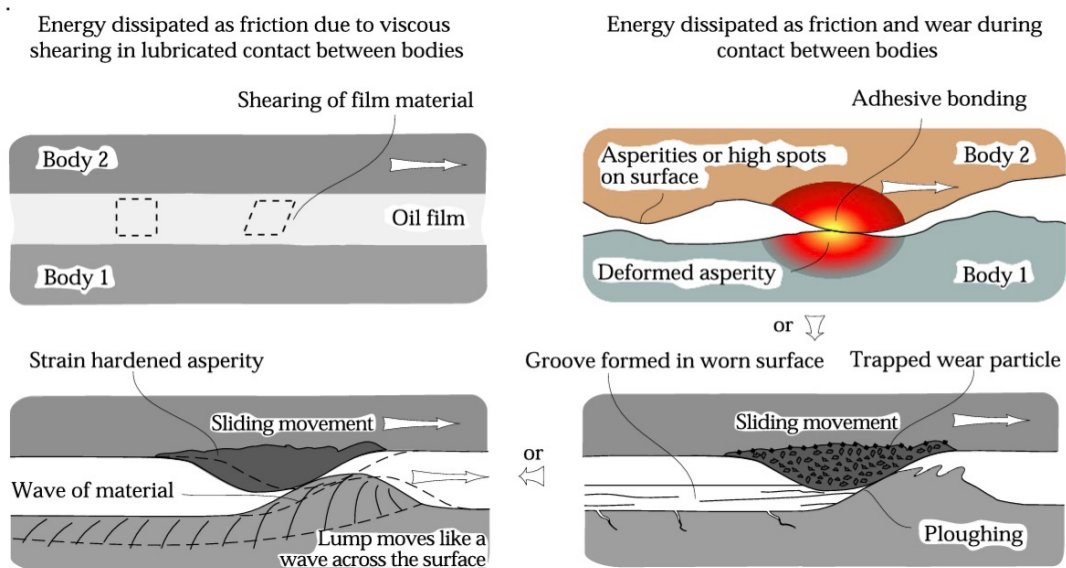


Figure 1.15: Schematic illustration of mechanisms of sliding frictional energy dissipation [1].

1.3.2 Wear

Wear is defined as the progressive damage or removal of material from a body surface during relative motion with another solid. In most cases, wear occurs due to surfaces asperities interaction. The first step of wear is usually a displacement of material on the contacting surface, with consequent alteration of the properties of the body near the surface, but little or no material is actually lost. After that, material may start to detach and may either break loose as a wear particle or transfer to the mating

surface. Erroneously, wear is considered as the loss of material but also the damage due to material displacement of a body is considered wear, even if no net change in weight or volume occurs.

It is important to know that wear is a system response and not a material propriety. By changing the operating conditions, wear will change. Wear, analogously to friction, can have either good or bad effect. For instance, wear is essential for writing with a pencil, polishing, machining, etc. On the other hand, it is an undesired phenomenon in almost all mechanical devices that are supposed to transfer any kind of motion (gear, bearing, seals, etc.). Wear involves several phenomena both mechanical and chemical, they can be divided in six principal types: adhesive, abrasive, fatigue, impact of erosion and percussion, corrosive, electrical-arc-induced wear [3]. Anyway, the most common ones are adhesive and abrasive wear. Since these two kinds of wear are the most frequently involved, they will be analyzed in the following section.

1.3.2.1 Adhesive Wear

Adhesion or bounding across the interface of two solid surfaces brought into contact can also occur during sliding contact. These adhesions are sheared by sliding and this may result in a detachment of material from one or both surfaces. Then, this material can either stick to the other surface or break loose as wear particle. According to the early theory of sliding wear, shearing can occur at the original surface or in the weakest region in one of the two bodies, Figure 1.16. In the first case, no wear occurs, and this happens when the strength of the interfacial adhesion is smaller compared to the breaking strength of neighboring local regions, Figure 1.16 (1). In the other case, a small fraction of material in one of the two bodies breaks and a small fragment, the shaded part in Figure 1.16, may become attached to the other surface due to adhesion, Figure 1.16 (2). Additional sliding may cause other fragments to remain adherent to a surface, transfer to the mating surface or become attached to another fragment (previously attached), with the consequence that a larger agglomerate may become detached as a large loose wear particle. The adherence of fragments has a strong bond between them and the surface they are attached to, this may avoid the formation of loose particle. However, some chemical changes occur to the fragments during sliding (like oxidation that decreases the adhesive strength) and the adhesion force may be reduced, breaking off the fragments.

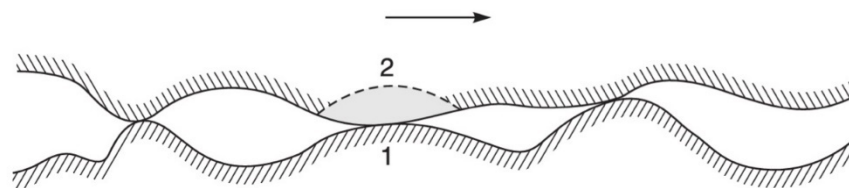


Figure 1.16: Schematic illustration of two break possibilities: at the interface (1) or at the weakest region of one body (2) [3].

There is an equation, based on experimental data of various unlubricated materials (mostly metals), that describes the adhesion wear. In fact, the volume of wear that is detached can be expressed as:

$$v = \frac{k W x}{H} \quad (1.11)$$

where k is the nondimensional wear coefficient and depends on the materials in contact and their cleanliness; W is the applied load; x is the sliding distance and H is the hardness of the surface being worn away. So, the amount of wear is generally proportional to the applied load and the sliding distance and inversely proportional to the hardness of the surface where the fragment is removed. Of course, there are other models for describing adhesive wear, but analyzing all of them is not the focus of this thesis[3].

1.3.2.2 Abrasive Wear

Abrasive wear occurs by plastic deformation or fracture of the softer surface when a harder one or harder particles slide on it. For metals and alloys, which are ductile materials with high fracture toughness, the hard asperities or hard particles cause the plastic flow of the softer material. In Figure 1.17, two general situations which can occur during abrasive wear are shown. In the first case, only the two rubbing surfaces are involved in the wearing. The hard asperities of one body or some abrasive grits mounted on the top surface result in damaging and wearing of the softer material, Figure 1.17(a). On the other case, three bodies are involved, and the wearing is caused by a small particle of abrasive caught between the two rubbing surfaces. Of course, this particle must be sufficiently harder to cause the wear and it can abrade either one or both the mating surfaces, depending on the hardness of the two materials. It is common that the wear mechanism starts as adhesive, then wear particles is created and gets trapped between the two interfaces resulting in abrasive wear. Usually, the visual result of this wear mechanism is a series of grooves parallel to the direction of sliding, which is usually called plowing. An example of this kind of scratching can be observed in Figure 1.18 [3].

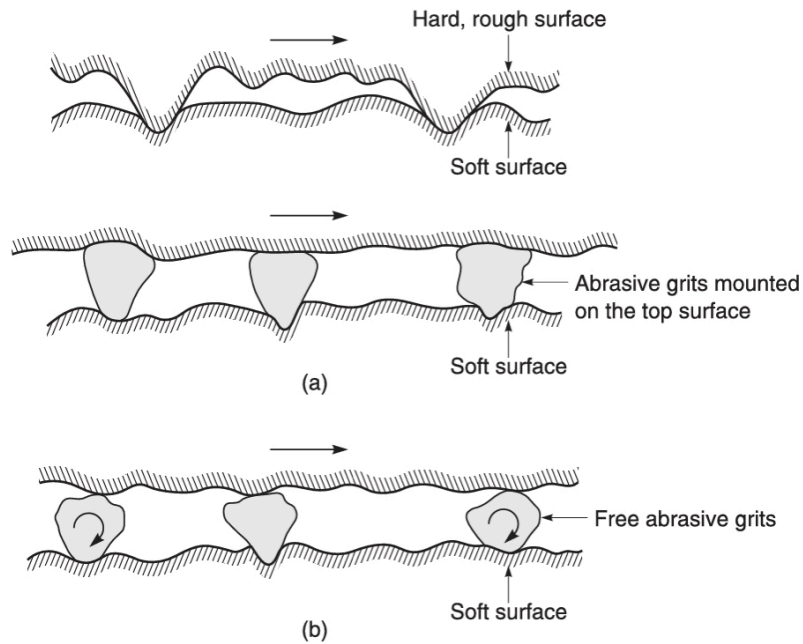


Figure 1.17: Schematics of (a) a rough, hard surface or a surface mounted with abrasive grits sliding on a softer surface, and (b) free abrasive grits caught between the surface with at least one of the surfaces softer than the abrasive grits [3].

Different deformation model can be involved during the material removal from a surface by abrasion. The three most common ones are shown in Figure 1.19: plowing, wedge formation and cutting. In plowing process, Figure 1.19(a), a series of grooves are created as a result of the plastic flow of the softer material. There is usually no loss of material because it is displaced from a groove to the sides, even if some fatigue mechanisms can occur and some material can be removed after several plowing process. Furthermore, this type of process may also cause subsurface plastic deformation, which may contribute to the nucleation of surface and subsurface cracks. If the material is very soft, for instance lead or indium, the amount of wear debris will be very small due to the deformed material which will be displaced along the sides of the groove. The wedge formation process, Figure 1.19(b), is quite similar to the plowing one because the tip of the hard material plows a groove, but with the difference that a wedge is developed on the front of the groove. So, some of the deformed material is displaced to the side instead, the remainder form a wedge. In the end, the cutting form of abrasive wear is a mechanism similar to the metal cutting operation. The hard material tip has a large attack angle and plows a groove removing the material in the form of shavings or discontinuous debris particles, Figure 1.19(c). This kind of process results in significant removal of material and very little material displacement [3].

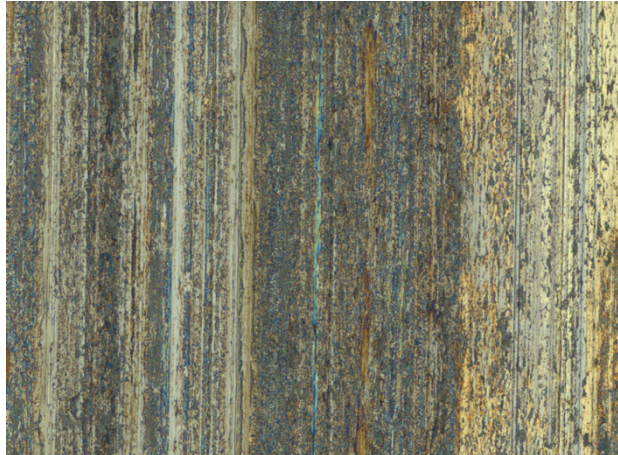


Figure 1.18: Optical microscope picture of a surface after the test. The sliding direction was along the vertical axis and it can be noticed that the scratches caused by abrasive wear are all parallel to the sliding direction.

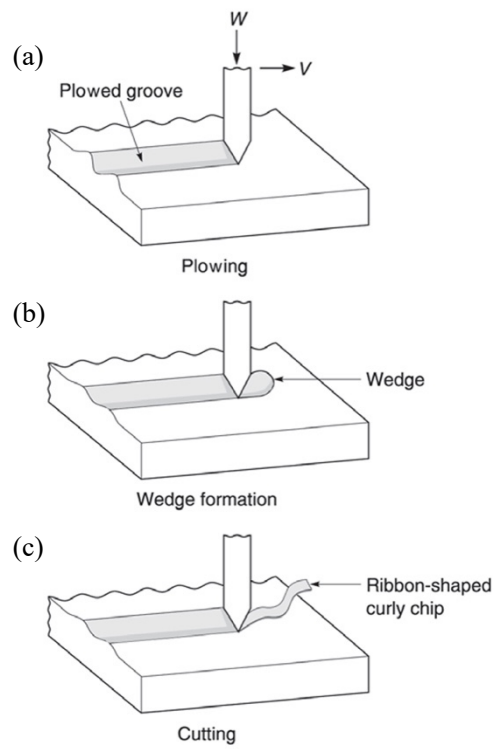


Figure 1.19: Schematics of abrasive wear processes as a result of plastic deformation by three deformation models [3].

1.4 Fluid Film Lubrication

Lubrication is one of the three main phenomena of Tribology science. The main purpose of lubrication is to avoid the direct contact between two mating surfaces during their relative motion. In absence of lubricant wear and friction could be too high and failures may occur. There can be both solid and liquid lubricant, the liquid ones, which are the most common, are analyzed in this thesis. The liquid lubricant creates a film which is able to separate the mating surfaces and reduce wear and friction. The thickness of the lubricant film depends on several variables and determines the regimes of lubricant. This aspect will be analyzed in the following sections. Furthermore, lubricants are also used to limit the interface temperature and to remove the wear particles created during the relative motion. The lubricant characteristics may be improved by adding some additives, which can modify either some physic proprieties (e.g., improving the viscosity variation with temperature) or some chemical proprieties (e.g., inhibitors of oxidation). There are many types of additive which may be added: based on the propriety to be modified there will be a specific additive which is optimal to that kind of situation. Anyway, including an overview of all the additives available on the market is not the focus of this thesis. A lot of books regarding this topic can be found in literature.

There are two main types of fluid film: in the first one, the fluid goes in the meatus between the mating surfaces and creates sufficient pressure to separate them. This method is based on fluid mechanics and depends on several liquid's proprieties, the most important one is viscosity. In this kind of lubrication, the two surfaces are completely separated, so wear and friction are usually very low. This type of lubrication is typical of fluid regimes like hydrodynamic, elasto-hydrodynamic or mixed lubrication, even if in the last one some contacts between the two surfaces could occur. Another type of lubrication is when the lubricant adheres to the surface forming a very thin layer which is able to support the load. The lubricant adheres to the surfaces due to either chemical reaction of the species within the liquid with the surfaces or to absorption of fluid molecules in the surfaces. This phenomenon is typical of boundary lubrication and usually viscosity does not affect wear and friction behavior.

Liquid lubricants have several characteristics, as density, vapor pressure, bulk modulus, etc. Anyway, the most important one is viscosity. This propriety plays an important role in fluid lubrication due to the thickness of the oil film, which is usually proportional to it. Thus, it is important to understand its meaning and what it depends on. For this reason, viscosity is discussed in the next section. However, the lubricant pressure, which separates the two mating surfaces, can also be provided by an external pump. This kind of lubrication regime is called hydrostatic and a thick film of lubricant is also maintained when there is little or no relative motion.

1.4.1 Viscosity

As mentioned above, viscosity plays an important role in fluid lubrication because the thickness of the fluid film is usually proportional to it. In literature, viscosity is expressed as either dynamic viscosity or kinematic viscosity. “The dynamic (or absolute) viscosity is the ratio of the share stress causing a flow to the resultant velocity gradient” [5]. It can be better understood looking at Figure 1.20, where two flat surfaces separated by a film, whose thickness is h , are presented.

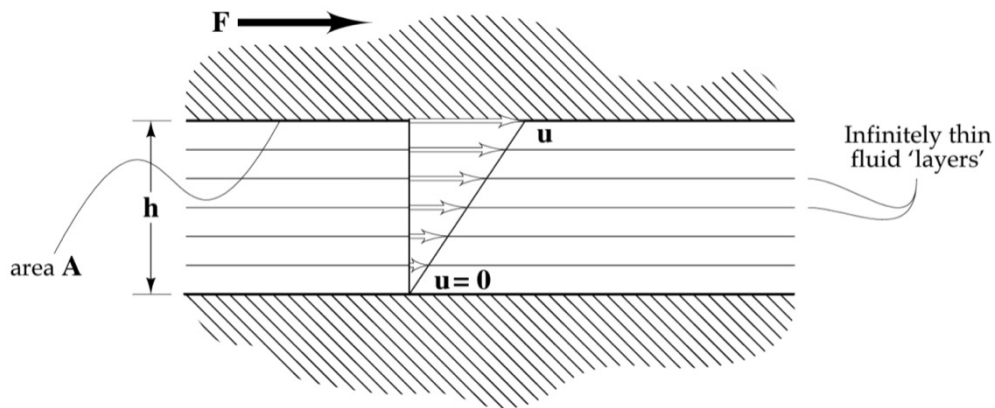


Figure 1.20: Schematic representation of the fluid separating the two surfaces [1].

The shear stress can be expressed as:

$$\tau = \frac{F}{A} \quad (1.12)$$

where F is the force required to move the upper surface and A is the area of the top surface wetted by the lubricant, Figure 1.20. In case of Newtonian fluids, the shear stress, τ , is proportional to the velocity gradient, u/h , and the proportionality coefficient is exactly the dynamic viscosity, η :

$$\tau = \eta \frac{u}{h} \quad (1.13)$$

The SI unit for dynamic viscosity is $Pa \cdot s$ (Pascal-second), however, the centipoise, cP , is also commonly used [1].

The kinematic viscosity is defined as the ratio of dynamic viscosity to fluid density:

$$\nu = \frac{\eta}{\rho} \quad (1.14)$$

where ν is the kinematic viscosity, η is the dynamic viscosity and ρ is the fluid density. The SI unit for kinematic viscosity is m^2/s , however the Stoke, S , is also commonly used [1].

Viscosity strongly depends on temperature, in particular with the increasing of temperature the viscosity decreases quite rapidly and, with it, the thickness of lubricant film. However, having a high viscosity is not always what it is wanted, in fact, more viscous oils do not only mean a thicker film and a better separation of the mating surfaces (which are positive effects) but it also means more power required due to shear stress. So, if the viscosity is too large, the power losses will be high, and heat will be generated. In this way, the temperature of the interface increases and may lead to the failure of the component. For this reason, it is important to know the viscosity of the different lubricants at the operating temperature in order to choose the best lubricant for the system, which minimizes friction and wear. There are several viscosity-temperature equations in literature, the most common ones are presented in §2.3 of [1]. They are both purely empirical and derived from theoretical models. Anyway, the most accurate of them is the Vogel equation, (1.15), which is very useful in engineering calculation. Furthermore, it is also used in numerical analysis. The variation of viscosity for several oils is presented in Figure 1.21 [1].

$$\eta = a e^{\frac{b}{T-c}} \quad (1.15)$$

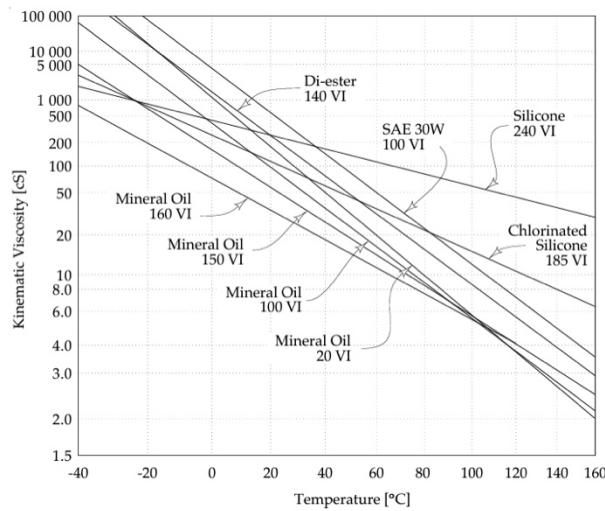


Figure 1.21: Viscosity-temperature characteristics of selected oils [1].

In addition to temperature, viscosity is also affected by the pressure which the lubricant is subjected to. In particular, oil viscosity increases with pressure and this effect becomes particularly important in the lubrication of heavily loaded concentrated contacts (e.g., gears) [1]. The most commonly used

equation to calculate the lubricant viscosity at pressures closed to atmospheric is the Barus' equation, (1.16). If pressure is below 0.5 GPa, this model works quite well, while if pressure is higher large error may occur [1].

$$\eta = \eta_0 e^{\alpha p} \quad (1.16)$$

where:

- η is the viscosity at pressure p , $Pa \cdot s$;
- η_0 is the atmospheric viscosity, $Pa \cdot s$;
- α is a coefficient typical of the lubricant, m^2/N ;
- p is the operating pressure, Pa .

In conclusion, viscosity is a very important lubricant propriety and choosing a correct value is essential in order to reduce wear and friction. In fact, the regime of lubrication is strongly influenced by viscosity.

1.4.2 Stribeck Curve

In case of lubrication without an external pumping agent, the different lubrication regimes can be observed in the Stribeck curve. This curve shows the dependence of the coefficient of friction in relation to the coefficient:

$$\frac{\text{Velocity} \times \text{Viscosity}}{\text{Pressure}} \quad (1.17)$$

A typical example of Stribeck curve is shown in Figure 1.22. In particular, at high pressure or with low speed and viscosity the lubrication film is thin, and surfaces may come into contact each other. This happen in clean surface or boundary lubrication, where the film between the two surfaces is extremally thin or absent so the surface asperities interact, involving plastic and elastic deformation and adhesive bounding. Therefore, high wear and friction occurs. On the other hand, by increasing lubricant viscosity and velocity or decreasing pressure, the lubrication film increases, and the surfaces come apart. Furthermore, the friction coefficient decreases. In full lubrication regimes, as elasto-hydrodynamic or hydrodynamic, the surfaces are completely separated so wear is negligible. The friction force is due to lubrication regimes and in particular because of viscous drag, this is also the reason why the friction force slightly increases with velocity. Mixed lubrication is a combination of boundary lubrication with hydrodynamic or elasto-hydrodynamic lubrication. A thin film of lubricant is present but sometimes it can break, and surface contacts may occur.

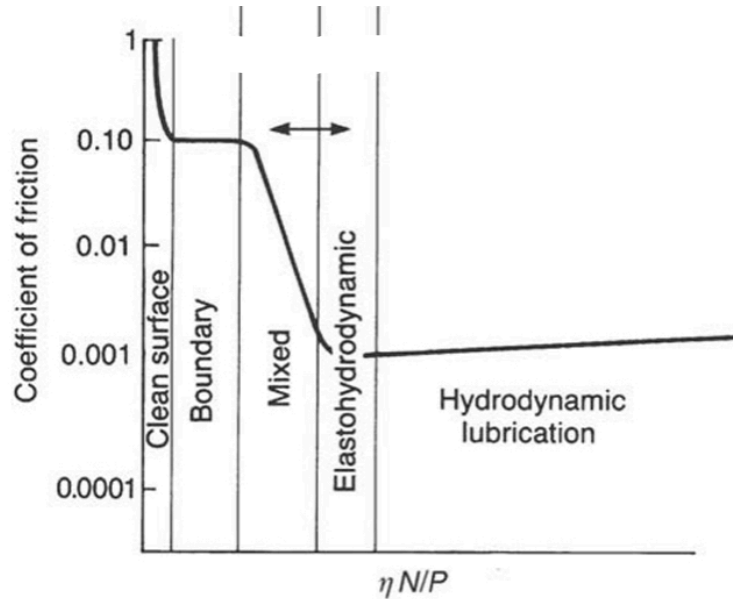


Figure 1.22: Stribeck curve and different lubrication regimes [3].

Specific thickness or *lambda ratio* Λ is a useful parameter to identify various lubrication regimes. It is defined as “the ratio of the minimum film thickness in the interface, h , to the composite root-mean square surface roughness” [5]:

$$\Lambda = \frac{h}{\sqrt{\sigma_1^2 + \sigma_2^2}} \quad (1.18)$$

where:

- h is the minimum film thickness in the interface;
- σ_1 is the root-mean-square roughness of surface 1;
- σ_2 is the root-mean-square roughness of surface 2.

Each lubrication regime has a typical value of the *lambda ratio*, Blau in [5] reports that: for boundary regimes usually $\Lambda \ll 1$, for the mixed regime $1 < \Lambda < 3$, for hydrodynamic regime $\Lambda \gg 6$ and for the elastohydrodynamic regime $3 < \Lambda < 10$.

Now, all the fluid lubrication regimes are presented in more detail.

1.4.2.1 Hydrodynamic Lubrication

Hydrodynamic lubricant, commonly referred to as HD, is a regime where the two surfaces are completely separated, and a thick film of lubricant is included between them. Two main conditions are necessary for the occurrence of this kind of lubrication:

- Relative motion between the two surfaces must occur and the velocity must be sufficient to allow the lubricant to provide a load-carrying capacity.
- Surfaces must be inclined at some angle to each other, otherwise the pressure field supporting the required load is not generated [1].

A schematic illustration on how the HD pressure is created between two non-parallel surfaces moving relatively to each other is shown in Figure 1.23. The bottom surface moves with a certain velocity and drag the lubricant along it into the meatus between the two surfaces. Since the upper surface is inclined, the exit flow would be lower than the entry flow (the cross section of the exit is smaller than the enter one) so a pressure field is generated in order to reduce the entry flow and increases the exit flow, as it can be seen in Figure 1.23. In fact, at the beginning of the wedge the pressure increases, and the fluid velocity decreases. On the other hand, at the exit the high pressure boosts the fluid outside, increasing its velocity. The pressure field separates the mating surface and can also support a certain load [1].

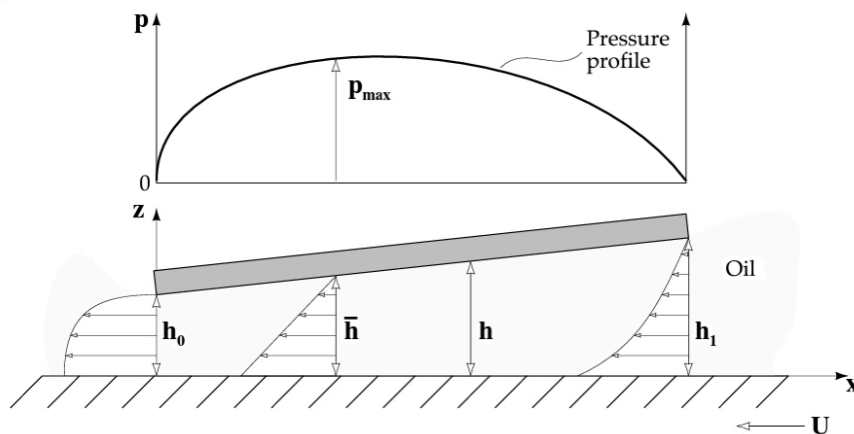


Figure 1.23: Principle of hydrodynamic pressure generation between non-parallel surfaces [1].

Anyway, fluid film can also be generated when a reciprocal motion in normal direction occurs. This can happen because a viscous fluid cannot be instantaneously squeeze out from the interface when two surfaces are placed in contact. It takes a certain time, during which a pressure is built up and so the fluid film is able to carry the load, keeping the two surfaces detached [3].

Hydrodynamic lubrication occurs when the tribo-system operates at high velocity and with fluids of high viscosity. In that situation, a high load capacity can be achieved. The typical thickness of lubrication film is from 5 to 500 μm , which is much bigger than the height of the asperities of surfaces so, the contact between the surfaces never occurs and the wear is very low. However, adhesive wear takes place during start-stop operation. Friction coefficient is usually very small, in the order of 0,001 and it increases slightly with the sliding speed due to viscosity drag. The behavior of this fluid regime is governed by the Reynolds equation and the bulk physical properties of the lubricant play an

important role, especially the viscosity. In fact, friction force in HD lubrication is only affected by the shearing of the viscous lubricant [3].

1.4.2.2 Elastohydrodynamic Lubrication

Elastohydrodynamic lubrication, commonly referred to as EHD, is a regime where the two surfaces are completely separated by a lubricant film, similar to HD, but elastic deformations of the solid bodies occur. EHD usually takes place in that application where heavy loads are applied, therefore high pressures are developed. The fluid film thickness is thinner in this kind of lubrication (typically 0,5-5 μm [3]) and the change of viscosity with pressure plays an important role. The high hydrodynamic pressure generated in the lubricant film deforms the contacting surface elastically [1]. Thus, the behavior of EHD lubrication involves simultaneously Reynolds equation, elastic deformation equation and viscosity-pressure equation.

Wear is generally low, however fatigue wear due to elastic deformation is very common. In addition, adhesive wear during start-stop operation occurs [3].

1.4.2.3 Mixed Lubrication

Mixed lubrication is the transition regime between hydrodynamic/elastohydrodynamic and boundary lubrication. Both lubrication mechanisms are involved, so part of the surface is detached by a partial hydrodynamic film but some asperities may come into contact. The wear rate increases in this kind of lubrication; in fact, solid contacts lead to adhesion, wear particle formation and metal transfer. Anyway, some additives may be added to the lubricant in order to prevent adhesion bounds.

Looking at Stribeck curve, Figure 1.22, friction coefficient drop-off greatly because less and less solid contacts occur, and the fluid regime becomes closer to hydrodynamic or elastohydrodynamic [3].

1.4.2.4 Boundary Lubrication

Boundary lubrication is usually referred to the plateau level on the Stribeck curve, Figure 1.22. It is a complex phenomenon and it occurs when the load is very high or when the speed and the fluid viscosity are very low. In these situations, the thickness of lubricant is very thin (monomolecular or multimolecular film), and it is not able to detach the surfaces. Thereby, surfaces are very closed and the interaction between surface asperities and monomolecular or multimolecular film dominates the contact. Anyway, boundary lubrication provides an excellent protection against adhesive and chemical wear. In fact, in clean surface contact, where the surfaces are “dry”, friction may become very high. Furthermore, additives are commonly added in the lubricant in order to provide a better lubrication,

improving the fluid film formation. The lubricant adheres to the surfaces due to either chemical reaction of the species within the liquid (including additives) with the surfaces or to absorption of fluid molecules in the surfaces. Since the fluid film is extremely thin, viscosity usually does not affect wear and friction.

In this kind of lubrication friction and wear are very high. The most common wear mechanisms are adhesive and chemical wear, and they usually occur when the boundary lubrication fail [3].

1.4.2.5 Hydrostatic Lubrication

Unlike the previous regimes of lubrication, hydrostatic lubrication supports loads thank to a thick fluid film, which is ensured by an external pump. The main advantage of this type of lubrication is that no relative motion is needed to build up the pressure required to separate the two surfaces, wear is also avoided during start-stop operation and with slow speed. In addition, hydrostatic lubrication supplies a high stiffness. Anyway, the pump requires additional space and its cost is relevant, so system with hydrostatic lubrication are bigger and more expensive.

1.5 Run-in

Run-in is the most common tribological transition. It is usually defined as “those processes which occur prior the *steady state* when two or more solid surfaces are brought together under load and moved relatively to one another” [6]. In fact, friction force and wear change substantially during the first time of work, and after such initial perturbations they reach a constant value. This condition, known as *steady state*, occurs where the tribosystem’s parameters, like the average kinetic friction coefficient, wear rate and others (temperature, concentration of debris, etc.), have reached a constant level. So, the whole phenomena between start-up and the beginning of *steady-state* are known as run-in. Anyway, *steady-state* may not be reached or reached for a short period, and the process continues to evolve while the friction force behaves erratically. On the other hand, friction coefficient of well-lubricated tribosystem remains low and steady during *steady-state*.

Friction transition could also occur after changes in the operating conditions of the tribosystem (e.g., changing the load, velocity, temperature, etc.) or due to materials and lubricants aging. Some machines or components are intentionally made work under certain run-in procedures (usually with low load or velocity) after initial assembly or after periodic maintenance in order to reach correctly the *steady-state*. Improper run-in can result in short lifetime of the component or erratic behaviour [5].

Some models, able to describe the changes of surface during run-in, can be found in literature, for instance, Jeng et al. [7] published a run-in wear model for surface with different heigh distribution.

Anyway, as reported by Blau [6], a lot of information about this phenomenon are kept secret because they may give a competitive advantage, so manufacturers prefer not to publish their discovery.

Run-in is a complex process that involves several phenomena, in addition to changes in friction and wear. First, changes in surface roughness and surface chemical conditions occur: the roughness could either increase or decrease, even if decreasing is most common because the highest asperities are broken by sliding; the kinetics of reaction between surface and environment usually change during run-in. Furthermore, other phenomenon as elastic and plastic deformation, thermal changes, microstructural changes are typical of run-in [6]. For this reason, understanding and interpreting run-in requires a multidisciplinary approach. Figure 1.24 shows eight common forms of friction-time curves, friction force may either increase or decrease during run-in. The causes for each of the eight shapes can be of various nature, the same curve may be obtained by different sets of interfacial processes. It is also important to understand that run-in is not only dependent on materials, but it is a characteristic of the whole tribosystem [5].

The time to reach *steady state* of wear could be different compared to that required to reach the *steady state* of friction. In fact, high friction is not necessarily correlated to high wear, frictional energy may be used for several purposes (to form oxide, heat surface, shear debris layer, etc.) including wear. So, this energy may be differently partitioned from one tribosystem to another and the resulting wear will not be the same.

Two characteristic terms of run-in process are: *asperity truncation* and *elastic shakedown*. Asperity truncation is the rapid truncation of high and sharp asperities during the sliding of two surfaces placed in contact. Of course, this leads to a change of surface roughness parameters and usually the surface becomes smoother; however, this is not always true and sometimes roughness could increase. *Elastic shakedown* is the process where “a (typically metal) surface that initially yields plastically during run-in eventually reaches an *elastic shakedown limit* at which the behaviour of the near-surface layers is no longer plastic but has reached a work-hardened condition sufficient to support the contact pressure in an elastic manner” [5].

In order to reduce run-in process, hard surfaces or wear-resistant coating or treatments can be used and some anti-wear additives can be added to the lubricant.

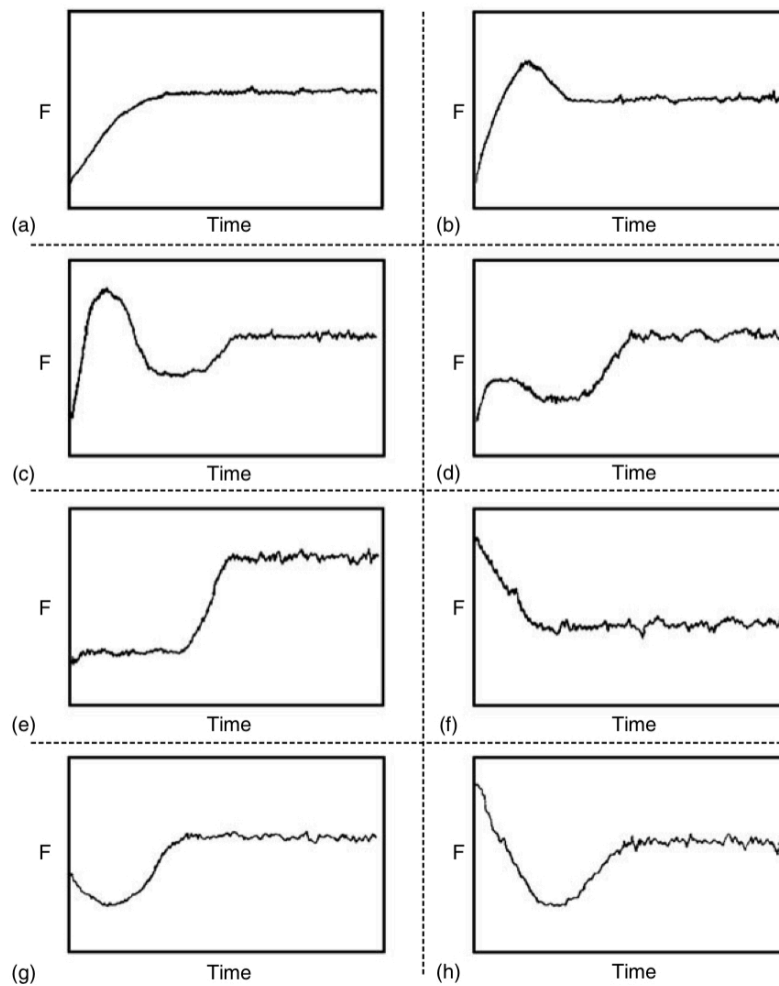


Figure 1.24: Eight common form of friction-time curves [5].

1.6 Flow Factors

In lubrication friction, surface roughness could play an important role, especially when the film thickness becomes thin. For example, in mixed lubrication, part of the load is carried by asperities interaction and the other part is carried by pressurized lubricant that percolates through the maze formed by asperities of both surfaces. If the film thickness of the lubricant is thin, the flow and the pressure of the lubricant are influenced by surface roughness also during hydrodynamic lubrication. For these reasons, the roughness of the two surfaces is very important and it must be taken into account. Anyway, asperities change rapidly compared to the geometrical shape of the surface, so a too dense mesh is required in order to consider the surface roughness in the simulation of fluid lubrication.

Therefore, there are no computers sufficiently powerful to compute the flow simulation also considering the surfaces roughness, many degrees of freedom would be required [8].

However, some averaging techniques are developed for studying the effects of surface roughness in hydrodynamic lubrication. One of them is the flow factor method by Patir and Cheng (P&C) [9] [10]. This method defines an average type of the Reynolds equation expressed in terms of flow factors [11]. The flow factors are computed by numerical flow simulation on a local roughness scale with the software *Tribo-x*. Once they are found, they could be included as coefficient in the average Reynolds equation to analyse how the roughness influences the pressure and shear driven flow. Thus, the average Reynolds equations are solved for a smooth surface and the flow factor included in the equation takes into account the roughness of the surface. However, the assumption that the surface roughness can be modelled as a periodic extension is done, so a representative part of the surface must be taken for the simulation of flow factors [11]. According to Sahlin et al. [12], the advantage of using P&C method is that profiles having the same Abbot curve are also shown to have the same flow factors. This implies that once the flow factors are calculated for several surfaces, then they can be used for similar surfaces, without computing them anymore.

The main problem of this theory is that no off-diagonal terms are present in the flow tensors. So, the effect due to anisotropic roughness or roughness having diagonal lay cannot be taken into account. Almqvist et al. in [11] compare the flow factor method by P&C and homogenization method. Homogenization method provides an accurate solution for arbitrary roughness. As presented by the authors, the two methods coincide if the roughness is symmetric, but they present some differences in the other condition.

As mentioned before, the flow factor theory is presented by Patir and Cheng in [9] [10]. In these articles, they defined the film thickness, h_T , as a function of a global parameter, h , and the two roughness parameters, δ_1 and δ_2 , see Figure 1.25.

$$h_T = h + \delta_1 + \delta_2 \quad (1.19)$$

where:

- h_T is the local film thickness;
- h is the nominal film thickness defined as the distance between the mean levels of the two surfaces;
- δ_1, δ_2 are the random roughness amplitudes of the surfaces, measured from their mean levels.

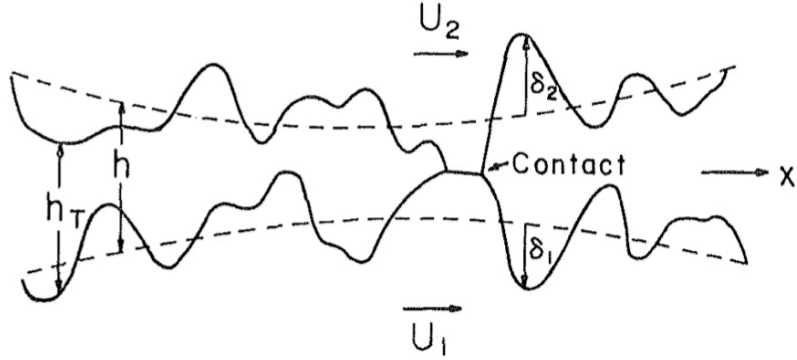


Figure 1.25: Film thickness [9].

Assuming that δ_1 and δ_2 have a Gaussian distribution of heights with zero mean and standard deviation σ_1 and σ_2 , the variance of the combined roughness $\delta = \delta_1 + \delta_2$ can be defined as:

$$\sigma^2 = \sigma_1^2 + \sigma_2^2 \quad (1.20)$$

In order to understand the effect of surface roughness in the lubrication regime, the ratio h/σ is very significant. In fact, it is known that for $h/\sigma \gg 3$ the lubricant film is sufficiently thin, and the surface roughness has no effect in the lubrication. On the other hand, when $h/\sigma \rightarrow 3$, the roughness effect becomes important. As h/σ decreases further, the contact between asperities starts and the roughness effect becomes increasingly important.

The average Reynolds equation found by P&C is defined as:

$$\frac{\partial}{\partial x} \left(\phi_x \frac{h^3}{12\mu} \frac{\partial \bar{p}}{\partial x} \right) + \frac{\partial}{\partial y} \left(\phi_y \frac{h^3}{12\mu} \frac{\partial \bar{p}}{\partial y} \right) = \frac{U_1 + U_2}{2} \frac{\partial \bar{h}_T}{\partial x} + \frac{U_1 - U_2}{2} \sigma \frac{\partial \phi_s}{\partial x} + \frac{\partial \bar{h}_T}{\partial t} \quad (1.21)$$

Where:

- \bar{p} is the mean pressure;
- μ is the absolute viscosity;
- \bar{h}_T is the average film thickness;
- U_1, U_2 are the velocity, along x-direction, of surfaces;
- ϕ_x, ϕ_y are the pressure flow factor;
- ϕ_s is the shear flow factor.

The flow factor ϕ_x, ϕ_y, ϕ_s are computed through a flow simulation. The pressure flow factor ϕ_x and ϕ_y compare the average pressure flow in a rough surface to that of a smooth surface. The shear flow factor ϕ_s represents the additional flow due to sliding. The procedure to obtain the flow factor starts by defining a rectangular part of the surface, whose area is ∂A_i . It is assumed that the surface is

approximated by a sequence of the previous rectangular. The area ∂A_i must be small relatively to the dimension of the total surface but large enough to include a large number of asperities, see Figure 1.26. The film thickness h is assumed to be constant. Then, the pressure flow factor will be calculated for each rectangular surface by applying the following boundary condition:

$$\begin{aligned} p &= p_A && \text{at } x = 0; \\ p &= p_B && \text{at } x = L_x; \\ \frac{\partial p}{\partial y} &= 0 && \text{at } y = 0 \text{ and } y = L_y; \end{aligned}$$

No flow at contact points;

and simulating the pressure flow by numerical methods. After that this flow is compared to that of a similar smooth surface. At the end, the flow factor can be obtained as a function of h considering different nominal film thickness (h) [9] [10].

In the following two sections, the pressure flow factors and the shear flow factor are explained.

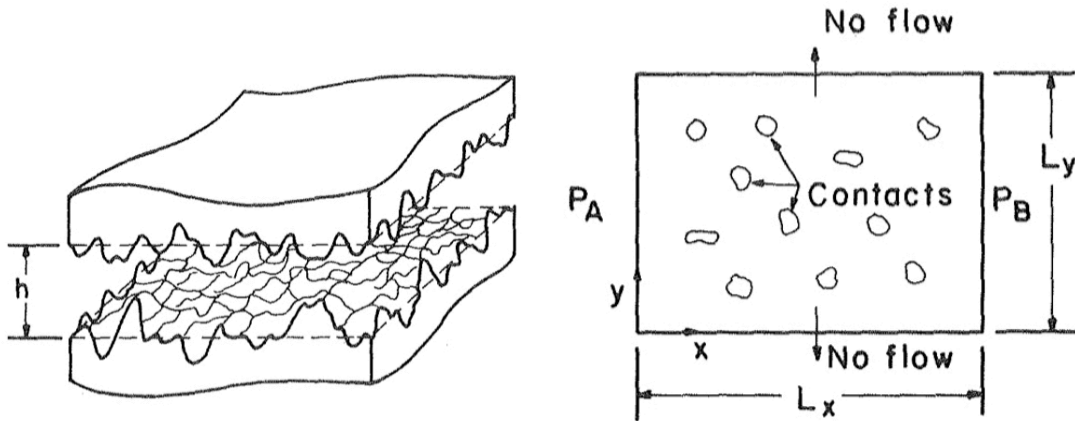


Figure 1.26: Model for flow factor simulation [9].

1.6.1 Pressure Flow Factors (ϕ_x, ϕ_y)

In order to understand what the pressure flow factors means, a new parameter, γ , is introduced. It is defined as the ratio of $\lambda_{0,5}$ lengths of the x and y profiles, where $\lambda_{0,5}$ is the length at which auto-correlation function of a profile reduces to 50 percent of its initial value.

$$\gamma = \frac{\lambda_{0,5 x}}{\lambda_{0,5 y}} \tag{1.22}$$

This parameter can be seen as the ratio of the length asperities and their width. Thus, for an isotropic roughness structure, $\gamma = 1$; for a purely transverse roughness patterns, $\gamma = 0$ and for a purely

longitudinal roughness pattern, $\gamma = \infty$. Figure 1.27 shows the typical contact area for surface roughness oriented different.

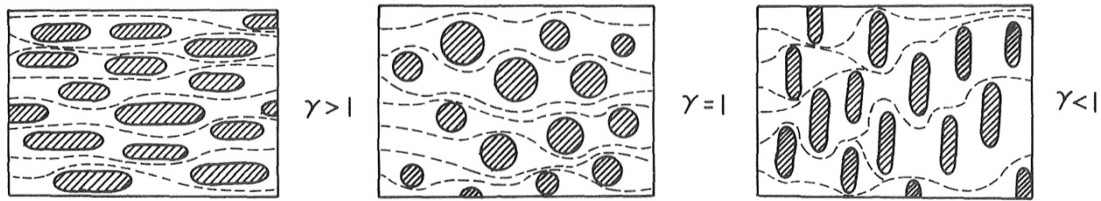


Figure 1.27: Typical contact areas for longitudinally oriented ($\gamma > 1$), isotropic ($\gamma = 0$) and transversely oriented ($\gamma < 1$) surfaces [9].

Changing the surface roughness orientation, the flow factors change too. In particular, for an isotropic structure the flow is equal in the two directions because there are no differences in the asperities shape between x- and y-direction. So, the two flow factors ϕ_x and ϕ_y should be equal. Figure 1.28 shows an example of the pressure flow factors ϕ_x and ϕ_y as a function of h/σ . Note that over $h/\sigma = 6$ the pressure flow factors are equal to 1, this means that the surface roughness does not influence the lubricant flow anymore and the average Reynolds equation is the same as that of smooth surfaces. Anyway, when the rate h/σ decreases, the roughness starts to modify the pressure and the flow of the lubricant and for $h/\sigma < 3$ the mixed lubrication occurs. The asperities start interacting with each other and the contact points form barriers to flow; for this reason the pressure flow factors are lower than 1.

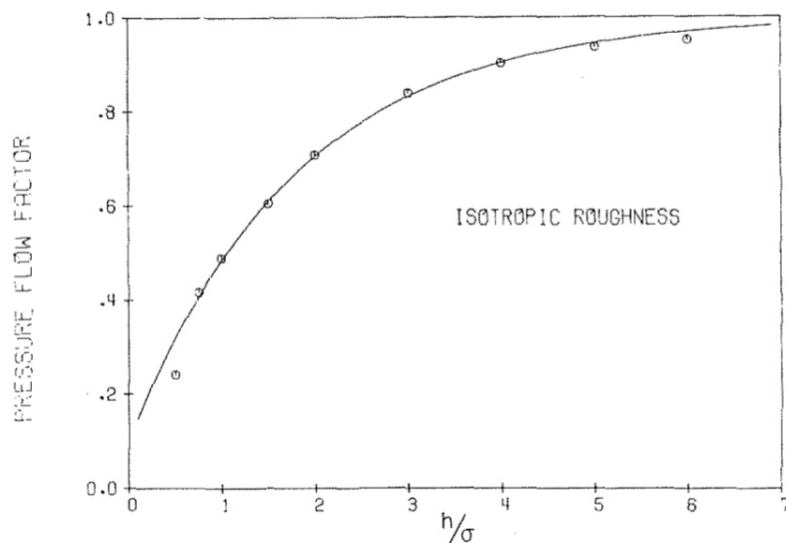


Figure 1.28: The pressure flow factors ϕ_x and ϕ_y for isotropic surfaces [9].

However, most engineering surfaces have directional patterns due to different manufacturing processes or due to run-in. For this reason, the roughness orientation is mostly in the longitudinal or transverse directions ($\gamma > 1$ or $\gamma < 1$). In that cases, the pressure flow factors in the two directions, ϕ_x and ϕ_y are different. In particular, for surfaces with a longitudinal direction ($\gamma > 1$), the pressure flow factor is greater than 1. While, for transverse direction ($\gamma < 1$), the pressure flow factor is smaller than 1. Figure 1.29 shows the variation of the pressure flow factor ϕ_x with different γ ratios. As shown in Figure 1.27, it is easy to understand that with longitudinally oriented contact areas ($\gamma > 1$), a little resistance is offered to the pressure flow and the resulting flow is greater than a similar smooth surface because the average gap is larger due to the valleys ($\phi_x > 1$). Furthermore, when h/σ decreases, the flow will be larger compared to the one of a smooth surface with the same gap, so the pressure flow factors will increase.

On the other hand, when γ decreases, small valley length occurs, and the contact asperities form a barrier to flow so the lubricant has to pass around the contact points. Thus, the pressure flow factor will be smaller than 1 because the resistance caused by the contact asperities leads to a larger mean gap compared to the smooth surfaces ($\phi_x < 1$) [9].

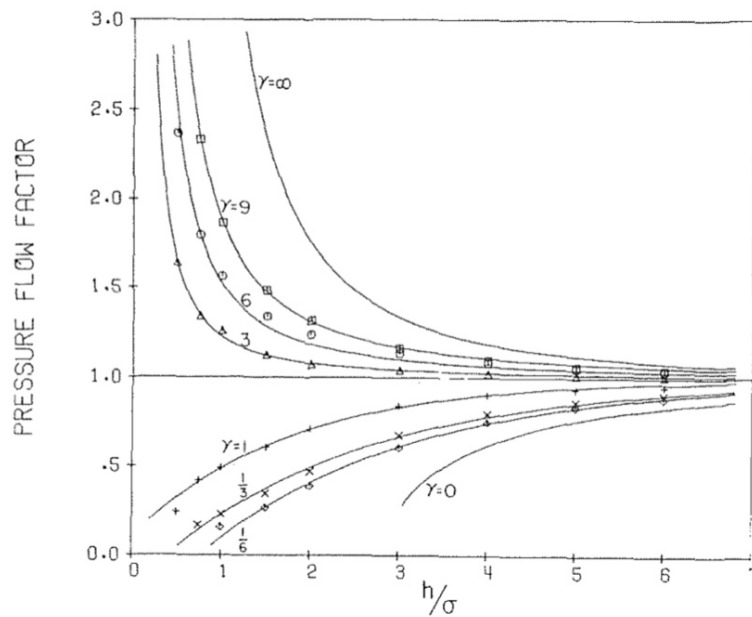


Figure 1.29: Effect of directional properties of roughness on pressure flow factor [9].

1.6.2 Shear Flow Factors (ϕ_s)

The shear flow factor is a function of the film thickness and roughness parameter only, but it does not depend on the combined roughness δ like the pressure flow factor. It depends on the statistical

parameter of δ_1 and δ_2 separately. Similarly to pressure flow factor, the shear flow factor ϕ_s is obtained by numerical flow simulation. However, the boundary conditions are a little bit different because no mean pressure gradient is introduced, so the pressure is set to a certain value both for $x = 0$ and $x = L_x$ (see Figure 1.26) and one of the two surface is moving. In this way, the simulating model becomes pure sliding of two nominally parallel surfaces. Then the simulation is computed for different surface distance. Note that in case of smooth surfaces, the pressure would be constant, and no flow would be present because no pressure gradient is imposed. However, the combined effect of sliding and roughness produces a net mean flow. In fact, the shear flow factor takes into account the increasing or decreasing of the flow due to the lubricant contained into the roughness valley and transported because of sliding. In order to understand, assume one surface is rough and the other is smooth and only one of the two is moving. When the rough surface is moving, the fluid carried in the valleys produces an additional flow transport and the mean flow increases ($\phi_s > 0$). On the other hand, if the smooth surface is moving, the asperities of the rough surfaces form a barrier and restrict the flow, so the mean flow decreases ($\phi_s < 0$). In the hypothetical case of two surfaces with statistically identical roughness configuration (in particular the same σ and γ), the shear flow factor will be zero ($\phi_s = 0$) because there is no net flow transportation due to the combined effect of sliding and roughness. Figure 1.30 shows typical shape of the shear flow factor varying γ .

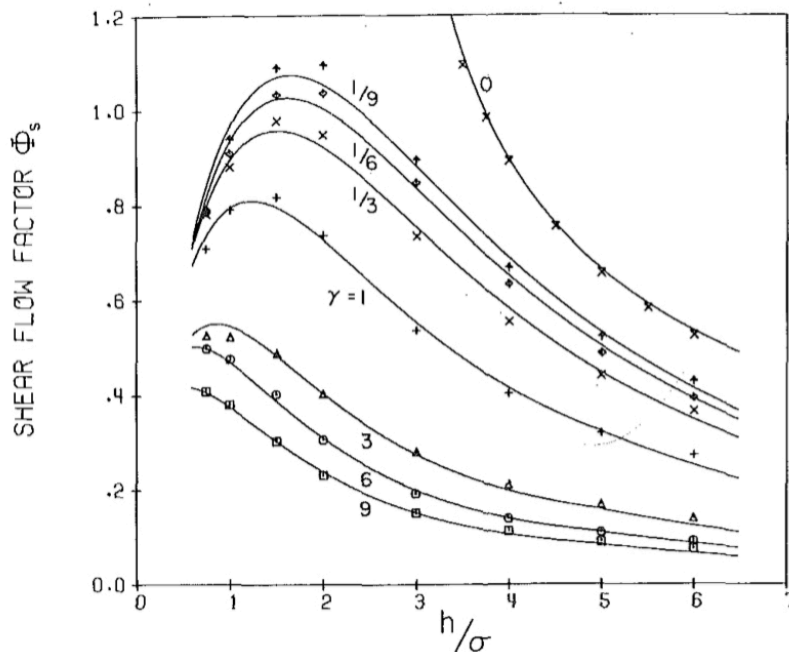


Figure 1.30: Shear Flow Factor ϕ_s [10].

Note that if h/σ is increased, the pressure flow factors ϕ_x and ϕ_y approach to 1 and the shear flow factor ϕ_s approaches to 0. This means that the average Reynold equation becomes equal to that of smooth surfaces. In fact, if the lubricant film thickness is thick, the surface roughness is not important anymore [10].

1.6.3 *Tribo-x*

“*Tribo-x* is a thermal elastohydrodynamic simulation software that allows the calculation of the stress, friction and temperature of lubricated systems. With *Tribo-X* a "numerical magnifying glass" is available, which allows a view into the frictional contact and thus contributes to a better understanding of the processes taking place there. *Tribo-X* can be used to optimize the friction and wear of lubricated systems to increase product efficiency and shorten product development cycles.” [13].

It has several modules: the one used to compute the flow factor is *MicroSim*. It is an Add-on module used in order to consider microdynamic and mixed friction. *MicroSim* calculates flow factors and contact pressure curves for measured rough surfaces. It can calculate the following parameters for consecutive steps, starting from a positive chosen distance (usually set to 30 μm) and decreasing step by step the surfaces distance up to a negative value (usually set to $-5 \mu\text{m}$):

- Nominal and deformed gap height;
- Real contact area;
- Mean contact pressure, based both on the nominal contact area and the real contact area;
- Pressure flow factor in x and y direction;
- Shear flow factor in x and y direction;
- Surface Factor.

Note that the nominal gap-height is zero when the surface asperities are for the first time in contact each other and the contact pressure increases. Then the software continues to decrease the nominal gap-height, reaching negative value. Anyway, the deformed gap-height is always positive due to the elastic and plastic deformations that occur in the highest peaks of the two surfaces.

1.7 Test Bench

The test bench used for the tests is a disc-on-disc tribometer, Figure 1.31. Two different discs are brought in contact and a normal force is applied by a hydraulic piston. Then, the upper disc is fixed and the lower one is placed in rotation by a hydraulic motor, Figure 1.32. The two discs are immersed in lubricant, and a pump allows the lubricant flow in a heat exchanger connected to a cooling system.

In this way, the lubricant temperature can be regulated. The friction force is measured by a force sensor, placed at a known distance, which measures the tangential force. Multiplying that force for the distance from the centre, the torque is found. Finally, from the torque it is possible to find the friction force.

The technical specifications are indicated in the following table:

<i>Mean friction diameter</i>	54 mm
<i>Wear track size</i>	5 mm
<i>Area of friction</i>	848,23 mm ²
<i>Typical load</i>	10 MPa
<i>Maximum load</i>	25 MPa
<i>Range of friction coefficient, μ</i>	0 – 0,1
<i>Maximum surface speed</i>	6 m/s

Table 1.2: Technical specification of the Test Bench.

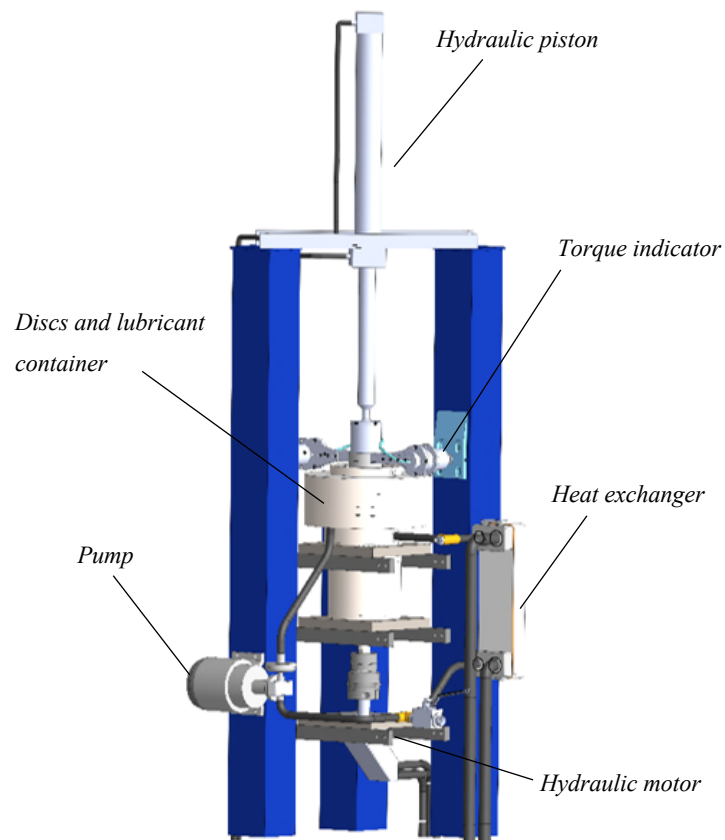


Figure 1.31: Test bench: disc on disc tribometer [14].

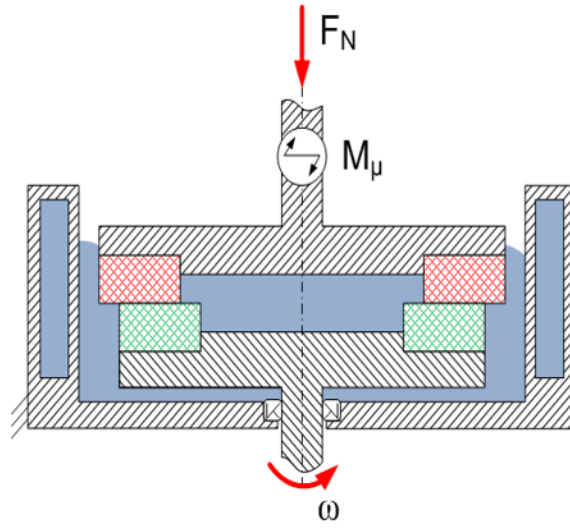


Figure 1.32: Tribometer scheme [14].

Chapter 2

MATLAB Code

The aim of the code is to find a submatrix of 300 for 300 points from the 3D vector obtained from the microscope scan. This matrix will be used as input matrix in the software “*Tribo-X*” to calculate the Flow Factors. In order to build the 300 for 300 matrix, a relevant distance between two relevant measurement points has to be found by studying the Power spectral Density both for x- and y-direction. Once the two PSD is calculated, a cut-off frequency has to be determined and then, with the Nyquist– Shannon sampling theorem, it is possible to obtain the relevant distance.

In this chapter each of the previous mentioned themes are clearly explained. Furthermore, the use of a Gaussian filter to avoid the noise originated from the scanning will be also discussed.

At the end of the chapter, the results using different cut-off frequency and different type of PSDs will be showed. In addition, a comparison between them will be done.

2.1 Data Structure

After the microscope scan the data has the structure shown in Figure 2.1(a). It is a 3D vector where in the first column there are x-values, in the second one y-values and in the last one the surface heights, $z(x, y)$. It is important to notice that the scan is done along y-direction. In fact, the microscope scans all the x-points for the same y point, afterwards it increases the y-value by one step and scans the same x-points again and so on.

This type of structure is difficult to handle. It is better to have a *z-matrix* where there are all the $z(x, y)$ values. Its columns correspond to the y-values and its rows to the x-values, Figure 2.1(b). In order to obtain this, it is necessary to think up an algorithm which is simple and lows computational time request. The computation time was the most difficult problem to solve. Different algorithms were tried but most of them required too much time. §2.1.1 shows how this problem was solved.

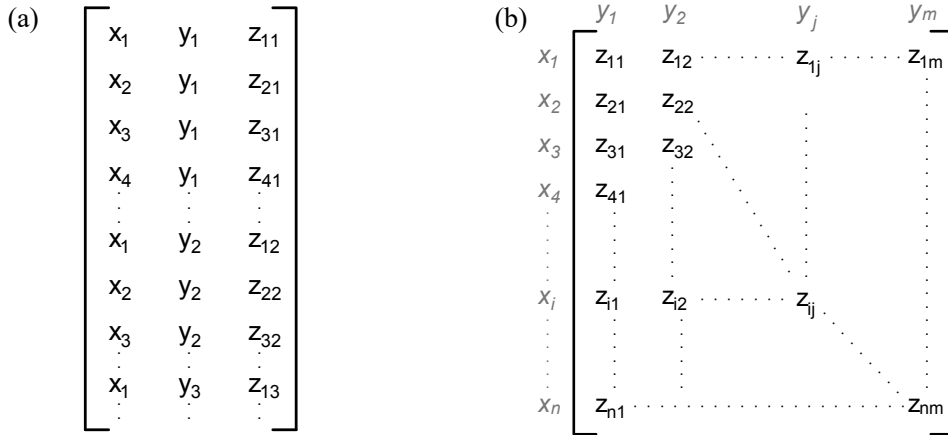


Figure 2.1: Data structure after the microscope scan (a) and z-Matrix including all the $z(x,y)$ surface values (b).

Moreover, there could be some missing points during the microscope scan due to the reflection of the light in the surface. Thus, these points will be replaced with a NaN (not a number) during the *z-matrix* construction, in this way it will be easier to recognize and delete them. In §2.1.2 how these points are processed will be explained.

Furthermore, the surface could be rotated after the scanning: for this reason, the program finds the plane which interpolates the data and calculates its rotation angles around x- and y-axis. Then, using the rotation matrixes, the surface is rotated.

2.1.1 Z-Matrix Construction

In this section the algorithm which is used to build the *z-matrix* from the 3D vector obtained by the microscope will be presented.

As it was said before, the main problem was the computational time. With the first attempted algorithms the matrix construction took too much time. In particular, it was discovered that the MATLAB function *'find'*, which is used to identify the vector indexes, takes excessive time if it is repeated for many cycles. This function was very useful to build the *z-matrix* because the x-values, differently from the y-values, are not in ascending order. So, it is important to know the index of the 3D vector where each x-value is repeated.

To avoid the use of the function *'find'*, the following method is used. First of all, three vectors have to be defined:

- *AllValue_x*: it contains all the x-values. Its length is equal to the number of x-points.
- *AllValue_y*: it contains all the y-values. Its length is equal to the number of y-points.

- *dim_y*: It is a row vector and its length is equal to the length of *AllValue_y*. Each value of it corresponds to a y-value: the first value is about the first y-point, the second value is about the second point and so on. The respective values in the vector are the number of x-points for a known y-point (for instance: if there are 5 x-points for the first y- and 8 for the second y-value, the first value of *dim_y* is 5 and the second one is 8).

These three vectors are used to build the *z-matrix*, how they are used will be explained in the next part. To obtain these vectors, you can proceed in two different ways for x- and y- direction. The reason is the structure of the 3D vector: y-values are simple to find because the microscope scans along y-direction. As it can be seen in Figure 2.1(a), each y-value is repeated for all x-values and they are sorted in ascending order. It is not the same for x-direction, the x-values are repeated for each y-values, so it is not easy to know all the index of each x-value. Furthermore, not for all y-values the same x-values are scanned. Indeed, as stated before, there could be some missing points. For this reason, it was decided to use the vector *dim_y*. In this way, it was possible to find out how many x-points there are for each y-values and it will be useful in the construction of the *z-matrix* as it will be seen later. In order to understand how these vectors are built, the two vectors *AllValue_y* and *dim_y* are first of all presented. To obtain these two vectors, other two vectors are needed, as it is showed in Figure 2.2. From the second column of the 3D vector, which contains y-values, the difference between the elements of the vector can be obtained and the results are stored in a vector called *diff_y*. Due to the structure of the second column of the 3D vector, *diff_y* is zero for most of the values and equal to the difference between two measurement points along y, *dy*, when the y-value changes.

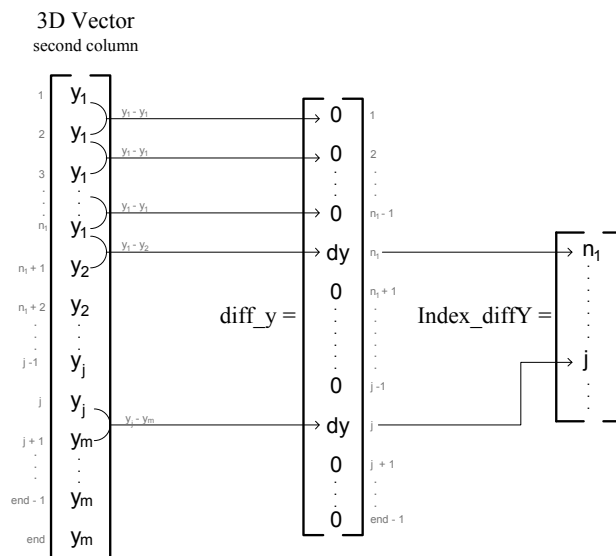


Figure 2.2: Construction of 'diff_y' and 'Index_diffY'

At this point, with the MATLAB function *'find'* it is possible to uncover the index where the y-value changes. This is what it is showed in the vector *Index_diffY*. Therefore, with these vectors it is possible to obtain the two vectors searched. Regarding *AllValue_y*, it can be easily found by taking only the rows of the second column of the 3D vector contained in *Index_diffY*. In this way, all the y-values will be obtained, except the last one, which is found by adding the last value of 3D vector (second column). The code relating to the part just mentioned is showed below:

```
AllValue_y = Surface_trasl(Index_diffY,2);
AllValue_y(end+1) = Surface_trasl(end,2);
```

On the other hand, the element of the vector *dim_y*, from the second to the penultimate, can be found thanks to the difference between the elements of *Index_diffY*. Then, the first element is obtained by taking the first value of *Index_diffY* and the last one calculating the difference between the length of the 3D vector and the last element of *Index_diffY*. The relative part of the code is shown below:

```
dim_y = Index_diffY(1);
dim_y(2:length(Index_diffY), 1) = diff(Index_diffY);
dim_y(end+1, 1) = length(Surface_trasl) - Index_diffY(end)
```

For the last vector *AllValue_x*, the procedure is quite similar to the one seen before, with the difference that the x-values are not sorted. So, what it was done is to sort the x-values to have a structure similar to the y-value. After that there will be a vector, *sort_x*, of two columns where in the first one there are the x sorted values and in the second one the real index that they had in the original vector, see Figure 2.3.

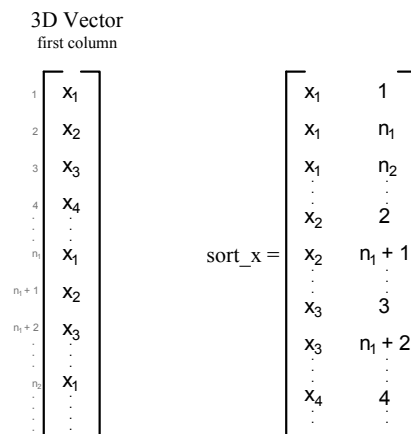


Figure 2.3: x sorted values used to find the vector with all x-values

Now, the procedure to obtain *AllValue_x* is the same as the previous one. The only difference is that attention must be paid to indexes. In fact, *diff_x* and *Index_diffX* (using the first columns of *sort_x*) has to be found, as it was done before. But the indexes just found are not the real ones because the vector was sorted so, in order to have the real indexes, it is necessary to use the second column of *sort_x*. The code relative to this part is shown below:

```
diff_x = diff(sort_x(:,1));
Index_diffX = find(diff_x ~= 0);
Index_diffX_Real = sort_x(Index_diffX, 2);
AllValue_x = Surface_trasl(Index_diffX_Real, 1);
AllValue_x(end+1) = Surface_trasl(sort_x(end,2), 1);
```

With these three vectors it is now possible to find the *z-matrix*. First of all, to obtain this matrix, a matrix of NaN (not a number) is created, whose size is the number of x-points for the rows and the number of y-points for the columns. Then, it will be filled with two ‘for’ cycles, one to check the y-values and the other one to check the x-values.

With the first ‘for’ cycle a matrix of two columns (*Supp*) is created for each y-values. In its first column there are the x-values for the analyzed y and in the second column there are the z-values for the same y. To obtain this matrix the vector *dim_y* can be used. In fact, this vector contains the number of x-values for each y-points, so the y-value to analyze is chosen with the ‘for’ cycle while the x- and z- values corresponding to the analyzed y are considered with the vector *dim_y*.

In fact, it is assumed that:

$$dim_x = [n_1, n_2, n_3, \dots, n_j, n_{end}] \quad (2.1)$$

It means that it will be n_1 x- and z-values for y_1 ($j = 1$), n_2 values for y_2 ($j = 2$) and so on. The first ‘for’ cycle goes from j equal to 1 to j equal to total number of y-values. So, it easy to understand that to achieve the matrix *Supp* for a certain value of j, what is needed is, from the 3D vector, the value of the first (for x-values) and of the last columns (for the z-values) of the 3D vector from $n_{j-1} + 1$ to $n_{j-1} + n_j$, see Figure 2.4.

It is important to notice that there are not the same x-values for every y-values due to the lack of some points during the microscope scanning. For this reason, another ‘for’ cycle is implemented and his aim is to identify, for each y, which x-points have a z-values and which one don’t. This cycle scans each value of the first columns of *Supp* and it locates the row of the z-matrix which corresponds to the same x-value. Then it fills the z-matrix in the correct location, that is row *i* and column *j*. For example, in case of a 3D vector like the one in Figure 2.4, for $j = 1$ the z-matrix from the second row of the

first column will be filled, the first value will be a NaN. For $j = 2$ the first two values of the second column will be NaN and so on.

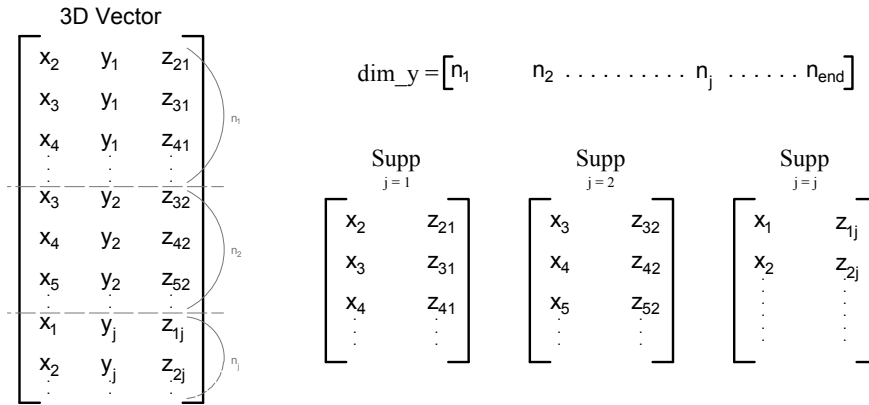


Figure 2.4: Structure of matrix 'Supp' used to build z-matrix.

So, a matrix is obtained where each column corresponds to one y-value and each row to one x-value. Its values are the heights of the surface, $z(x, y)$ (Figure 2.5). There will also be a few NaN, which means that the microscope could not scan that point (an error occurred). In the following section the problem of the lacked points and its possible solution will be examined.

2.1.2 Missing points

The real structure of the z-matrix is not exactly the same as shown in Figure 2.1(b) but it has some NaNs inside, especially in the first and last columns and rows. An example of it can be seen in Figure 2.5.

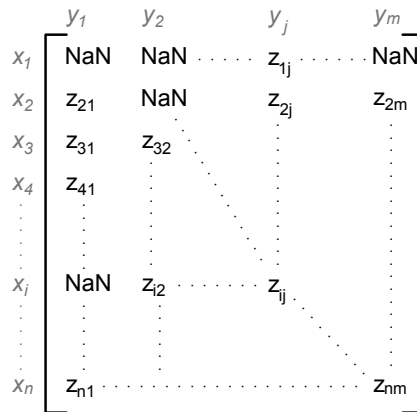


Figure 2.5: Real structure of z-matrix.

Since the most missing points are usually in the first and last 10 columns and rows, it has been decided to delete them. So, it will be a submatrix of *z-matrix* in the range from $x_{10} \div x_{end-10}$ and $y_{10} \div y_{end-10}$, in this way most of NaNs are deleted. Nevertheless, sometimes there could be some lack of points also in the middle of the matrix and of course also these values have to be replaced. To obtain this, the MATLAB function ‘*fillmissing*’ is used. This function is able to find the missing points and replace them with a ‘spline’ interpolation. However, if there are several missing points in a row the interpolation does not work well. With some attempts it was found that up to 100 NaNs in a row, the approximation is correct. If they are more, that function cannot be used because the error would be too high. In that case, the NaN values are substituted with zero and a warning message shows up. It was decided to replace with zero because that value does not modify the PSD. The warning message is useful for the users to understand that they have to pay attention to choose the 300×300 matrix without those zero values. This is easy verifiable by plotting the graph of the 300x300 matrix and seeing if there are some flat zones.

At this point, *z-matrix* is complete (without any missing points) and the PSD can be calculated. However, it is better to filter the surface data before, in order to avoid the noise originated from the measurement. How the filter is used is explain in §2.2.

2.2 Gaussian Filter

After a microscope scanning, the data could have some noise. It is important to remove it, otherwise the Power Spectral Density could be modified. In order to do it, a filter must be used. There are different kinds of filter but typically the Gaussian filter is employed to reduce the noise from data.

The Gaussian filter is an image-blurring filters that uses a Gaussian function for calculating the transformation to apply to each point in the matrix. It could be both one- and two-dimensional. In this case, two-dimensional one was used; the formula of a Gaussian function in two dimensions is:

$$G(x, y) = \frac{1}{2\pi \sigma^2} e^{-\frac{x^2+y^2}{2\sigma^2}} \quad (2.2)$$

Where σ is the standard deviation of the Gaussian distribution, x is the distance from the origin in the horizontal axis and y is the distance from the origin in the vertical axis. This formula produces a surface, and each section of this surface has a Gaussian distribution from the center points, Figure 2.6.

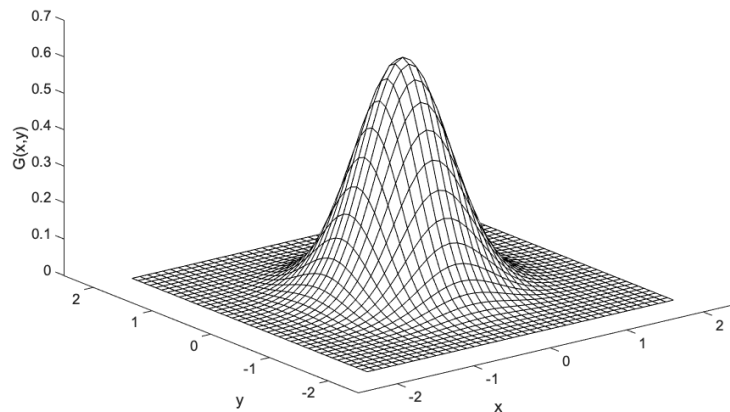


Figure 2.6: 2D Gaussian distribution with mean(0,0) and $\sigma = 0,5$

A convolution matrix is built from values of this distribution and it is applied to the original matrix. Each point of the original matrix is set to a new value which is a weighted average of the points' value neighbourhood of it. The central point's value has the heaviest weight (having the highest Gaussian value) and neighbouring points receive smaller weights as their distance to the central point increases. So, the effect of this kind of filter is a blur where boundaries and edges are preserved.

In theory, the Gaussian function is non-zero in every point of the matrix, meaning that the entire original matrix in the calculation for each point would be included. However, it is known that points at a distance of more than 3σ have a small enough influence to be considered zero. Thus, the points outside that range can be ignored [15].

An example of Gaussian filter's effect can be seen in Figure 2.7. The sample's material is steel before it was tested, so its surface is very smooth. On the upper left of the figure the filter is not applied, and it seems flat because the measurement noise is too high. When increasing the sigma value, the filter's effect increases, and the edges and boundaries of the rough surface show up clearly.

2.3 Power Spectral Density

The power spectral density can be seen as the power of the signal in the frequency domain and is very useful to describe the surface. Indeed, it contains all the information about the roughness property of the surface. Furthermore, it is unbiased by the particular scan size and resolution chosen. It can be used for different purposes, for instance the research paper [16] shows how to calculate the RMS (root-mean-square) roughness by using PSD. There are different ways to find the power spectral density for a surface, in article [17] all of them are present. In addition, in [17] there is an overview about how to analyse topography measurements to reconstruct a reliable PSD.

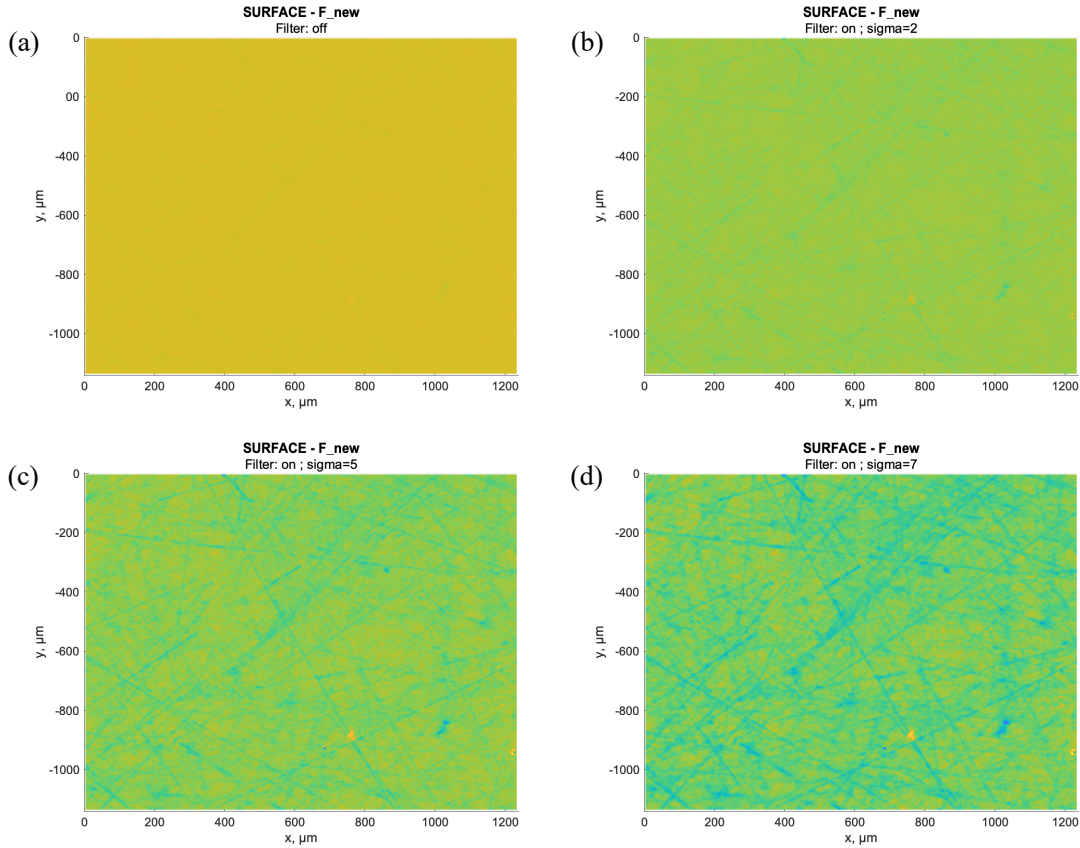


Figure 2.7: Gaussian filter's effect. Panel (a) shows the original surface, without filter, panels (b)-(d) shows the filter's effect increasing standard deviation (σ). Respectively $\sigma=2$ (b), $\sigma=5$ (c) and $\sigma=7$ (d).

In this thesis the PSD is used to analyse the power spectrum of the surface in order to find a relevant distance between two measurement points of the surface. This distance has to be as big as possible (to take a part of the surface as wide as possible) but it has also to be able to reconstruct the original surface without errors. This necessity comes up because the software “*Tribo-x*”, which calculates the flow factors, takes as input a matrix of 300x300 points but, after the microscope scan, there are much more points. IFAS’s measurement system can scan up to 10000×10000 data points for a surface of $1\text{mm} \times 1\text{mm}$ at highest resolution. Thus, taking a submatrix of that matrix of 300×300 data points would lead to having a very tiny surface and it would not characterize the roughness of the total surface. For instance, a typical distance between two measurements points is $0,37 \mu\text{m}$ so, taking 300 near points means obtaining a surface whose area is only $0,01 \text{mm}^2$.

Therefore, the idea is to study the PSD of the surface and find a correct cut-off value, $f_{\text{cut-off}}$. In fact, over a certain value the information is not important anymore. The value of the cut-off frequency is analysed in §2.4. In Figure 2.8 there is an example of cut-off frequency.

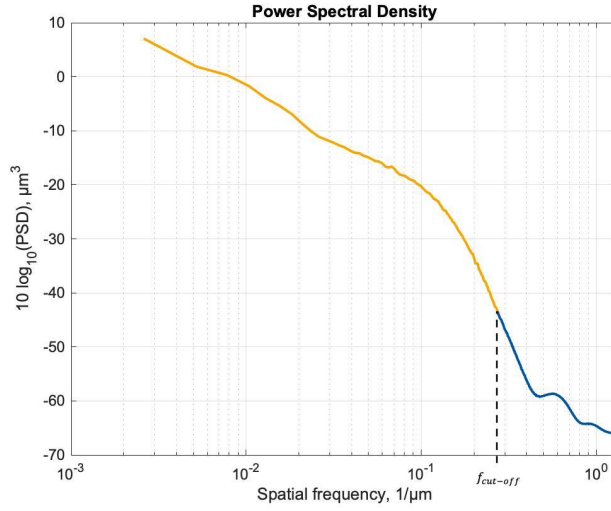


Figure 2.8: Power Spectral Density where shows an example of what the cut-off frequency means.

After the cut-off frequency is found, the Nyquist-Shannon theorem is used to calculate the relevant distance between two measurements points:

$$f_{Nyquist-Shannon} > 2 f_{cut-off}. \quad (2.3)$$

Given that the surface behaviour is studying both along x- and y- direction, there will be two different cut-off frequencies and two different relevant distances, ω_x for x-direction and ω_y for y-direction. It should be noted that in equation (2.3) is indicated the wavevector², in $1/\mu m$, whereas the relevant distance is the wavelength, in μm . So, ω_x and ω_y are its reciprocal:

$$\omega_x = \frac{1}{f_{Nyquist-Shannon_x}} ; \quad (2.4)$$

$$\omega_y = \frac{1}{f_{Nyquist-Shannon_y}}. \quad (2.5)$$

Where $f_{Nyquist-Shannon_y}$ and $f_{Nyquist-Shannon_x}$ are found using as coefficient of Nyquist-Shannon theorem three.

Once these two values are found, they are used to create the 300×300 matrix, called *Flow Matrix*. This matrix will be used as input of the software *Tribo-x* to calculate the flow factor. Figure 2.9 shows

² The wavevector k is defined as: $k = \frac{1}{\lambda}$ in μm^{-1} , where λ is the wavelength in μm

an example that explains the meaning of the *Flow matrix*: a submatrix of 300×300 points is taken from the total scanned surface.

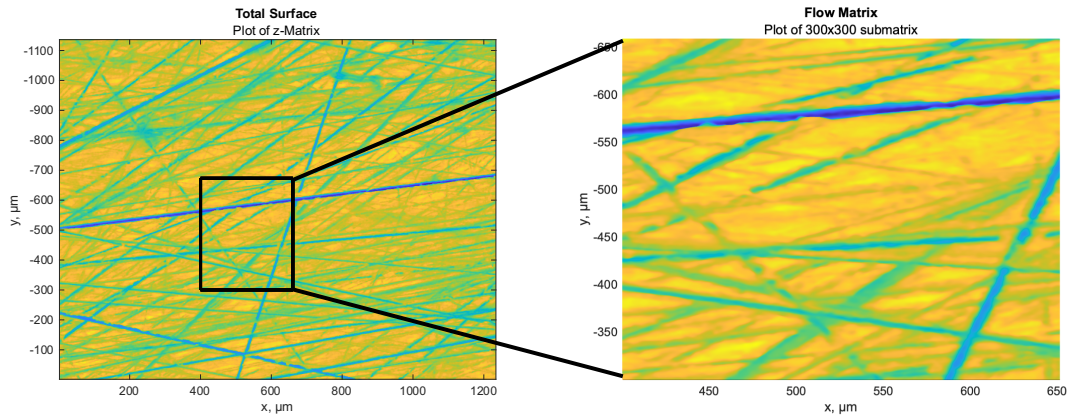


Figure 2.9: Example of Flow Matrix creation.

In Figure 2.10 is shown how that matrix is built and what ω_x and ω_y mean. The first point, which will be called start point, is located with x_{start} and y_{start} . There is an interface in the MATLAB code where the user can enter these two values. In order to help the user to make the right choice, the top view of the surface is plotted and the user should identify a pattern. Then, the *Flow Matrix* creation will start from that point. Furthermore, attention should be paid to avoid the artifacts arising from the measurement.

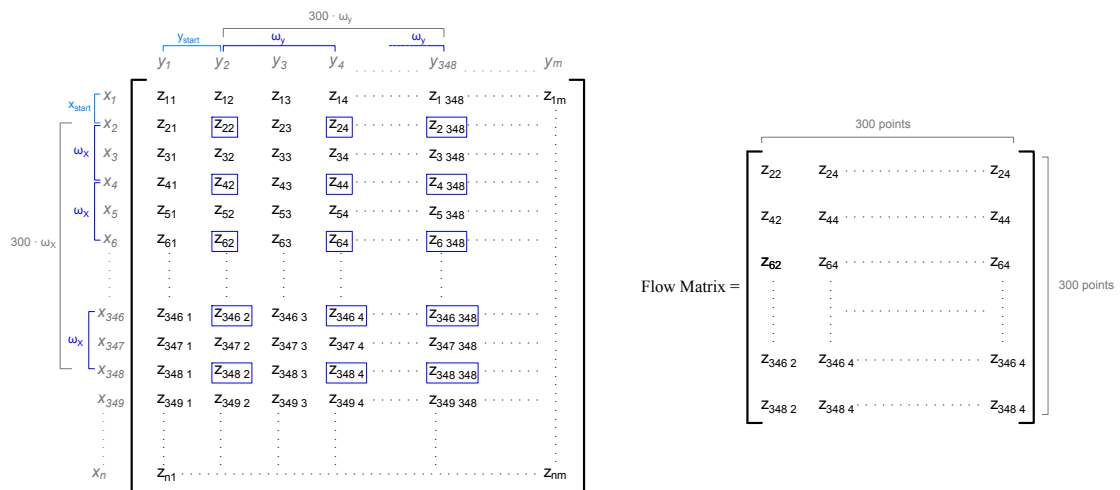


Figure 2.10: Construction of the Flow Matrix. On the left there is the z-matrix and an explanation of how the Flow Matrix is built, whereas on the right there is the Flow Matrix.

The PSD is calculated using two different ways. The first is found with the Welch's method, whereas the other is found using directly the FFT and then normalized. They are presented in §2.3.1 and §2.3.2. It should be noticed that the first one (with Welch's method) is preferred because the result is more accurate. In fact, the PSD using the FFT is sometimes not correct and may lead to errors.

Anyway, the PSD along x is calculated for each x-sections and the PSD along y is computed for each y-section. Then, the average between every section is taken for both directions, these are the two final PSD. Due to the structure of the z-matrix (see §2.1.1) each row corresponds to a x-section and each column to a y-section. So, to find the PSD along x it is necessary to calculate it for each row of z-matrix and for PSD along y for each column of the same matrix.

In order to have an averaged result, the mean between 5 rows of z-matrix (for x-PSD) and 5 columns of z-matrix (for y-PSD) is computed, then the PSD is found using this new averaged z-matrix.

2.3.1 Welch's Method

Welch's method takes its name after Peter D. Welch and it is an approach for spectral density estimation. The idea behind this method is to take the data and split it up into segments. After that, each segment is multiplied for a window function and the periodogram is computed from each segment. In the end, the results are the average of the periodograms just calculated. The aim is to reduce the variance associated with the periodogram estimate of the power spectrum. In [18] this method is explained, a short summary of Welch's works is presented below.

Let $x(j)$, $j = 0, \dots, N - 1$ be the signal which PSD has to be calculated. Segments of length L and starting point equal to D are taken, unit apart. Possibly, these segments have to be overlapping. They are defined in equations (2.6), (2.7) and (2.8). It is assumed that there will be K such segments and they cover the entire signal $x(j)$, i.e., that $(K - 1)D + L = N$. This kind of segmentation is shown in Figure 2.11.

$$x_1(j) = x(j) \quad j = 0, \dots, L - 1 \quad (2.6)$$

$$x_2(j) = x(j + D) \quad j = 0, \dots, L - 1 \quad (2.7)$$

And so on, finally:

$$x_K(j) = x(j + (K - 1)D) \quad j = 0, \dots, L - 1 \quad (2.8)$$

Now a data window is selected, $W(j)$, $j = 0, \dots, L - 1$ and each segment is multiplied for that window function to obtain the sequences $x_1(j) W(j), \dots, x_k(j) W(j)$. In the end, the periodogram is calculated for each segment and the PSD will be the average of them [18].

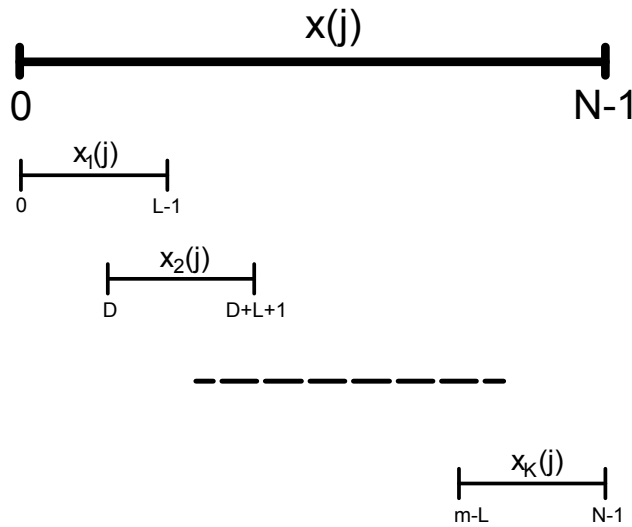


Figure 2.11: Welch's method segmentation [18]

The window function is a mathematical function that is zero-valued outside of the chosen interval. It can be of different types (rectangular, triangular, Gaussian, ...), for this study the “Hamming window” has been chosen, Figure 2.12.

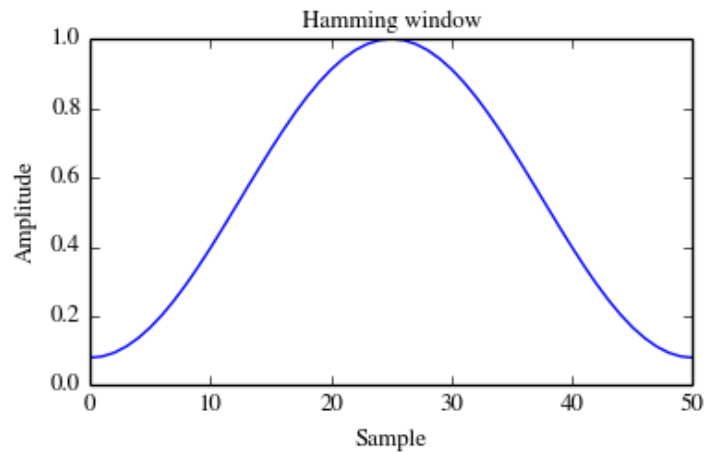


Figure 2.12: Hamming window

2.3.2 PSD computed directly from FFT

In addition to the PSD found with the Welch's method, it was decided to calculate another PSD using directly the FFT, with no windowing, in order to compare the two results. In fact, the PSD can also be computed as the square of the Fourier transform of the surface height, $z(x, y)$. As reported in [19], if the surface is periodic both the PSD with windowing and the PSD without windowing works equally well. On the other hand, the windowing is required for non-periodic data, otherwise some errors may occur. So, the PSD with the Welch's method must be used in that case.

In Figure 2.13 these two types of PSD are compared for two different surfaces used for tests.

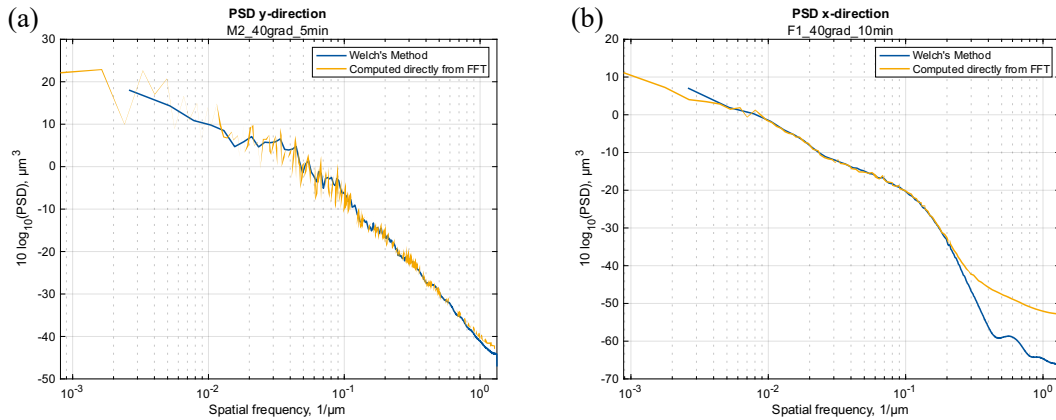


Figure 2.13: Comparison between PSD with Welch's method and PSD computed directly from FFT. Two surfaces are analysed: in the first one (a) the two results look very similar, in the second one (b) the two PSD are a little bit different, especially with large wavevector.

As it can be seen, two different results are presented: in Figure 2.13(a) the two PSD are almost the same (predictably, the one found with Welch's method is smoother); in Figure 2.13(b) the results are quite different for large wavevector. This difference might be caused by non-periodicity of the surface, in fact, as presented in [19] (section 3), for non-periodic surface the PSD without windowing picks up an artificial contribution at large wavevector. So, it is usually preferable to use the Welch's method, but sometimes the power spectral obtained using a straight FFT gives a better result.

Furthermore, the PSD obtained directly from the FFT is normalized, see Figure 2.14.

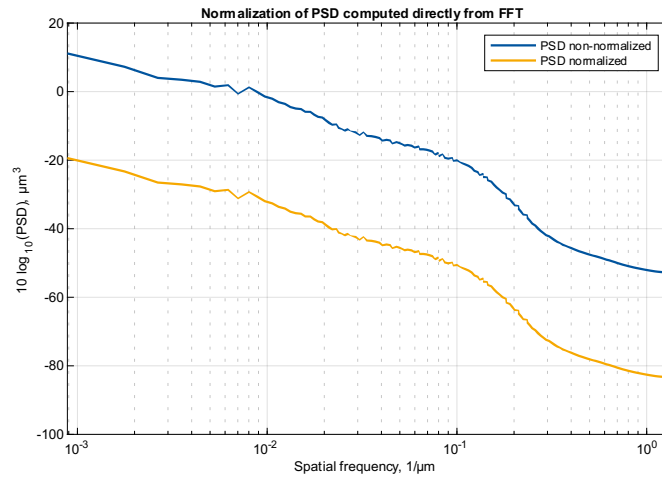


Figure 2.14: Normalization of PSD computed directly from FFT

2.4 Cut-Off Frequency

The cut-off frequency, presented in §2.3, is the PSD wavevector above which the contribution of the surface wavelengths is not important anymore. There is not a universal value that is correct for every surface, so the aim of this section is to analyze the PSD of several surfaces and try to find a typical value that gives suitable results for most surfaces.

It is important to find a correct cut-off value because it will define the relevant distance between two measurement points (ω_x or ω_y) in the constriction of *Flow matrix*. If it is too small, a lot of information will get lost and a high error will occur when the surface is rebuilt from the *Flow matrix*. On the other hand, if it is too large, the relevant distance will be small, and the part of the surface taken by the *Flow matrix* will not be large enough to characterize the surface roughness. So, an accurate value has to be found.

In order to obtain this value, three different methods are defined:

1. *Area method*: the cut-off frequency is identified when the area under the PSD graph reaches a certain percentage of the total area.
2. *Minimum method*: the cut-off frequency is identified when the PSD value reaches a certain percentage of its minimum value.
3. *Error method*: this is an atypical method which does not take into account the PSD but it studies how the error increases when the relevant distance increases. As it will be discussed in the following section, this method is only used in some cases: when a particular error or an improvement of the final result are needed.

Each method has a parameter which can be modified in order to find the best cut-off frequency. Since a parameter to evaluate the goodness of the results is needed, the parameter err_{perc} is calculated. This variable takes into account the number of points of the crapped surface (*Flow matrix* data), which, compared to the surface real points, has an error bigger than a threshold error value.

Let err be the threshold error and its value fixed to 45 nm, that is half of the microscope resolution (being 90 nm). Now, the difference between the *Flow matrix* value and the *z-matrix* value for each points of the *Flow matrix* is found and, if this difference is bigger than the threshold error, that points will be considered as an error. After that, the number of points considered as an error is counted:

$$number\ of\ error\ points = \sum_{i=m}^k \sum_{j=n}^l FlowMatrix(i, j) - zMatrix(i, j) > err \quad (2.9)$$

Where m , n , k and l are respectively the index of the *z-matrix* of x_{start} , y_{start} , x_{out} and y_{out} . Let $x_{out} = x_{start} + 300 \times \omega_x$ and $y_{out} = y_{start} + 300 \times \omega_y$ be the last taken point by *Flow Matrix*.

And err_{perc} is calculated dividing that number for the total number of points:

$$err_{perc} = \frac{number\ of\ error\ points}{total\ number\ of\ zMatrix(x_{start}:x_{out}, y_{start}:y_{out})} \quad (2.10)$$

So, this value establishes the percentage of the points of *Flow Matrix* that has an error bigger than the threshold error (err) and it is useful to understand whether the cut-off frequency is correct and so the 300×300 matrix reproduces the original surface well. In case err_{perc} is large, it means that too much information has been cut (cut-off frequency must be increased). On the other hand, if err_{perc} is around zero and the size of the cropped surface by *Flow Matrix* is tiny, it means that the cut-off frequency could be decreased in order to take a large portion of the total surface.

2.4.1 Area method to determine cut-off frequency

This method defines the cut-off frequency where the area under the PSD reaches a certain percentage, n_{Area} , of the total area (Figure 2.15).

$$f_{cut-off} \rightarrow Area_{PSD} = n_{Area} \cdot Area_{PSD_{tot}} \quad (2.11)$$

2.4 – Cut-Off Frequency

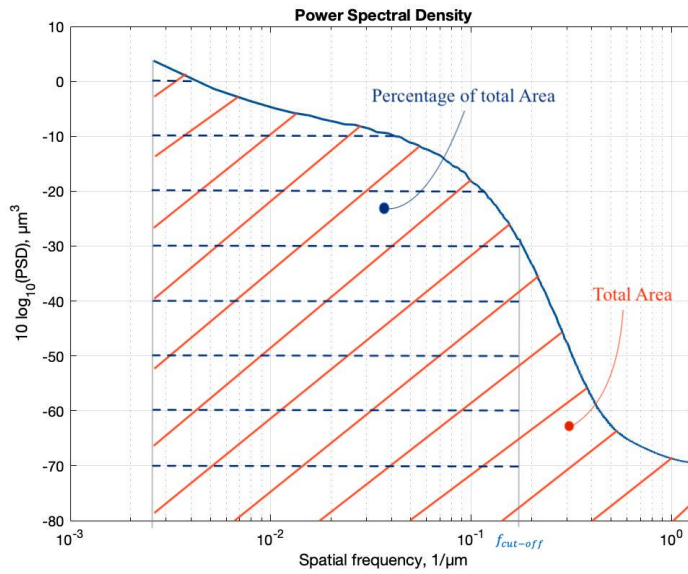


Figure 2.15: Cut-off frequency determined with area method

The parameter n_{Area} can be modified in order to change the cut-off frequency. If its value is increased, the cut-off wavevector will be greater, therefore the relevant distance ω_x or ω_y will be smaller. On the other side, if n_{Area} is decreased, the relevant distance will be greater (the cut-off frequency will be smaller). Figure 2.16 shows how the cut-off frequency changes varying the parameter n_{Area} .

At this stage, the typical value for n_{Area} can be studied. The samples analysed are the ones used during the tests (see §3.1 and §3.2) and for each one the best value of the area's percentage is searched. In Table 2.1 the best n_{Area} values for some of the samples are presented. As it can be seen, the value for n_{Area} varies from 30 to 50%. In order to choose the best value of the percentage, the parameter err_{perc} is kept below 5%. The two values, *Range x* and *Range y*, represent the length of the cropped surface by the 300×300 matrix in x- and y-direction:

$$Range\ x = 300 * \omega_x; \quad (2.12)$$

$$Range\ y = 300 * \omega_y. \quad (2.13)$$

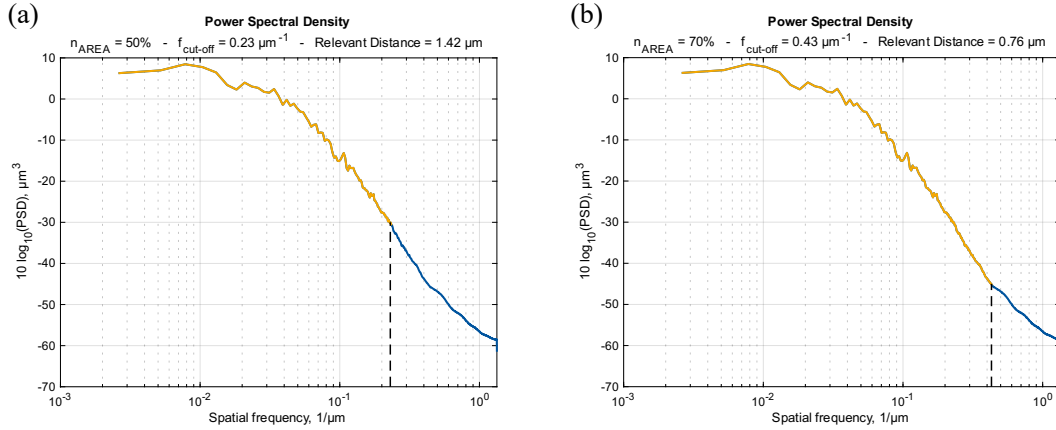


Figure 2.16: Variation of n_{Area} in cut-off area method. With $n_{Area} = 50\%$ (a) the cut-off frequency is smaller, so the relevant distance is greater, with $n_{Area} = 70\%$ (b) the cut-off value is bigger (relevant distance smaller).

Surface Name	n_{Area} [%]	ω_x [μm]	ω_y [μm]	err_{perc} [%]	Range x [μm]	Range y [μm]	R_a
M1_40grad_10min	40	1,50	-1,88	3,95	449	561	0,335
F1_40grad_5min	40	2,2	-2,24	0,73	658	670	0,15
M1_40grad_5min	35	1,50	-1,88	5,26	449	562	1,145
M_new	40	1,5	-1,42	0,09	449	425	0,09
M1_40grad_5min	50	0,85	-1,12	0,37	254	335	1,14
F1_40grad_60min	30	2,63	-2,63	2,03	786	786	0,199
M1_40grad_10min	50	1,14	-1,26	0,58	342	378	0,34

Table 2.1: Optimal n_{Area} value for different samples. The two relevant distances (ω_x and ω_y), err_{perc} , the roughness R_a and the length of the Flow Matrix in x-direction (Range x) and in y-direction (Range y) are also indicated).

In order to understand how the parameter n_{Area} influences the relevant distance, ω_x or ω_y , Figure 2.17 shows some x-sections of the original surface compared with the same sections but of the cropped surface by the 300×300 matrix for different values of n_{Area} . The surface under consideration is the one named as “M0,5_40grad_15min”. It may be noticed that the length of the *Flow Matrix* section increases when n_{Area} increases because the relevant distance ω_x becomes bigger. Of course, if the relevant distance is bigger, the error will be also bigger. In fact, the err_{perc} value increases with the increasing of n_{Area} . In Figure 2.18 there is a magnification of Figure 2.17(d) in order to observe that, with the percentage set to 25%, the error of the *Flow Matrix* is too large, and the surface is not reconstructed well.

2.4 – Cut-Off Frequency

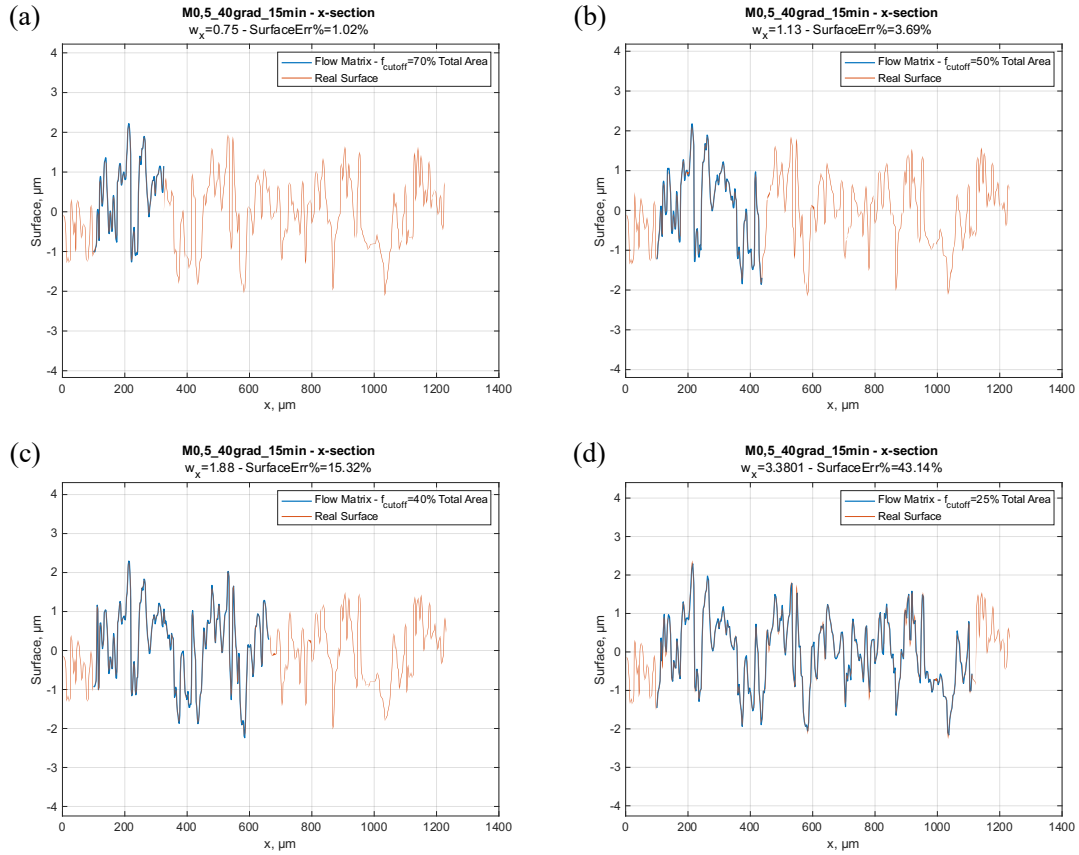


Figure 2.17: x -section of the sample $F0,5_{40grad_{15min}}$ compared with its Flow Matrix graph with different values of n_{Area} : 70% (a), 50% (b), 40% (c) and 25% (d). The relevant distance w_x and err_{perc} as $SurfaceErr\%$ is also indicated.

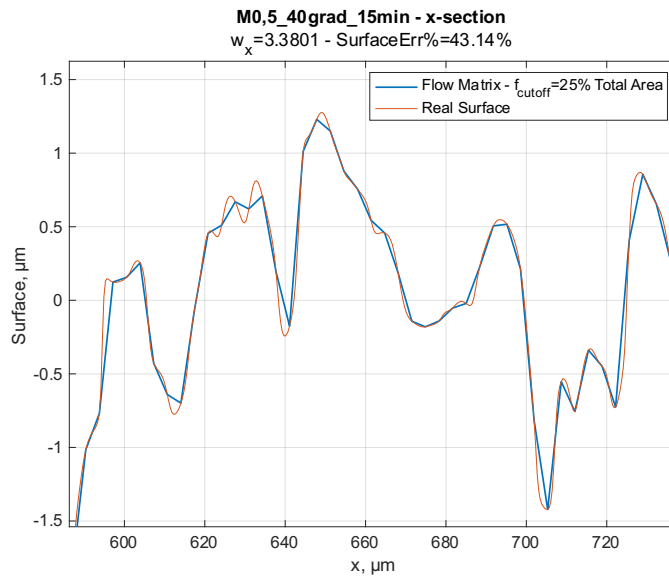


Figure 2.18: Magnification of Figure 2.17(c).

2.4.2 Minimum method to determine cut-off frequency

This method defines the cut-off frequency as the wavevector where the PSD reach a certain percentage, n_{Min} , of its minimum value, Figure 2.19.

$$f_{cut-off} \rightarrow PSD = n_{Min} \cdot \min(PSD). \quad (2.14)$$

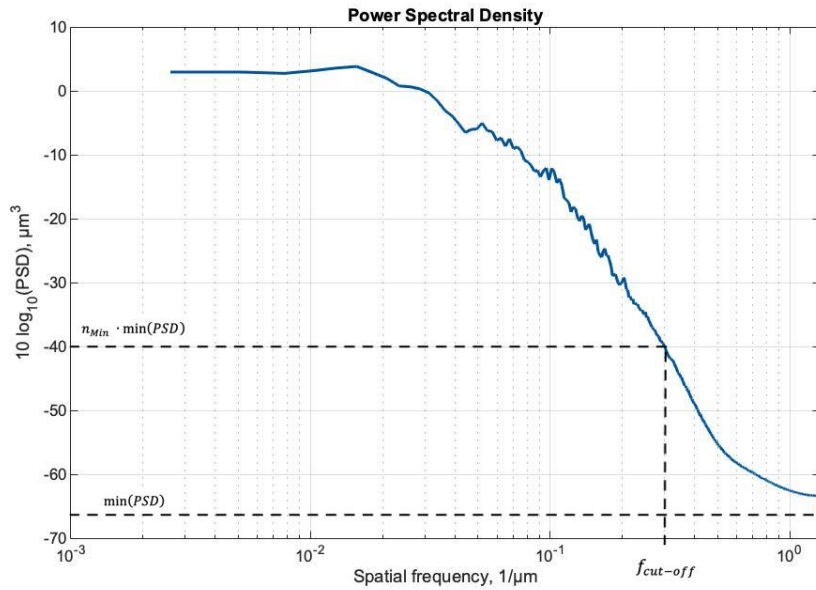


Figure 2.19: Cut-off frequency determined with area method

In this case, the parameter of variation is n_{Min} and it works similarly to n_{Area} . In fact, if this value is increased, the relevant distance will decrease because the cut-off frequency increases. Quite the opposite, if n_{Min} is decreased, the cut-off wavevector will also decrease and the relevant distance increases.

Even in this case, therefore, the typical values of n_{Min} are studied for the samples used during the test. In Table 2.2 the best values of n_{Min} for some of the samples are presented. It is remembered that, in order to choose the best value for the percentage of the PSD min, the parameter err_{perc} is kept below 5%. Looking at the table it can be noticed that the n_{Min} values are more random than the n_{Area} values found in the previous method. In fact, the range where the percentage of the min varies is very large here. For some samples it is 40%, while for others it is 80%. So, there is not a real typical value or range for n_{Min} because this method is strongly influenced by the material and its roughness. For this reason, using this method is a little more complex and sometimes a lot of attempts are required to

obtain the perfect n_{Min} value. Anyway, this is presented in this thesis because it gives the best results for some samples.

<i>Surface Name</i>	n_{Min} [%]	ω_x [μm]	ω_y [μm]	err_{perc} [%]	<i>Range x</i> [μm]	<i>Range y</i> [μm]	<i>Ra</i>
F0,5_40grad_5min	40	2,13	-2	0,62	637	598	0,11
F1_40grad_5min	50	1,85	-1,48	0,51	553	443	0,15
F1_40grad_10min	40	2,1	-1,91	0,59	628	571	0,15
M2_40grad_5min	80	0,79	-0,41	0,79	236	122	0,69
M2_40grad_10min	80	0,41	-0,39	0,55	123	117	0,88
M3_40grad_5min	55	1,52	-1,05	0,71	455	314	0,65

Table 2.2: Optimal n_{Min} value for different sample. The two relevant distance (ω_x and ω_y), err_{perc} , the roughness R_a and the length of the Flow Matrix in x-direction (*Range x*) and in y-direction (*Range y*) are also indicated.

2.4.3 Error method to determine cut-off frequency

The input of this method is the value of err_{perc} which is wanted as target. Then, the relevant distance, ω_x and ω_y , is set up to zero and it is increased step by step until the value of err_{perc} reaches the target. This method does not take into account the PSD and, for this reason, it is useful only to refine the final results. In other words, it could happen that, with the other two methods, it is not possible to find a certain result because the cut-off frequency could not vary linearly and sometimes it could change a lot with a little increase of input parameter. So, if a defined relevant distance is wanted, this method will allow to obtain it.

2.4.4 Comparison between filter and no filter surfaces

When the filter (§2.2) is applied, the large wavevectors are modified. In fact, the Gaussian filter is a low-pass filter and this behavior can be noticed looking at the PSD of the surface with and without filter, Figure 2.20. The graphs show the PSD for the same surface in x-direction, Figure 2.20 (a), and y-direction, Figure 2.20 (b), with different intensity of the filter. When the intensity of the filter increases (σ increases) the PSD at large wavevector decreases and the bigger the sigma, the more the PSD changes. So, if the filter is applied, the cut-off frequency will be modified: in particular, its value will be bigger because the information about the larger wavevectors is erased by the filter.

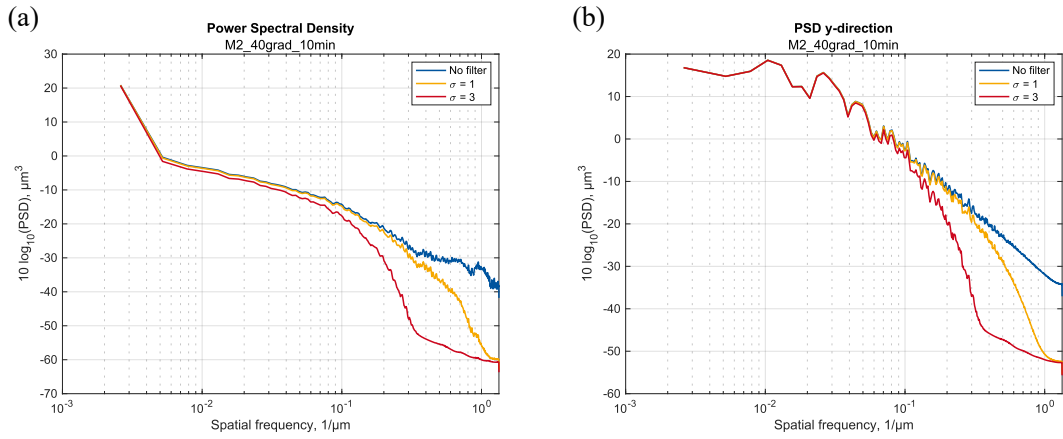


Figure 2.20: Power Spectral density in x-direction (a) and y-direction(b) for different value of filter intensity.

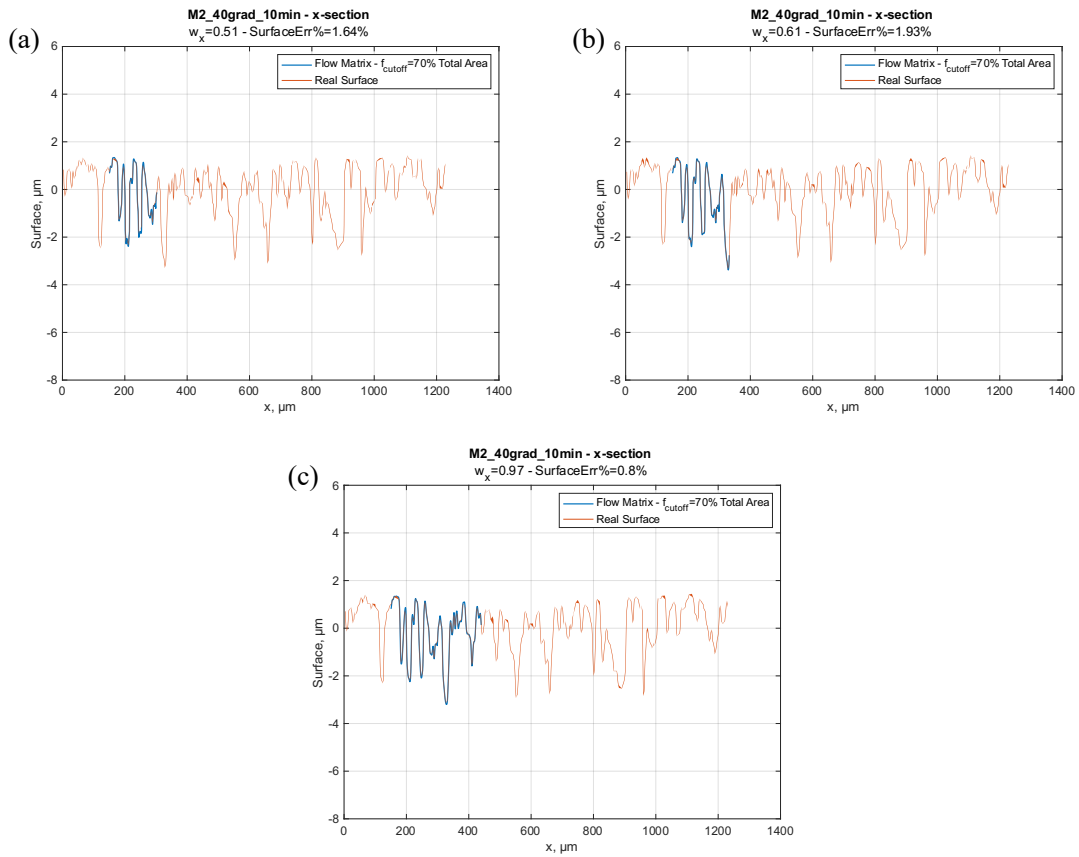


Figure 2.21: Relevant distance for the same surface and same percentage of the cut-off method but with different intensity of the filter: no filter (a), $\sigma = 1$ (b) and $\sigma = 3$ (c).

Figure 2.21 shows an example: all the three images are about the same surface and the same cut-off frequency (with the area method and $n_{Area} = 70\%$). In Figure 2.21(a) the filter is not applied, in Figure 2.21(b) the filter is applied with $\sigma = 1$ and in Figure 2.21(c) the filter is applied with $\sigma = 3$. It can be seen that the relevant distance ω_x increases if the intensity of the filter increases, the reason is

that the cut-off frequency shifts on the left due to the modification of the PSD by the filter. So, if the cut-off wavevector is smaller the relevant distance will be bigger. Furthermore, it is also interesting to observe the err_{perc} value: as expected, in Figure 2.21(b) it is bigger than Figure 2.21(a), being ω_x , but in Figure 2.21(c) err_{perc} is the smallest even if ω_x is the biggest. The reason is that the filter was too powerful, and the surface becomes smoother: in this way, even with a bigger relevant distance, the error is smaller. Of course, it is important to use the filter with moderation, even if a lot of information about the surface would get lost.

2.4.5 Grid size influence

During the measurement scanning, the grid size of the measured points can be chosen. If this size is small, the precision of the measurement will be higher. It is seen that this dimension influences the PSD (Figure 2.22) and, in this way, it also influences the two relevant distances, ω_x and ω_y .

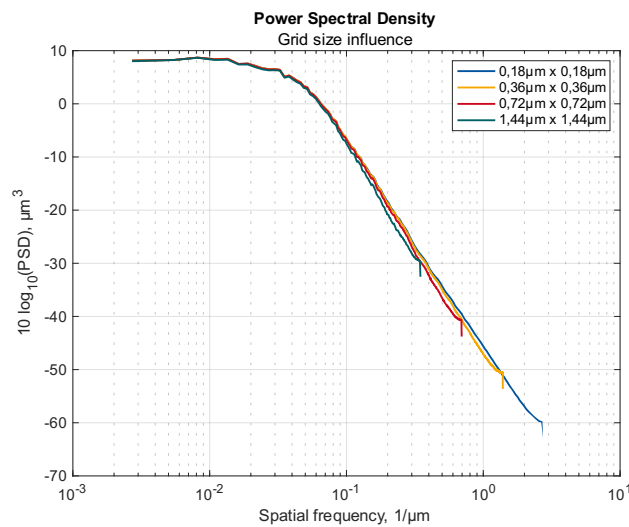


Figure 2.22: Influence of grid size in the calculation of Power Spectral Density.

In particular, if the grid size is small, the relevant distance will also be small; if the grid size increases, the relevant distance will also increase; an example is presented in Figure 2.23. The surface, the cut-off method chosen, and its relative percentage are the same for all the four graphs, the only difference is in the grid size. In Figure 2.23(a) the grid size is the smallest and the relevant distance is the smallest too, but from Figure 2.23(b) to (d) the grid size increases and the relevant distance increases with it.

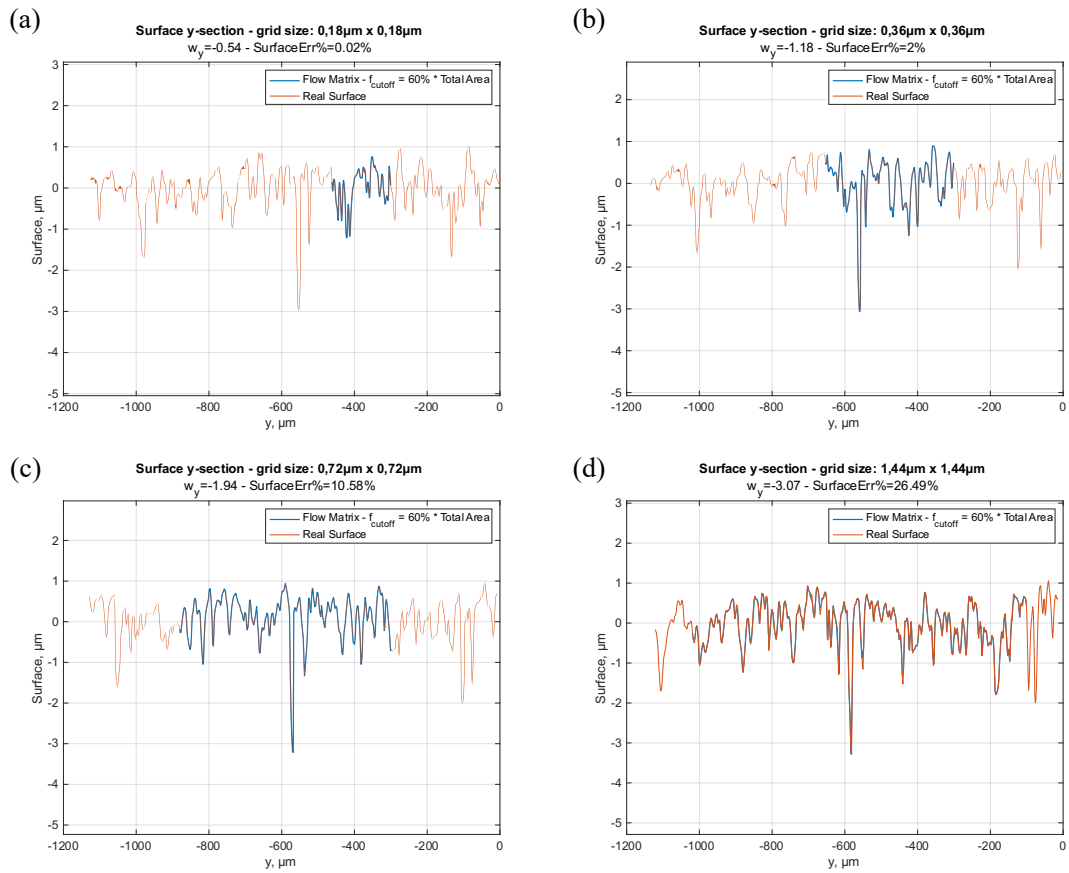


Figure 2.23: Grid size influence on the determination of the relevant distance ω_y . The surface, the cut-off method and the percentage of the cut-off method are the same for all the graphs. The only difference is the grid size of the measurement scanning: $0,18\mu\text{m} \times 0,18\mu\text{m}$ (a), $0,36\mu\text{m} \times 0,36\mu\text{m}$ (b), $0,72\mu\text{m} \times 0,72\mu\text{m}$ (c) and $1,44\mu\text{m} \times 1,44\mu\text{m}$ (d).

Chapter 3

Experimental Tests and Results

This chapter will present the experimental tests carry out and the reason why that kinds of parameters are chosen. Three parameter variations are investigated: time influence, load influence and oil temperature influence. The surface variations and the flow factor variations will be shown for each parameter. Furthermore, the sample dimensions and the material proprieties will be specified.

3.1 Samples

As indicated in §1.7, the test bench is a disc-on-disc tribometer. This means that the two samples will be two discs: one of them will be fixed, the other will rotate instead. Their dimensions and materials are different. For the fixed one the material chosen is steel, the opposite disc is made of brass. Their proprieties are indicated in Table 3.1 and a photo of them is shown in Figure 3.1. The upper disc (the fixed ones, the one on the left in Figure 3.1) has an outer diameter bigger than the opposite disc and has two groves in order to improve the tribosystem behavior, reducing the friction and providing a better lubrication. The contact area is the one between the outer diameter of the rotating disc (the one on the right in Figure 3.1) and the inner diameter if the fixed disc (the one on the left in Figure 3.1).

		<i>Steel</i>	<i>Brush</i>
<i>Bulk modulus</i>	<i>MPa</i>	210000	90000
<i>Poison number</i>	—	0,3	0,3
<i>Plastic flow pressure</i>	<i>MPa</i>	650	300

Table 3.1: Material proprieties.



Figure 3.1: Photos of the two sample. The stationary steel disc is on the left and the rotating brass disc is on the right.

3.2 Experimental tests

Tribosystems are affected by several parameters: time, temperature, type of oil, type of material, speed rotation, etc. Studying all of them would be impossible, so the three most important were considered: time, oil temperature and normal load. Once the parameters to study are chosen, some typical values for each of them must be decided, in order to have a perfect representation of their influence. The durations of the tests are correlated to the run-in process: the different test durations will be chosen so that surfaces would be undergoing different modification up to the steady state. The oil temperature influences the viscosity of the oil, reducing the fluid film thickness: its values will be chosen from a low value, where the oil viscosity is high, to a temperature where the oil viscosity is very low. At the end, the normal load increases the friction force and influences surface wear: its values are chosen from a very low (low friction force) to a high value, which involves a high pressure and friction force. Given that there are four couples of discs, four values will be chosen for each parameter. They are presented in Table 3.2. It should be noticed that for the temperature there is one more value because all the tests for the time and load were performed at 40°, then the tests for the oil temperature variation are carried out for the other four temperatures.

<i>Time</i>	<i>Load</i>	<i>Oil Temperature</i>
<i>5 min</i>	<i>0,5 MPa</i>	<i>40°</i>
<i>10 min</i>	<i>1 MPa</i>	<i>50°</i>
<i>15 min</i>	<i>2 MPa</i>	<i>60°</i>
<i>60 min</i>	<i>3 MPa</i>	<i>70°</i>
		<i>80°</i>

Table 3.2: Time, load and oil temperature values for the performed tests.

3.2 – Experimental tests

At this point, the combinations between those values need to be define, in order to take as less tests as possible. So, first of all the load and time influence was studied, setting the oil temperature to 40°. Before each test, the disc surfaces were grinded with the sandpaper in order to have a very smooth surface. As previously said, there were four couples of discs, so for every day of testing, all the loads were tested for a certain test duration and then the surfaces were scanned with the microscope. After that, all the disc surfaces were grinded with the sandpaper in order to have the same surface as the beginning of the previous test and then the next test was performed. The plan of the tests is clearly presented in Table 3.3. Note that the loads are expressed in terms of pressure, the test bench applies a normal force with a hydraulic piston instead. The normal force is easy to compute from the pressure when knowing the nominal contact area.

Once the load and time influence were carried out, the oil temperature influence was analysed. Looking at the result of the previous tests, it was observed that: the two most significant loads were 1 MPa and 2 MPa; the most significant duration was 15 min. Thus, the temperature variation was applied for the previously mentioned load with a duration of 15 min, see Table 3.4.

	<i>1° day of testing</i>	<i>2° day of testing</i>	<i>3° day of testing</i>	<i>4° day of testing</i>
<i>0,5 MPa</i>	5 min	10 min	15 min	60 min
<i>1 MPa</i>	5 min	10 min	15 min	60 min
<i>2 MPa</i>	5 min	10 min	15 min	60 min
<i>3 MPa</i>	5 min	10 min	15 min	60 min

Table 3.3: Plan of the tests for load and time influence, oil temperature set to 40°.

	<i>1° day of testing</i>	<i>2° day of testing</i>
	<i>1 MPa</i>	<i>2 MPa</i>
<i>50°</i>	15 min	15 min
<i>60°</i>	15 min	15 min
<i>70°</i>	15 min	15 min
<i>80°</i>	15 min	15 min

Table 3.4: Plan of tests for oil temperature influence.

After each test, all the samples were denominated with a code. The structure of the code is composed by letter and number. The first letter specifies the type of disc:

- *F* means the stationary disc.
- *M* means the rotating disc.

Immediately after there is a number indicating the value of the pressure applied to the samples. Then, an underscore divides the load information to the oil temperature information and after another underscore the information about the duration of the test is specified. For instance, the stationary disc of the five minutes runtime test, with 1 MPa of load and 40° of oil temperature, is denominated as: *F1_40grad_5min*.

3.3 Surface Variation during run-in period

In this section the surface variation during the first period of work is presented. Roughness and contact area changes will be discussed. Furthermore, the friction torque as function of time for different load will be analysed in order to understand the run-in phenomenon.

Understanding that the run-in depends on several factors is crucially important: if one of them is changed, the run-in behaviour changes as well. In this thesis, the focus is on load and temperature variations. Figure 3.2 shows the coefficient of friction as a function of time for different loads. It can be seen that the friction behaviour is very different when changing the load. In particular, friction starts with very high values for all the loads, except for 3 MPa, where the torque has an oscillatory behaviour. A possible cause could be that the pressure is too high, and the surfaces change very much and quickly. In fact, in Table 3.5 this behaviour is clear. In this table the roughness of the two discs after the 3MPa tests for different duration are presented and, when looking at the rotating disc it is clear that also the roughness has an oscillatory behaviour: for 5 min the roughness increases very much, which means that the surface was subjected to a high run-in process and several effects occur in the surface, like erosion, chemical reaction, etc. Then, the friction increases rapidly and the surface becomes smoother, there is a very high peak of torque before the 10 min runtime, so maybe the highest asperities broke and thus the roughness decreases, see Table 3.5. As the surface is very smooth, the friction decreases until around 25 minutes and then increases again. After 60 minutes the surface roughness is very high but, in this case, the steady-state is not reached because it takes more time with such a high load. The stationary surface is the steel disc, which is harder than the brass one, indeed its roughness changes less and it is almost constant from 5 min to 10 min see Table 3.5. Then, it starts to increase, which means that wear, erosion and chemical effects began.

On the other hand, with the other three loads the steady-state is reached. The best behaviour is obtained with 2 MPa: after an initial period with a very high friction, the surface reaches the steady-state and the friction coefficient remain low and constant for the rest of the time. A similar behaviour is observed for 0,5 MPa and 1 MPa, but in those cases the steady-state is not fully reached and the

friction is a little bit higher. For 0,5 MPa, after a couple of minutes the steady-state is reached but it is only temporary. In fact, after 40 minutes the friction torque increases a little bit and another steady-state is reached but the friction here is higher and unstable. On the other hand, for 1 MPa the friction torque increases slightly during the whole period. The roughness variations for those tests are reported in Appendix A. What is usually expected is that friction increases by increasing the load. The reason why with 2 MPa the friction is lower than the one with smaller pressures could be due to the control system of the test bench. Of course, the normal force is not perfectly constant, it has some fluctuation. Thus, if the load is low, these fluctuations could lead to a loss in the contact between the two surfaces, involving the subsequent impact when they return in contact, or they can rotate increasing the wear of surfaces. This behaviour is also confirmed by looking at the relative contact area after 5 minutes for different loads, see Figure 3.3. Here, it can be seen that the relative contact area for 0.5 MPa starts to be different from zero for a highest value compared to the other loads. This means that the surface is rougher and has asperities with a highest height. On the other hand, when the load is higher, the contact loss is more difficult but of course friction force tends towards a highest value due to more load. However, the best compromise is probably reached with 2 MPa.

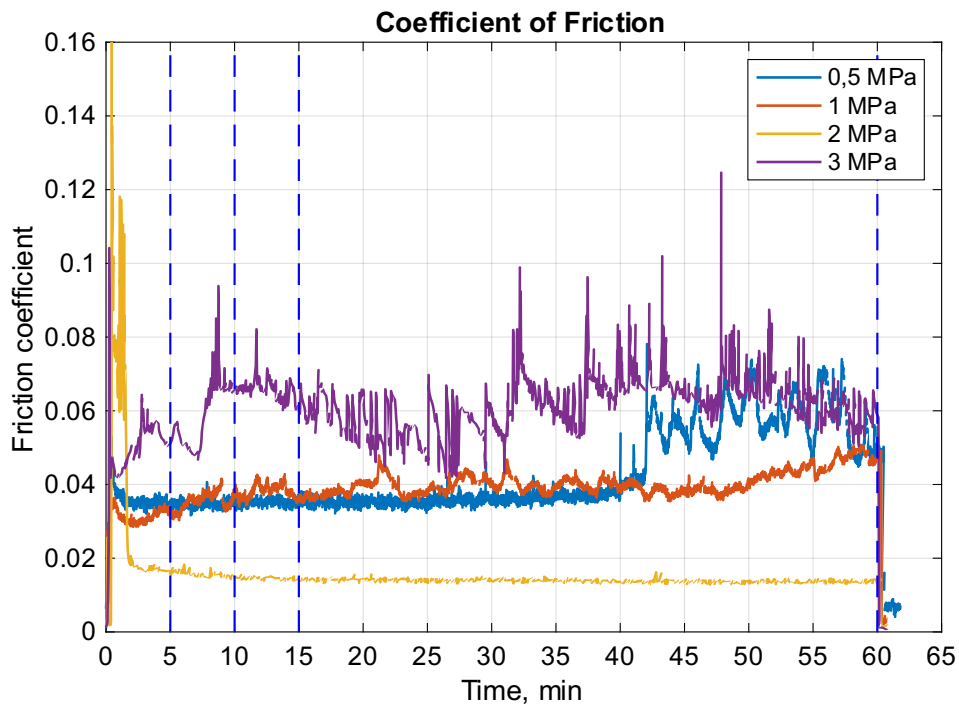


Figure 3.2: Coefficient of friction as a function of time for different load pressures. The blue dotted lines specify the duration for which tests are carried out.

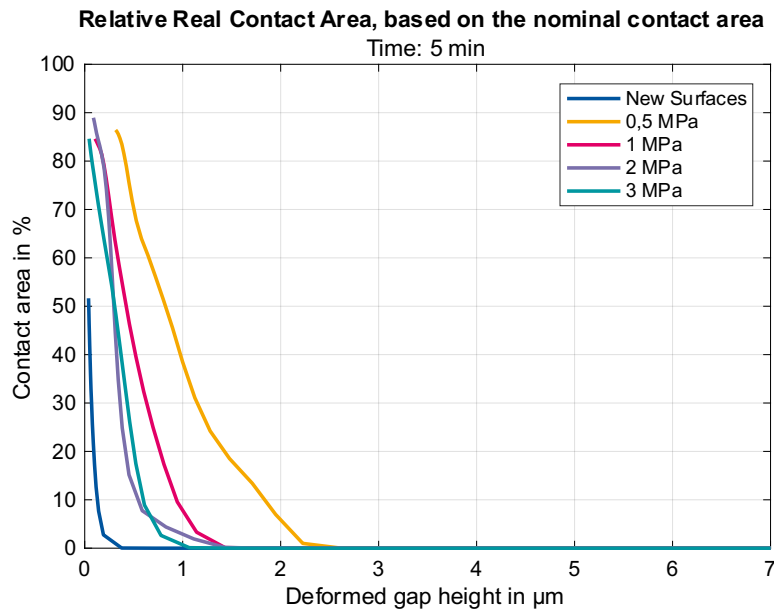


Figure 3.3: Relative contact area computed as the ratio between the real contact area and the nominal contact area after 5 minutes runtime for different loads.

<i>Rotating discs</i>			<i>Stationary discs</i>		
	<i>Ra</i>	<i>Rq</i>		<i>Ra</i>	<i>Rq</i>
<i>M_new</i>	0,094	0,766	<i>F_new</i>	0,053	0,072
<i>M3_40grad_5min</i>	0,654	0,834	<i>F3_40grad_5min</i>	0,141	0,204
<i>M3_40grad_10min</i>	0,305	0,394	<i>F3_40grad_10min</i>	0,120	0,165
<i>M3_40grad_15min</i>	0,477	0,709	<i>F3_40grad_15min</i>	0,233	0,287
<i>M3_40grad_60min</i>	1,895	2,954	<i>F3_40grad_60min</i>	1,262	1,637

Table 3.5: Roughness variation of the test with 3 MPa for different durations.

Regarding the oil temperature influence, Figure 3.4 shows friction torque variations for different oil temperature for a load of 2 MPa and 15 minutes of test duration. For an oil temperature set to 40 degree, the friction is the lowest one. In fact, the oil has a higher viscosity and the lubricant thickness is thicker. For 60 degree the behaviour is almost the same, although the run-in effect is a little bit longer. By increasing the temperature, the fluid viscosity decreases and so the lubricant thickness also decreases. The final result is an increasing of the friction force. Anyway, a strange behaviour is observed with 50°. In fact, what is expected is that the coefficient of friction for 50° is almost the same of 60° or 40°, maybe an intermediate condition. But it is the one with the highest coefficient of friction. There is not a clear explanation for this, maybe a problem during the test occurs. More inspections

have to be done in order to understand the causes. By decreasing the load, see Figure 3.4 and Figure 3.5, the oil temperature influence decreases. Figure 3.5 shows friction coefficient variation for different oil temperature for a load of 1 MPa and 15 minutes of test duration. The friction seems more stable for all the temperatures, of course with the maximum temperature the friction is the highest because of the reduction of the lubricant viscosity. Anyway, the friction for 40°, 50° and 70° is almost the same, differently from what happened for 2 MPa. The lowest friction force occurs for 60°, so may be this is the best oil temperature because the friction torque is the lowest one with both loads.

What is also remarkable about the temperature influence on the surface roughness is that by increasing the oil temperature, the roughness decreases. Table 3.6 and Table 3.7 show this behavior: for 2 MPa it is well clear, for 1 MPa the roughness increases a little bit for 70° but then it decreases again. In both cases for 80° the surfaces are very smooth. The reason is probably due to the breaking of asperity peaks because of the decreasing of the lubricant viscosity. In fact, the viscosity decreases when the temperature is higher: with a smaller viscosity the lubricant film is thinner and the asperities may come into contact more frequently, breaking the highest peaks.

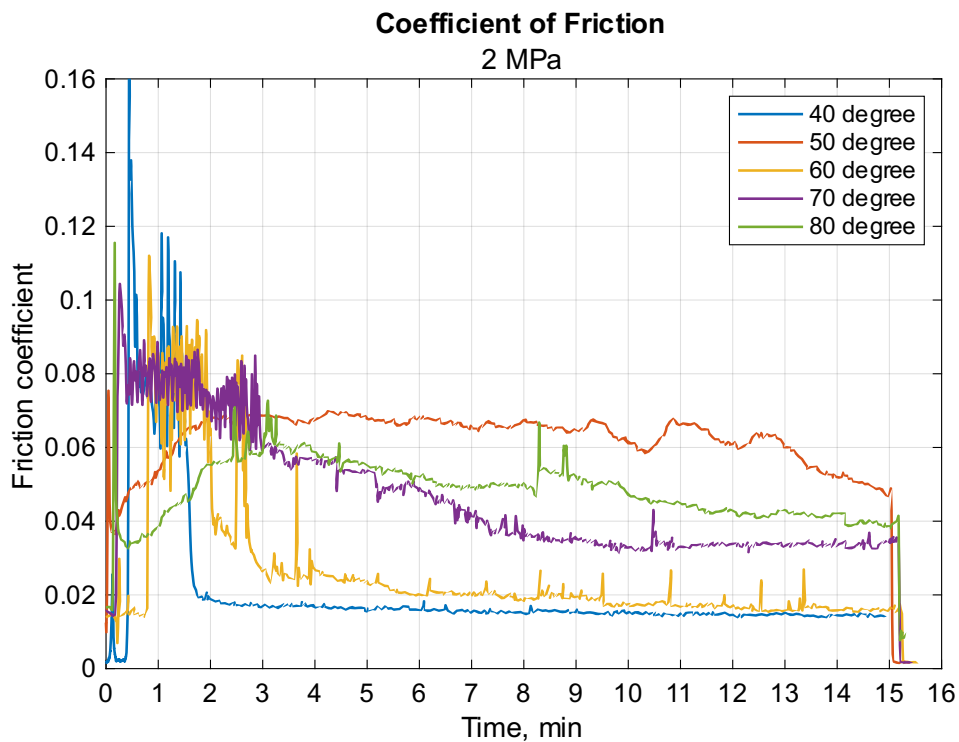


Figure 3.4: Coefficient of friction as a function of time for different oil temperature. The load is set to 2 MPa.

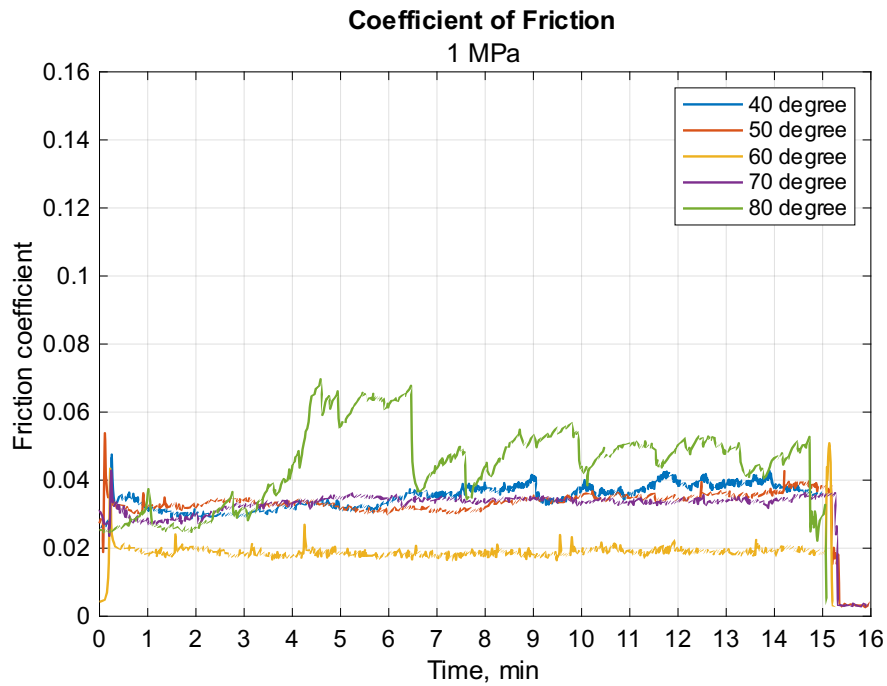


Figure 3.5: Coefficient of friction as a function of time for different oil temperature. The load is set to 1 MPa.

<i>Rotating discs</i>			<i>Stationary discs</i>		
	<i>Ra</i>	<i>Rq</i>		<i>Ra</i>	<i>Rq</i>
<i>M1_40grad_15min</i>	0,620	0,781	<i>F1_40grad_15min</i>	0,266	0,994
<i>M1_50grad_15min</i>	0,459	0,673	<i>F1_50grad_15min</i>	0,148	0,230
<i>M1_60grad_15min</i>	0,482	0,682	<i>F1_60grad_15min</i>	0,075	0,098
<i>M1_70grad_15min</i>	0,619	0,752	<i>F1_70grad_15min</i>	0,142	0,180
<i>M1_80grad_15min</i>	0,196	0,279	<i>F1_80grad_15min</i>	0,111	0,143

Table 3.6: Roughness variation of the 15 min runtime and 1 MPa tests for different oil temperature.

<i>Rotating discs</i>			<i>Stationary discs</i>		
	<i>Ra</i>	<i>Rq</i>		<i>Ra</i>	<i>Rq</i>
<i>M2_40grad_15min</i>	0,847	2,042	<i>F2_40grad_15min</i>	0,128	0,181
<i>M2_50grad_15min</i>	0,702	2,721	<i>F2_50grad_15min</i>	0,119	0,163
<i>M2_60grad_15min</i>	0,493	0,611	<i>F2_60grad_15min</i>	0,093	0,127
<i>M2_70grad_15min</i>	0,407	0,533	<i>F2_70grad_15min</i>	0,216	0,277
<i>M2_80grad_15min</i>	0,285	0,391	<i>F2_80grad_15min</i>	0,199	0,380

Table 3.7: Roughness variation of the 15 min runtime and 2 MPa tests for different oil temperature.

3.3 – Surface Variation during run-in period

Studying the contact area and the solid contact pressure for different test duration is also very interesting. Figure 3.6 shows the relative contact area computed as the ratio between the real contact area and the nominal contact area, so it is a percentage. It can be noticed that with the lowest load, 0,5 MPa, the surface undergoes most of the changes during the first 5 minutes, then it has little changes and after 60 minutes it reaches an intermediate condition between the 10 minutes runtime and 15 minutes runtime. When increasing the load, the surfaces after 5, 10 and 15 minutes come into contact for a lower gap height. This is probably due to the highest asperities broken under high load. In this way, the asperities height is lower and the contact starts for a smaller gap height. This is also confirmed by looking at the abbot curve, Figure 3.7. Abbot curves for different load are plotted for 5 minutes runtime because it is the duration that shows more clearly this phenomenon. For the stationary surface, the changes of the topography of the surface are very little, as expected, because it is the hardest material. On the other hand, it is clear that the surface peaks decrease with the increasing of the load. For 0,5 MPa, the 0% of material is reached around $2,5 \mu\text{m}$, for 3 MPa it is reached under $1 \mu\text{m}$ instead.

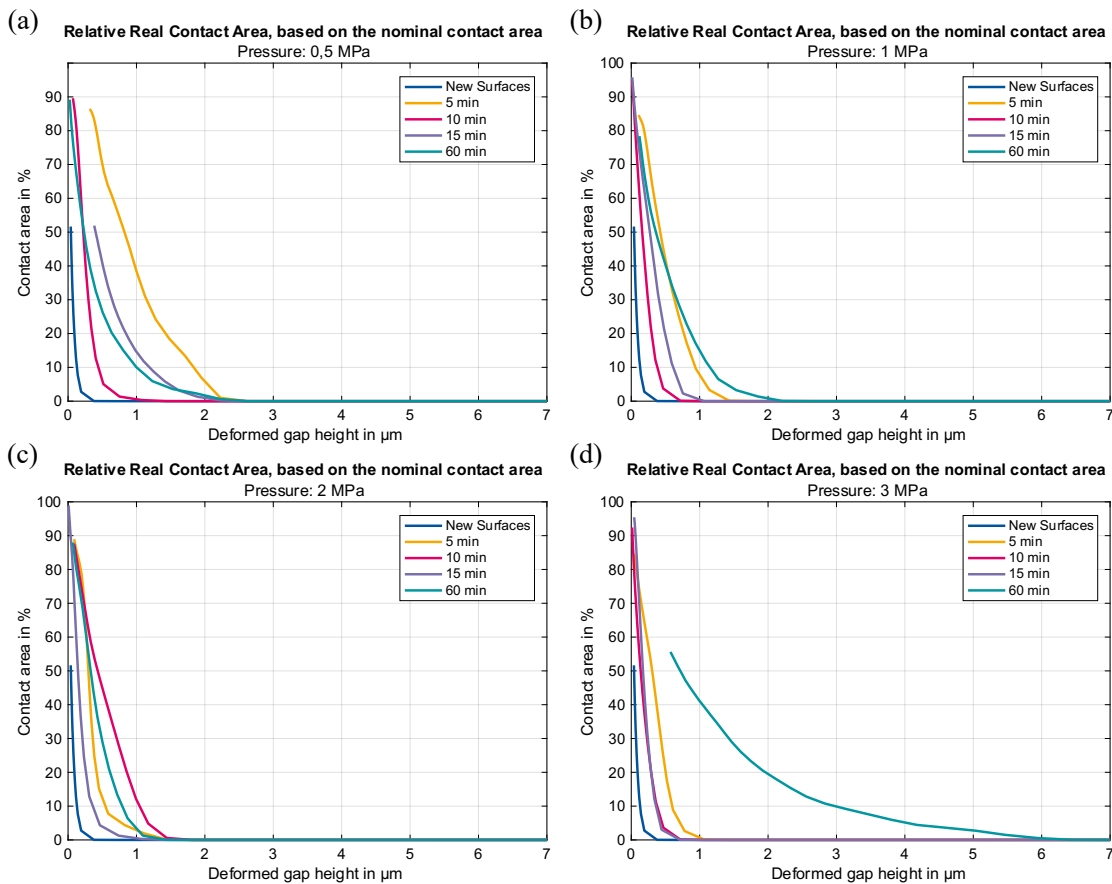


Figure 3.6: Relative contact area computed as the ratio between the real contact area and the nominal contact area. (a) is for a pressure of 0,5 MPa, (b) for 1 MPa, (c) for 2 MPa and (d) for 3 MPa.

For 3 MPa, the load is very high, and the surface after 60 minutes is very rough, see Figure 3.6(d). Anyway, from 10 minutes and 15 minutes a wear steady-state is reached and both the surface and the contact area remain almost the same. The wear steady-state and the friction steady-state are usually correlated but they are not the same thing and sometimes only one of them could be reached.

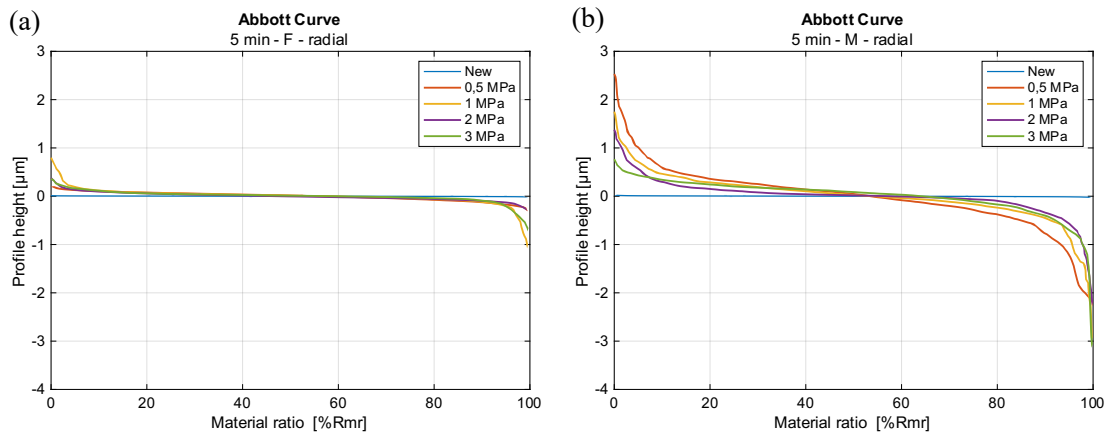


Figure 3.7: Abbot curve direction of 5 min runtime tests for different loads. On the left the Abbot curve of the stationary discs in the radial direction and on the right the one of the rotating discs, always for the radial direction.

3.4 Flow Factors

In this section, the Flow Factors will be analysed. Tests using different load, duration and oil temperature will be compared. In order to have a better comparison, all the graphs are plotted for the same ordinate range. In this way it is easy to compare the different graphs. Furthermore, all the graphs are drawn as function of the deformed gap-height and, since the most common gap-heights in hydraulic systems are in the range from $3 \mu\text{m}$ to $30 \mu\text{m}$, the x graph values are in the same range.

The pressure flow factor in x- and y-directions and the shear flow factor in x- and y- directions will be examined. Regarding the pressure flow factor, positive values are expected for the x-direction and negative ones for the y-direction. This is because the scratches due to the sliding are in y-direction, see Figure 3.8. Thus, given that the calculation of the pressure flow factor along x is done by applying a pressure gradient in x-direction and so the fluid flow is on y-direction, the flow will be assisted by the grooves of the surfaces; on the other hand, the calculation for pressure flow factor in y-direction is done by applying a pressure gradient in y-direction (flow along x), so the grooves will obstruct the flow and the pressure will increase. In other word, the γ value defined in §1.6.1 is greater than 1 in x-direction and lower than 1 in y-direction.

The expected shear flow factors will be almost zero in x-direction, because the direction of the lay is aligned with the main flow direction. So, there is not an increasing or decreasing flow due to lubricant trapped into the roughness valleys. On the other hand, the expected shear flow factors for the y-direction will be negative due to the flow stuck into the roughness valleys.

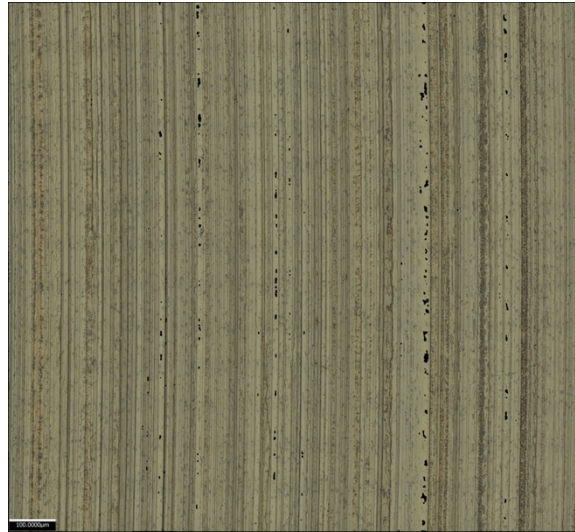


Figure 3.8: Surface of brass disc after 10 minutes of work under 2 MPa of normal load and 40° of oil temperature. The grooves are verticals because the sliding was in y-direction.

3.4.1 Influence of Time

The influence of time on the flow factor is carried out for each of the four contact pressure applied (0.5, 1, 2 and 3 MPa), with the oil temperature set to 40°. The four different durations studied are: 5, 10, 15 and 60 minutes. Anyway, the most relevant ones are for 1 MPa and 2 MPa. Figure 3.9 and Figure 3.10 show the pressure flow factor in the two dimensions for those two pressures. It can be noticed from these graphs that after 5 minutes and after 60 minutes the pressure flow factors are equal. This may mean that after 5 minutes the steady state is reached but only temporarily. Then, another run-in process starts, and the final steady-state is definitely reached after 60 minutes. Furthermore, by increasing the load the influence of flow factors decreases a little bit and the reason may be that more load makes the surface smoother, thus its influence is smaller. Moreover, the pressure flow factor for 10 minutes runtime and 2 MPa (Figure 3.10) increases its values compared to the 5 minutes runtime, but it decreases with 1 MPa instead (Figure 3.9). Then, after 15 minutes the pressure flow factor values in x-direction for 2 MPa (Figure 3.10) are almost the same of the 1 MPa test after 10 minutes. This could be because the run-in process takes more time with more load. So, the same surfaces topography

could be reached either after 10 min and 1 MPa or after 15 minutes and 2 MPa. Notice that the pressure flow factors are equal to 1 for the new surfaces for all the deformed gap-heights because the surfaces are very smooth and their influence is negligible. In addition, if the deformed gap-height is high enough, the pressure flow factors are equal to 1 as well, because the surface roughness does not influence the lubricant flow anymore.

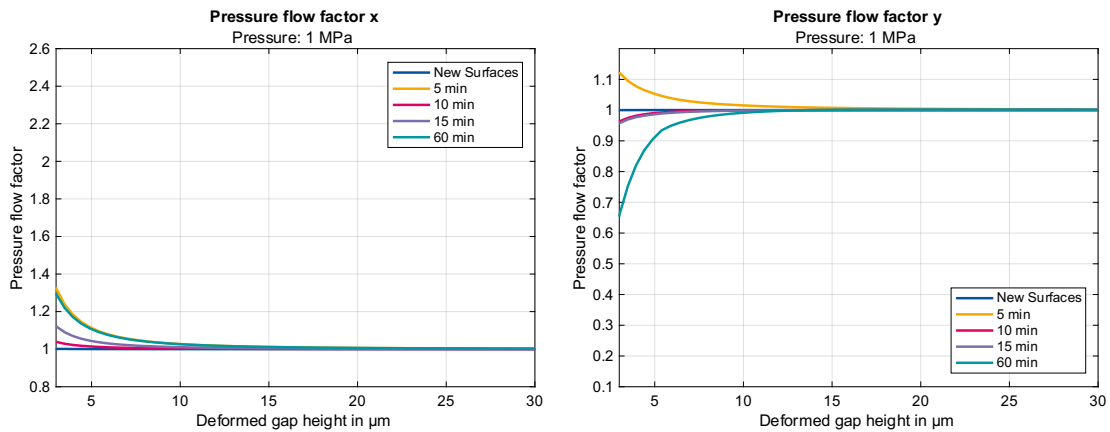


Figure 3.9: Pressure flow factor in x- and y-direction with 1 MPa of pressure load.

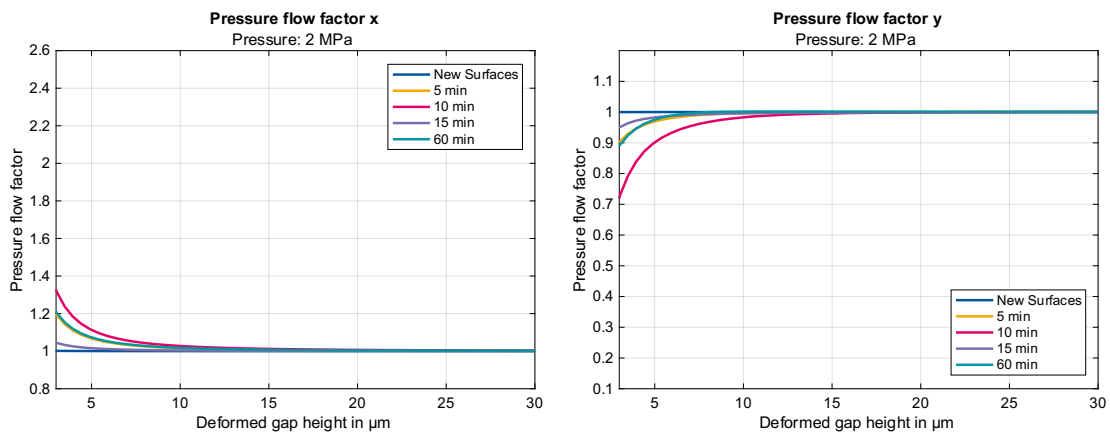


Figure 3.10: Pressure flow factor in x- and y-direction with 2 MPa of pressure load.

The pressure flow factor curve in y-direction for 1 MPa and 5 minutes of runtime in Figure 3.9 is positive because the direction of the scratches are not perfectly vertical, see Figure 3.11. Thus, the flow in y-direction is not totally impeded by the roughness as it could be if they were vertical.

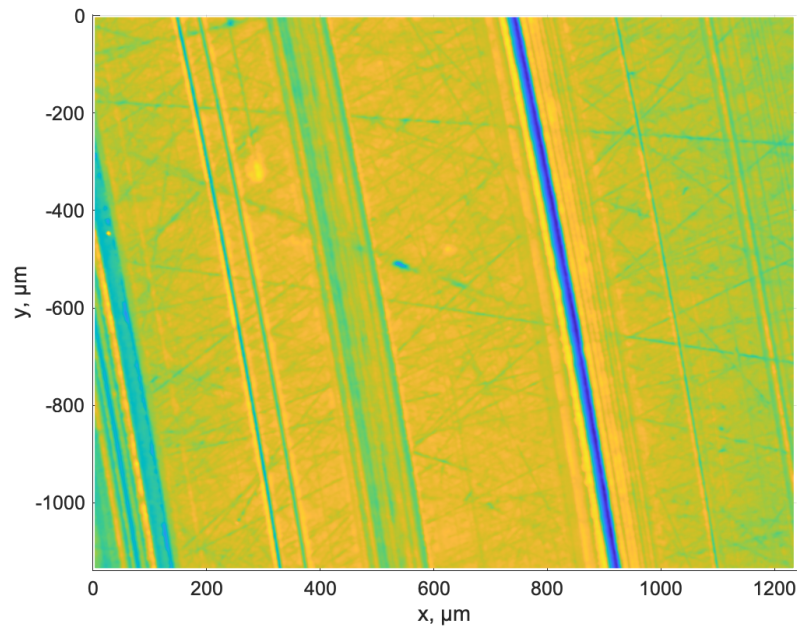


Figure 3.11: Steel surface after 5 minutes of testing with 1 MPa. Note that the scratches are not perfectly vertical so the flow factor along y is not negative.

The time comparison for the shear flow factor is presented in Figure 3.12 and Figure 3.13. As expected, the shear flow factors for x-direction are zero for all the deformed gap-height because the directions of the scratches are aligned with the main flow direction. So, there is no variation of the net mean flow due to the lubricant contained in the roughness valley. On the other hand, there is a reduction of the net mean flow in y-direction because of the lubricant stuck in the valley of the rough surface during the sliding. The behavior of the surface with different loads for the same runtime is very different and it seems that there is no correlation between them. In the test with 1 MPa the highest influence is reached after 60 minutes but, with 2 MPa as contact pressure, it is reached only after 10 min. Furthermore, the surface influence with 2 MPa (Figure 3.13) dropped after 15 minutes, reaching almost the zero value. In this condition the net mean flow is practically not influenced by the surface roughness.

Another important thing to observe is that the shear flow factor does not reach completely the zero value, so this means that the roughness surfaces have a small influence in the shear flow also for a gap-height of $30 \mu\text{m}$.

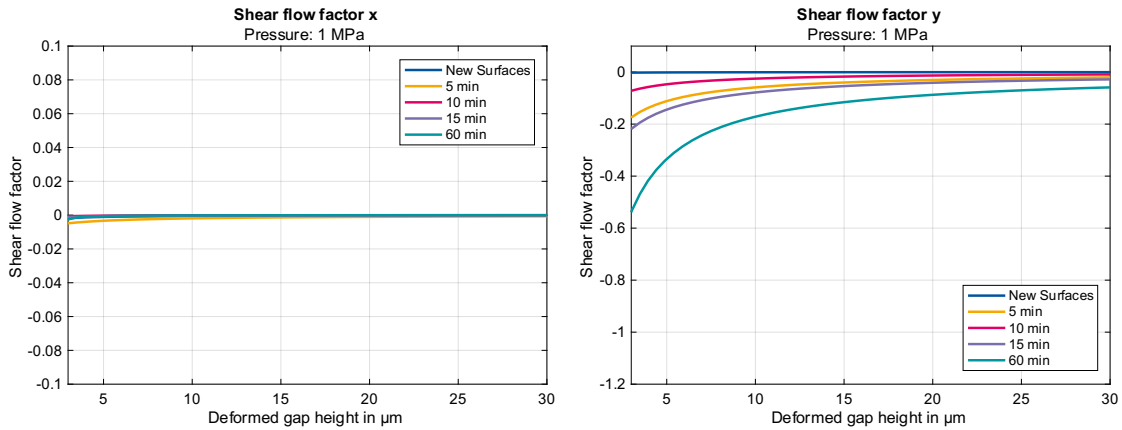


Figure 3.12: Shear flow factor in *x*- and *y*-direction with 1 MPa of pressure load.

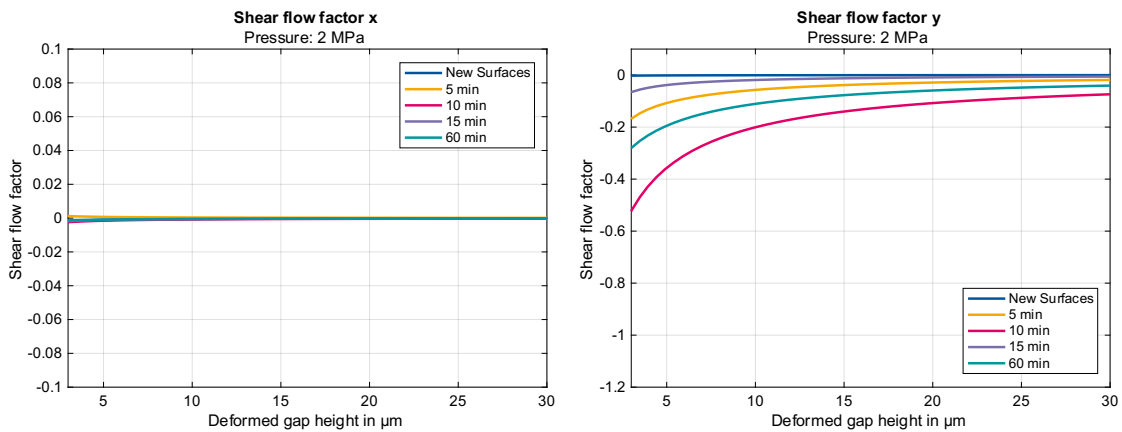


Figure 3.13: Shear flow factor in *x*- and *y*-direction with 2 MPa of pressure load.

3.4.2 Influence of Load

The influence of load of flow factor is carried out for each of the four test durations (5, 10, 15, 60 minutes), with the oil temperature set to 40°. The four different loads studied are: 0,5 MPa, 1 MPa, 2 MPa and 3 MPa. What is immediately clear looking at Figure 3.14 and Figure 3.15 is that within the first 15 minutes the surface influence is greater for the lowest pressure, 0,5 MPa, contrarily to expectation. The causes could be various, maybe the main reason may be that the surface undergoes more effects, such as erosion and chemical reaction during the initial phases of working time with a smaller load. Another possible cause could be the control system of the test bench, which cannot keep a perfectly constant normal force, as mentioned before. In this way, if the load is low, the surfaces could lose their contact because of the fluctuations of the normal force and then they could slam into each other, increasing the wear. It is a very unexpected phenomena and it could be interesting to do

3.4 – Flow Factors

more tests in order to better understand the reasons why this strange surface behaviour occurs. Furthermore, for the other loads the pressure flow factors are more or less the same. Thus, during the first 15 minutes of work the surface effect in the lubrication regimes stay steady using load from 1 MPa to 3 MPa. Anyway, by increasing the duration of the sliding contact the effect of the load starts to be observed. In fact, the surface influence of the 3 MPa test for 60 minutes of work is clearly larger compared to the other loads, see Figure 3.16.

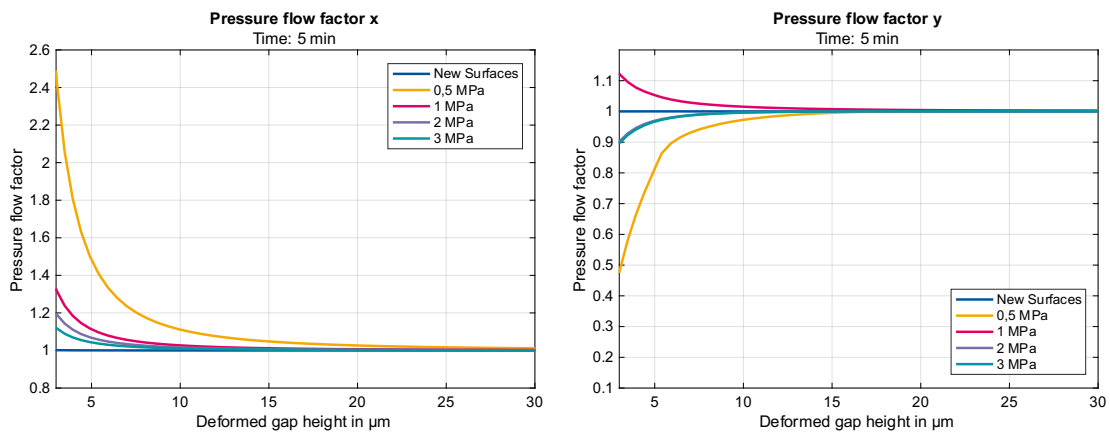


Figure 3.14: Pressure flow factor in x- and y-direction for 5 minutes runtime.

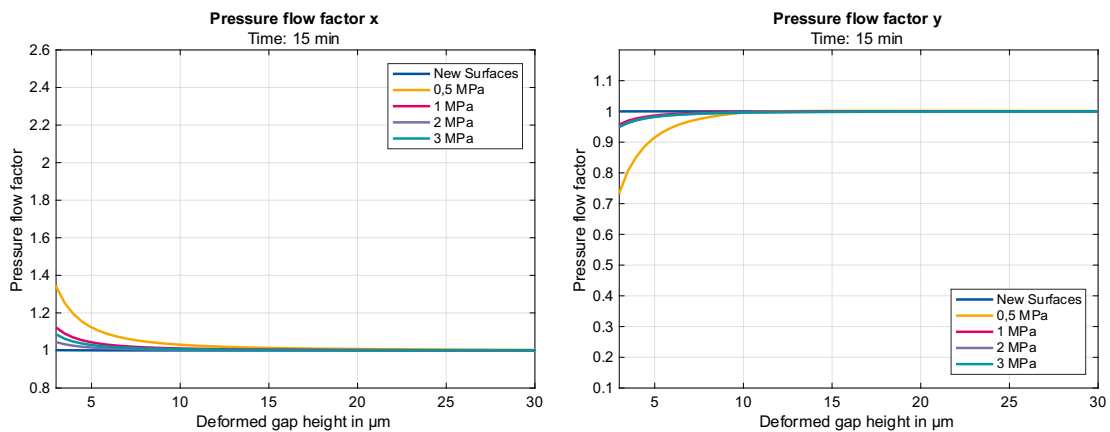


Figure 3.15: Pressure flow factor in x- and y-direction for 15 minutes runtime.

The pressure flow factor y in Figure 3.14 for 1 MPa is positive for the same reason said before. In fact, the directions of the scratches are not perfectly vertical, see Figure 3.11.

3 – Experimental Tests and Results

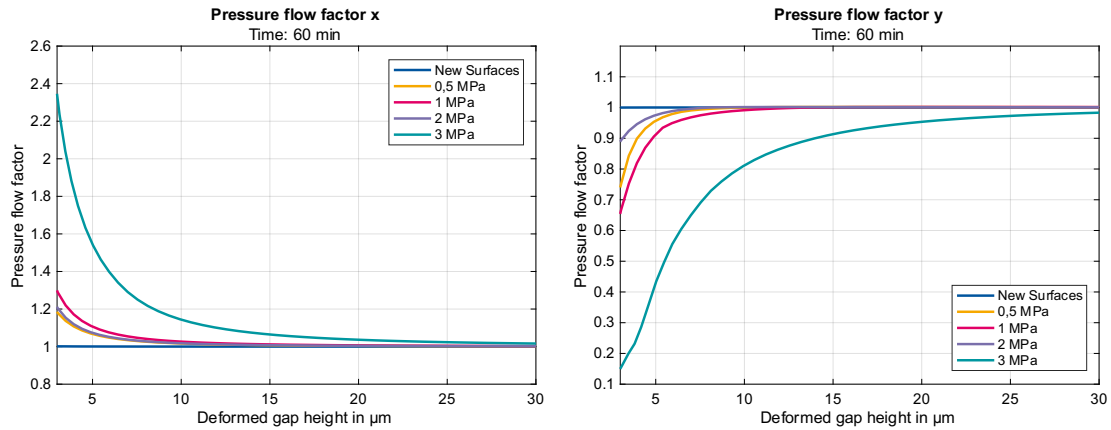


Figure 3.16: Pressure flow factor in x- and y-direction for 60 minutes runtime.

Similar observation can be done for the shear flow factors, Figure 3.17 and Figure 3.18: during the first 15 minutes the test with 0,5 MPa of contact pressure has the most influence on the shear flow, reducing the net mean flow significantly. Furthermore, surfaces have the same influence on the shear flow by applying pressure from 1 MPa to 3 MPa during the first 5 minutes. However, after 15 minutes of test the surface influence is slightly different with 1 MPa, indeed the shear flow factors are a little smaller than the ones of the tests with 2 MPa and 3 MPa. Also in this case, the shear flow factors in x-direction are zero and thus the surface influence on the net mean flow in that direction tends to zero.

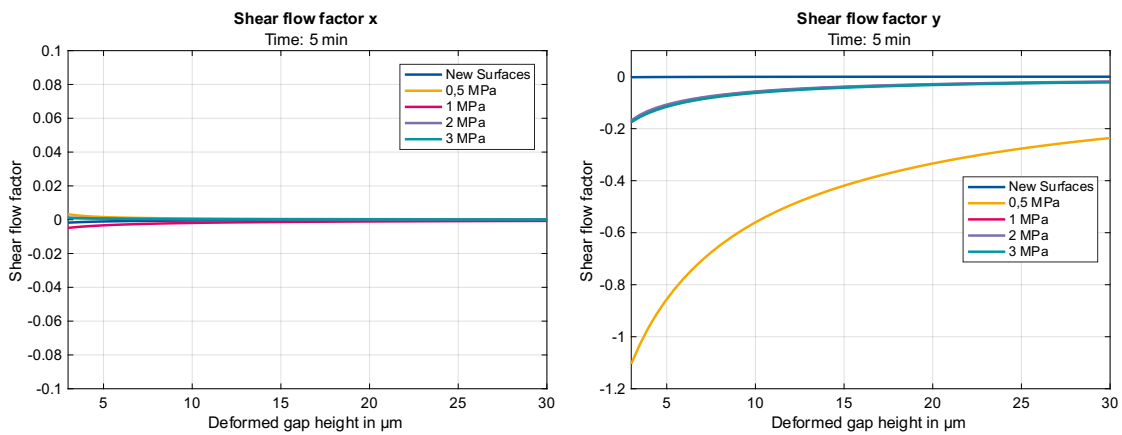


Figure 3.17: Shear flow factor in x- and y-direction for 5 minutes runtime.

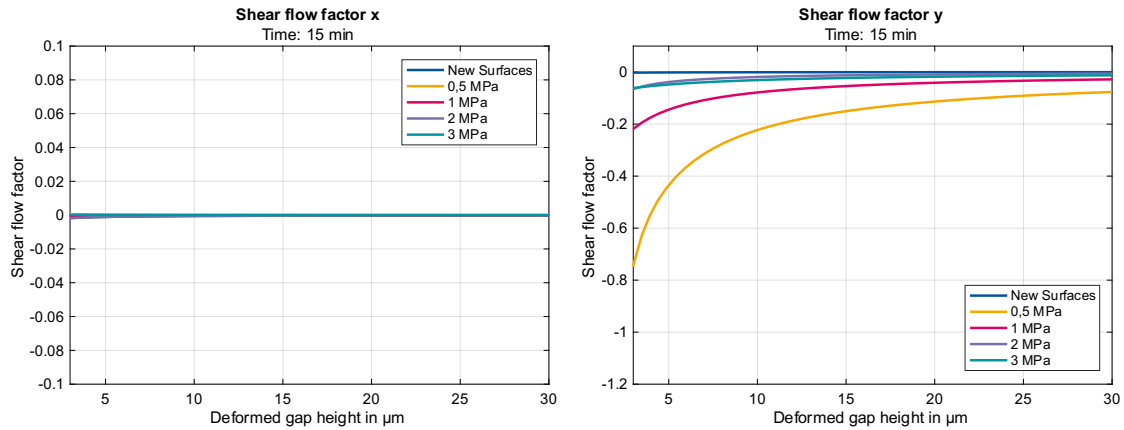


Figure 3.18: Shear flow factor in x- and y-direction for 15 minutes runtime.

3.4.3 Influence of Temperature

In this section the lubricant temperature influence in the flow factor is carried out. Five different temperatures were studied: 40°, 50°, 60°, 70° and 80°. The duration of the test was 15 minutes and the test were done for two different contact pressures: 1 MPa and 2 MPa. Looking at Figure 3.19 and Figure 3.20 it can be observed that there is not a clear correlation between the oil temperature and the flow factor value. Indeed, for 1 MPa (Figure 3.19) the most influence is obtained with 70 degrees of lubricant temperature; on the other hand, for 2 MPa (Figure 3.20) the most influence effect is obtained for 50 degree. Thus, the tribosystem behaviour with a certain oil temperature is different for each load. The best temperature is the one where friction and wear are as small as possible and so the surface remains sufficiently smooth to avoid a high influence in the lubrication regime also for small gap-height (in other words: pressure flow factor equal to 1 and shear flow factor equal to 0). As mentioned before, the best lubricant temperature is 60° in term of friction, but also in term of flow factor the surface influence is low with 60°. Thus, it can be said that the best oil temperature is 60°.

3 – Experimental Tests and Results

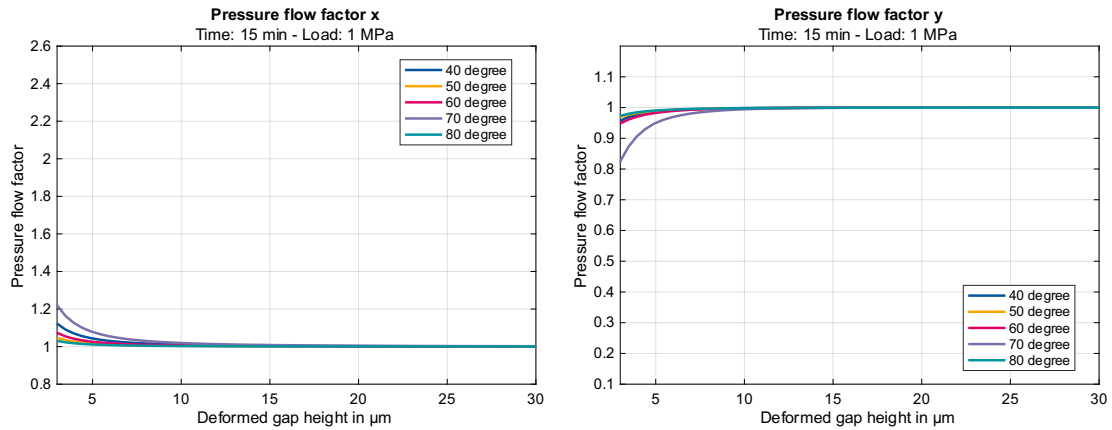


Figure 3.19: Pressure flow factor in x- and y-direction for different oil temperature and 15 minutes runtime with 1 MPa of contact pressure.

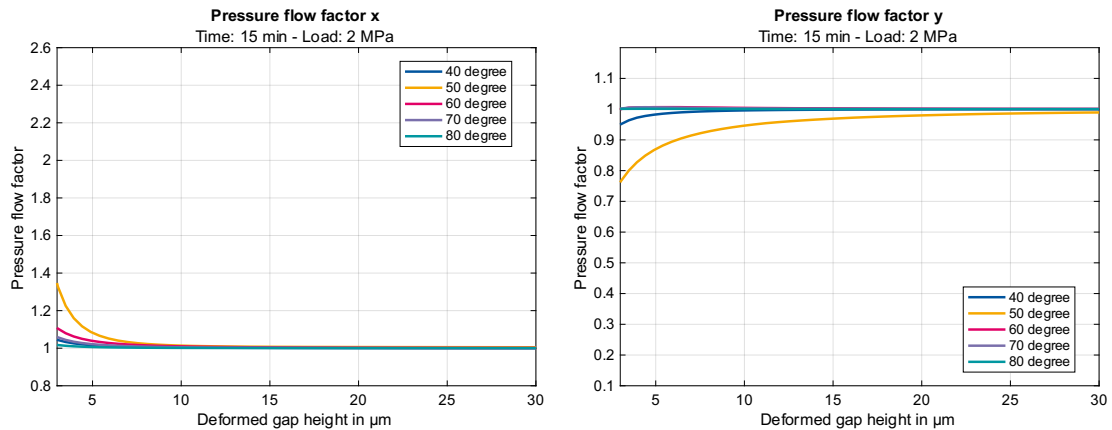


Figure 3.20: Pressure flow factor in x- and y-direction for different oil temperature and 15 minutes runtime with 2 MPa of contact pressure.

Figure 3.21 and Figure 3.22 show the shear flow factor comparing different oil temperature. It is remarkable that for 2 MPa, Figure 3.22, the influence of surface roughness on the shear flow is extremely high with an oil temperature equal to 50° . Furthermore, it remains very high also for $30 \mu\text{m}$ of gap-height, where usually the surface influence is usually very low or negligible.

3.4 – Flow Factors

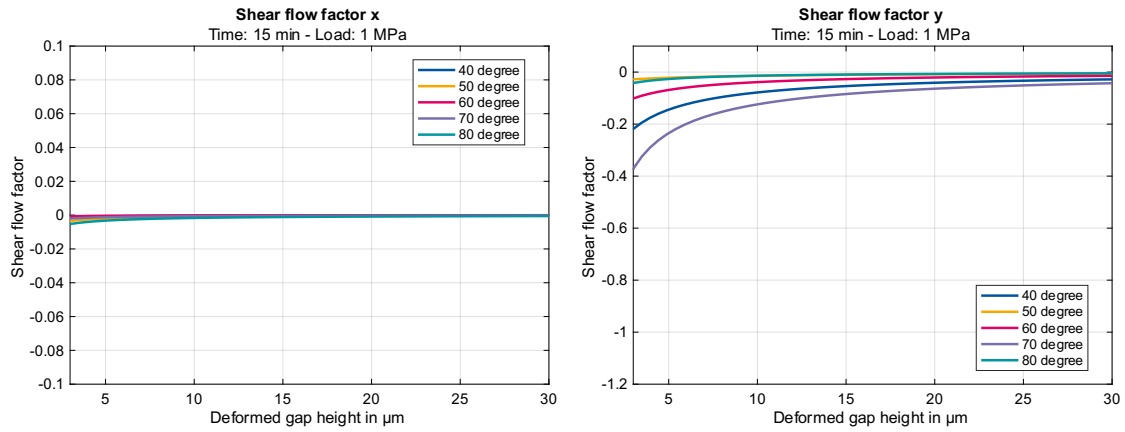


Figure 3.21: Shear flow factor in x- and y-direction for different oil temperature and 15 minutes runtime with 1 MPa of contact pressure.

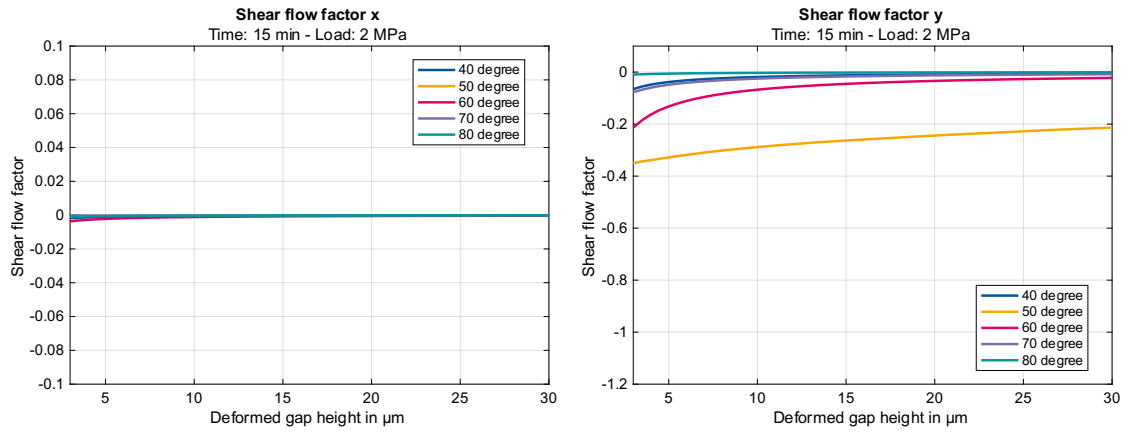


Figure 3.22: Shear flow factor in x- and y-direction for different oil temperature and 15 minutes runtime with 2 MPa of contact pressure.

Chapter 5

Conclusion and Future Work

This research aimed at overcoming the size limitation for the input matrix in the simulation software. In fact, the software used to simulate the flow factor takes as input a matrix of 300x300 points. Since after microscope scanning there are many more points, involving a submatrix of 300x300 points of the microscope data would lead to consider a very tiny portion of the surface, which is not representative of the surface topography, Figure 4.1. For this reason, a MATLAB code is created in order to: handle the microscope data, find a relevant distance between two measurement points and create the matrix for the simulation software, by considering a larger portion of surface.

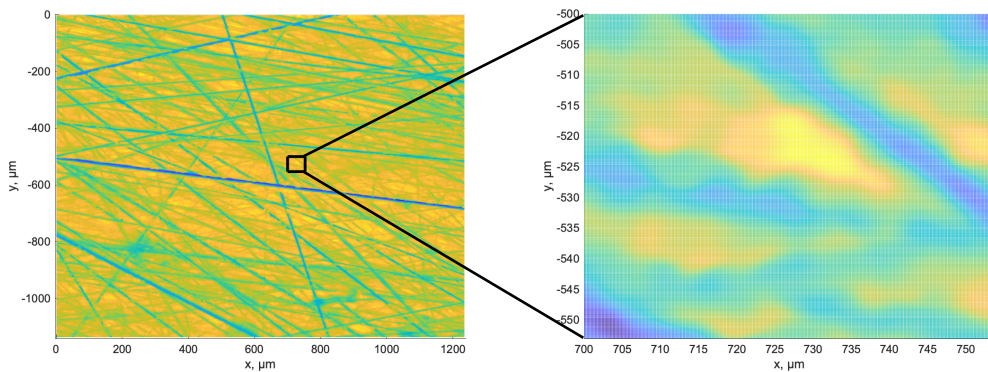


Figure 4.1: Example that shows the tiny portion of the total microscope data considered by taking a 300x300 submatrix. On the left there is the total surface scanned by the microscope, on the right there is the submatrix taken by conspiring a submatrix of 300x300 points. This is tiny and it is not representative of the total surface topography.

The idea to increase the surface taken by the 300x300 matrix is to study the Power Spectral Density. It is computed in both x- and y-direction, for each direction a cut-off value is found. Then the Nyquist-Shannon theorem is applied to compute the wavevector, its unit of measure is one over μm . So, finally,

the relevant distance is its reciprocal. The cut-off value needs to be as small as possible, in order to consider a larger portion of the surface; but if it is too small, the relevant distance will be too large, and the surface will not be equal to the real one anymore because a lot of information will get lost. Thus, finding the correct cut-off value is crucial.

Three different methods to identify the cut-off frequency are analyzed. The most suitable one is the area method, which takes as cut-off frequency the value where the PSD reaches a certain percentage of the total area. The typical percentage values are from 30 to 40% of the total area. Figure 4.2 shows the surface considered by the 300x300 matrix studying the PSD. It is clearly bigger and it better represents the total surface topography.

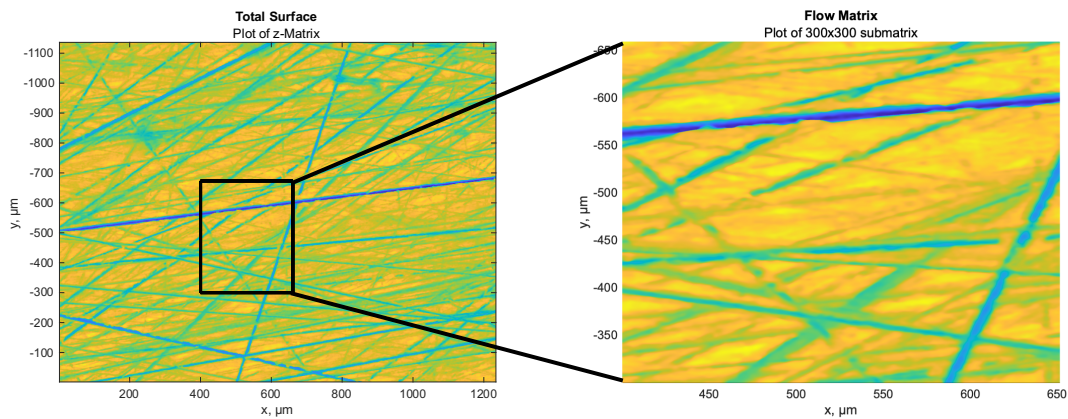


Figure 4.2: Portion of surface taken by studying the PSD. It is clearly bigger and it is representative of the surface roughness.

In conclusion, the MATLAB code allows to identify easily the correct portion of the surface with a helpful graphic interface.

Furthermore, the influence of three parameters is analyzed. Some interesting behaviors are found. Anyway, what was expected was a tendency between the variation of one parameter and the flow factor values. But there are not clear correlations, they have a random behavior. In fact, for instance, the load influence on flow factor is different when changing the load and vice versa. Therefore, more tests need to be done to have a greater knowledge about their behavior under different conditions.

In any case, what is remarkable is that the surface influence on the lubricant flow is not so high. Before this works, it was thought that the surface could influence highly the lubricant regime. Looking at the results, the surface influence appears to be usually from 20 or 30% with the smallest gap-heights. So, in most cases, the error done by not considering the surface roughness could be negligible, especially if the lubricant film is thick enough.

4.1 Future Work

This section gives some suggestions for future work to implement the code and to examine in depth the variation of flow factor during run-in process. These suggestions are:

- The surface sometimes has not the direction of lays perfectly vertical after the microscope scan. Figure 3.11 shows an example. This could lead to a strange behavior on the flow factor, so trying to rotate the surface around z-axis is a good point. Some attempts were done, see Figure 4.3, but the problem was that after the rotation the *z-matrix* cannot be built anymore because the data has not a matrix structure: after the rotation all points have different x and y values. Thus, finding a method to overcome this problem would be interesting.

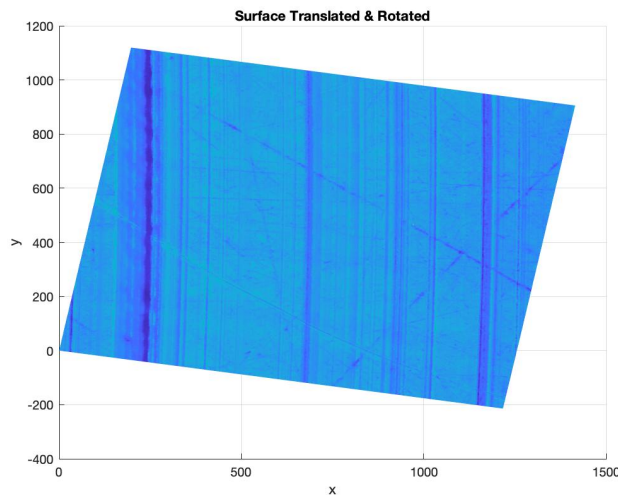


Figure 4.3: Surface rotation around z-axis in order to have vertical oriented lay.

- Another important suggestion may be the study of a possible correlation between the percentage of the area used to determine the cut-off frequency and the surface topography. At the moment that value is chosen by the operator for each surface. Anyway, there seems to be some kind of relation between the roughness values of the surface and the percentage of the PSD area used to determine the relevant distance. If there is a correlation between them, the cut-off frequency will be found automatically and the creation of the input matrix for the Tribo-x software will be easier and faster.
- During the load comparison, a very interesting phenomenon is observed: with a contact pressure equal to 0,5 MPa, the flow factors have the greatest influence, even if it is the

lowest contact pressure. Thus, doing more test could be interesting in order to better understand the reasons why this strange surface behaviour occurs.

Appendix

5.1 Appendix A

In this appendix roughness values for different load, time and temperature are presented. Note that, in order to better understand each parameter variation effect, the values are shown as function of time, load and temperature.

In the following tables the time effect on roughness is presented:

<i>Rotating discs</i>			<i>Stationary discs</i>		
	<i>Ra</i>	<i>Rq</i>		<i>Ra</i>	<i>Rq</i>
<i>M_new</i>	0,094	0,766	<i>F_new</i>	0,053	0,072
<i>M0,5_40grad_5min</i>	1,494	1,930	<i>F0,5_40grad_5min</i>	0,115	0,156
<i>M0,5_40grad_10min</i>	0,439	0,618	<i>F0,5_40grad_10min</i>	0,131	0,178
<i>M0,5_40grad_15min</i>	0,707	0,863	<i>F0,5_40grad_15min</i>	0,155	0,253
<i>M0,5_40grad_60min</i>	1,022	1,261	<i>F0,5_40grad_60min</i>	0,287	0,391

Table 5.1: Roughness variation of the test with 0,5 MPa for different durations.

<i>Rotating discs</i>			<i>Stationary discs</i>		
	<i>Ra</i>	<i>Rq</i>		<i>Ra</i>	<i>Rq</i>
<i>M_new</i>	0,094	0,766	<i>F_new</i>	0,053	0,072
<i>M1_40grad_5min</i>	1,145	1,440	<i>F1_40grad_5min</i>	0,153	0,256
<i>M1_40grad_10min</i>	0,335	0,478	<i>F1_40grad_10min</i>	0,153	0,210
<i>M1_40grad_15min</i>	0,620	0,781	<i>F1_40grad_15min</i>	0,266	0,994
<i>M1_40grad_60min</i>	0,667	0,810	<i>F1_40grad_60min</i>	0,199	0,279

Table 5.2: Roughness variation of the test with 1 MPa for different durations.

<i>Rotating discs</i>			<i>Stationary discs</i>		
	<i>Ra</i>	<i>Rq</i>		<i>Ra</i>	<i>Rq</i>
<i>M_new</i>	0,094	0,766	<i>F_new</i>	0,053	0,072
<i>M2_40grad_5min</i>	0,693	0,944	<i>F2_40grad_5min</i>	0,131	0,441
<i>M2_40grad_10min</i>	0,880	1,100	<i>F2_40grad_10min</i>	0,125	0,172
<i>M2_40grad_15min</i>	0,847	2,042	<i>F2_40grad_15min</i>	0,128	0,181
<i>M2_40grad_60min</i>	0,691	0,889	<i>F2_40grad_60min</i>	0,140	0,182

Table 5.3: Roughness variation of the test with 2 MPa for different durations.

<i>Rotating discs</i>			<i>Stationary discs</i>		
	<i>Ra</i>	<i>Rq</i>		<i>Ra</i>	<i>Rq</i>
<i>M_new</i>	0,094	0,766	<i>F_new</i>	0,053	0,072
<i>M3_40grad_5min</i>	0,654	0,834	<i>F3_40grad_5min</i>	0,141	0,204
<i>M3_40grad_10min</i>	0,305	0,394	<i>F3_40grad_10min</i>	0,120	0,165
<i>M3_40grad_15min</i>	0,477	0,709	<i>F3_40grad_15min</i>	0,233	0,287
<i>M3_40grad_60min</i>	1,895	2,954	<i>F3_40grad_60min</i>	1,262	1,637

Table 5.4: Roughness variation of the test with 3 MPa for different durations.

In the following tables the load effect on roughness is presented:

<i>Rotating discs</i>			<i>Stationary discs</i>		
	<i>Ra</i>	<i>Rq</i>		<i>Ra</i>	<i>Rq</i>
<i>M0,5_40grad_5min</i>	1,494	1,930	<i>F0,5_40grad_5min</i>	0,115	0,156
<i>M1_40grad_5min</i>	1,145	1,440	<i>F1_40grad_5min</i>	0,153	0,256
<i>M2_40grad_5min</i>	0,693	0,944	<i>F2_40grad_5min</i>	0,131	0,441
<i>M3_40grad_5min</i>	0,654	0,834	<i>F3_40grad_5min</i>	0,141	0,204

Table 5.5: Roughness variation of the 5 min runtime tests for different loads.

5.1 – Appendix A

Rotating discs			Stationary discs		
	<i>Ra</i>	<i>Rq</i>		<i>Ra</i>	<i>Rq</i>
<i>M0,5_40grad_10min</i>	0,439	0,618	<i>F0,5_40grad_10min</i>	0,131	0,178
<i>M1_40grad_10min</i>	0,335	0,478	<i>F1_40grad_10min</i>	0,153	0,210
<i>M2_40grad_10min</i>	0,880	1,100	<i>F2_40grad_10min</i>	0,125	0,172
<i>M3_40grad_10min</i>	0,305	0,394	<i>F3_40grad_10min</i>	0,120	0,165

Table 5.6: Roughness variation of the 10 min runtime tests for different loads.

Rotating discs			Stationary discs		
	<i>Ra</i>	<i>Rq</i>		<i>Ra</i>	<i>Rq</i>
<i>M0,5_40grad_15min</i>	0,707	0,863	<i>F0,5_40grad_15min</i>	0,155	0,253
<i>M1_40grad_15min</i>	0,620	0,781	<i>F1_40grad_15min</i>	0,266	0,994
<i>M2_40grad_15min</i>	0,847	2,042	<i>F2_40grad_15min</i>	0,128	0,181
<i>M3_40grad_15min</i>	0,477	0,709	<i>F3_40grad_15min</i>	0,233	0,287

Table 5.7: Roughness variation of the 15 min runtime tests for different loads.

Rotating discs			Stationary discs		
	<i>Ra</i>	<i>Rq</i>		<i>Ra</i>	<i>Rq</i>
<i>M0,5_40grad_60min</i>	1,022	1,261	<i>F0,5_40grad_60min</i>	0,287	0,391
<i>M1_40grad_60min</i>	0,667	0,810	<i>F1_40grad_60min</i>	0,199	0,279
<i>M2_40grad_60min</i>	0,691	0,889	<i>F2_40grad_60min</i>	0,140	0,182
<i>M3_40grad_60min</i>	1,895	2,954	<i>F3_40grad_60min</i>	1,262	1,637

Table 5.8: Roughness variation of the 60 min runtime tests for different loads.

In the following tables the load effect on roughness is presented:

<i>Rotating discs</i>			<i>Stationary discs</i>		
	<i>Ra</i>	<i>Rq</i>		<i>Ra</i>	<i>Rq</i>
<i>M1_40grad_15min</i>	0,620	0,781	<i>F1_40grad_15min</i>	0,266	0,994
<i>M1_50grad_15min</i>	0,459	0,673	<i>F1_50grad_15min</i>	0,148	0,230
<i>M1_60grad_15min</i>	0,482	0,682	<i>F1_60grad_15min</i>	0,075	0,098
<i>M1_70grad_15min</i>	0,619	0,752	<i>F1_70grad_15min</i>	0,142	0,180
<i>M1_80grad_15min</i>	0,196	0,279	<i>F1_80grad_15min</i>	0,111	0,143

Table 5.9: Roughness variation of the 15 min runtime and 1 MPa tests for different oil temperature.

<i>Rotating discs</i>			<i>Stationary discs</i>		
	<i>Ra</i>	<i>Rq</i>		<i>Ra</i>	<i>Rq</i>
<i>M2_40grad_15min</i>	0,847	2,042	<i>F2_40grad_15min</i>	0,128	0,181
<i>M2_50grad_15min</i>	0,702	2,721	<i>F2_50grad_15min</i>	0,119	0,163
<i>M2_60grad_15min</i>	0,493	0,611	<i>F2_60grad_15min</i>	0,093	0,127
<i>M2_70grad_15min</i>	0,407	0,533	<i>F2_70grad_15min</i>	0,216	0,277
<i>M2_80grad_15min</i>	0,285	0,391	<i>F2_80grad_15min</i>	0,199	0,380

Table 5.10: Roughness variation of the 15 min runtime and 2 MPa tests for different oil temperature.

Bibliografy

- [1] Stachowiak, G., & Batchelor, A. W. (2016). *Engineering Tribology* (4th ed.). Butterworth-Heinemann.
- [2] Hamrock, B. J., Schmid, S. R., & Jacobson, B. O. (2004b). *Fundamentals of Fluid Film Lubrication (Dekker Mechanical Engineering)* (2nd ed.). CRC Press.
- [3] Bhushan, B. (2013a). *Introduction to Tribology* (2nd ed.). Wiley.
- [4] Leach, R. (2013). *Characterisation of Areal Surface Texture* (2013th ed.). Springer.
- [5] Blau, P. J. (2019b). *Friction Science and Technology: From Concepts to Applications, Second Edition* (2nd ed.). CRC Press.
- [6] Blau, P. J. (1991). Running-in: Art or engineering? *Journal of Materials Engineering*, 13(1), 47–53. <https://doi.org/10.1007/bf02834123>.
- [7] Jeng, Y.-R., Lin, Z.-W., & Shyu, S.-H. (2004). Changes of Surface Topography During Running-In Process. *Journal of Tribology*, 126(3), 620–625. <https://doi.org/10.1115/1.1759344>.
- [8] Sahlin, F., Larsson, R., Almqvist, A., Lugt, P. M., & Marklund, P. (2009). A mixed lubrication model incorporating measured surface topography. Part 1: Theory of flow factors. *Proceedings of the Institution of Mechanical Engineers, Part J: Journal of Engineering Tribology*, 224(4), 335–351. <https://doi.org/10.1243/13506501jet658>.
- [9] Patir, N., & Cheng, H. S. (1978). An Average Flow Model for Determining Effects of Three-Dimensional Roughness on Partial Hydrodynamic Lubrication. *Journal of Lubrication Technology*, 100(1), 12–17. <https://doi.org/10.1115/1.3453103>.
- [10] Patir, N., & Cheng, H. S. (1979). Application of Average Flow Model to Lubrication Between Rough Sliding Surfaces. *Journal of Lubrication Technology*, 101(2), 220–229. <https://doi.org/10.1115/1.3453329>.
- [11] Almqvist, A., Fabricius, J., Spencer, A., & Wall, P. (2011). Similarities and Differences Between the Flow Factor Method by Patir and Cheng and Homogenization. *Journal of Tribology*, 133(3), 1–5. <https://doi.org/10.1115/1.4004078>.
- [12] Sahlin, F., Almqvist, A., Larsson, R., & Glavatskih, S. (2007). Rough surface flow factors in full film lubrication based on a homogenization technique. *Tribology International*, 40(7), 1025–1034. <https://doi.org/10.1016/j.triboint.2006.09.007>.
- [13] <https://www.tribo-technologies.com/en/tribo-x> (February 2021).

- [14] Otto, N.: „Experimentelle Untersuchung nachhaltiger Hydraulikfluide auf Ester- und Wasserbasis“, Ph.D. thesis RWTH Aachen, 2018, Aachen.
- [15] https://en.wikipedia.org/wiki/Gaussian_blur, (December 2020).
- [16] Gong, Y., Misture, S. T., Gao, P., & Mellott, N. P. (2016). Surface Roughness Measurements Using Power Spectrum Density Analysis with Enhanced Spatial Correlation Length. *The Journal of Physical Chemistry C*, 120(39), 22358–22364. <https://doi.org/10.1021/acs.jpcc.6b06635>.
- [17] Jacobs, T. D. B., Junge, T., & Pastewka, L. (2017). Quantitative characterization of surface topography using spectral analysis. *Surface Topography: Metrology and Properties*, 5(1), 013001. <https://doi.org/10.1088/2051-672x/aa51f8>.
- [18] Welch, P. (1967). The use of fast Fourier transform for the estimation of power spectra: A method based on time averaging over short, modified periodograms. *IEEE Transactions on Audio and Electroacoustics*, 15(2), 70–73. <https://doi.org/10.1109/tau.1967.1161901>.
- [19] Jacobs, T. D. B., Junge, T., & Pastewka, L. (2017a). Quantitative characterization of surface topography using spectral analysis. *Surface Topography: Metrology and Properties*, 5(1), 013001. <https://doi.org/10.1088/2051-672x/aa51f8>.

